

Chromate-free pre-treatment of aluminium for adhesive bonding

by

Otto Lunder

*Thesis submitted in partial fulfilment of the
requirements for the degree*

Doktor Ingeniør

Norwegian University of Science and Technology
Department of Materials Technology

May 2003

Preface

The work presented in this thesis was carried out at the Department of Materials Technology, Norwegian University of Science and Technology, and at SINTEF Materials Technology, in the period April 2000 to May 2003. Financial support by the Norwegian Research Council through SINTEFs Strategic Institute Programme (SIP) on “Surface Engineering” is gratefully acknowledged.

First of all I would like to thank my supervisor, Professor Kemal Nisancioglu, for his encouragement and good advice during these three years, and for inspiring collaboration over many years.

I would also like to thank my colleagues at SINTEF Materials Technology, particularly everyone involved in the SIP, for many interesting discussions and for making it an enjoyable project to participate in. Furthermore, thanks to everyone at the Department of Materials Technology for making these three years a pleasant experience.

Finally, thanks to Kristin, Mari and Mia for your care and support.

Trondheim, May 2003

Otto Lunder

Contents

Preface	iii
Contents	v
Summary	ix
1. Introduction.....	1
Background	1
Objective of present work	2
Structure of Thesis	2
References	3
2. Adhesive bonding of aluminium.....	5
Intrinsic adhesion	5
Objectives of the pre-treatment	7
Pre-treatments for structural bonding	8
Aerospace industry	8
Automotive industry	9
Environmental degradation	10
Corrosion of the substrate	12
Discussion	14
Chemical pre-treatment	14
Anodising	15
Environmental degradation	16
References	17
3. Formation and characterisation of a chromate conversion coating on AA6060 aluminium.....	21
Abstract	21
Introduction	22
Experimental	24
Materials	24
Chromating procedure	25
Electrochemical measurements	25
Surface characterisation	26
Results	26

Microstructure of the test materials	26
Electrochemical behaviour during CCC formation	28
Surface characterisation of AA6060	29
Growth of CCC on AlMg0.5Si0.4	34
Electrochemical behaviour in chloride solution	37
Discussion	40
Morphology of the conversion coatings	40
Behaviour of coated surfaces in chloride solution	43
Conclusions	44
Acknowledgements	45
References	45
4. Formation and characterisation of Ti-Zr based conversion layers on AA6060 aluminium.....	47
Abstract	47
Introduction	47
Experimental	48
Materials	48
Pre-treatment procedure	50
Surface characterisation	51
Electrochemical measurements	51
Results	52
SEM, EPMA and TEM observations	52
Surface analyses	58
Electrochemical behaviour of AA6060 and its phases in the conversion bath	60
Effect of pre-treatment on electrochemical behaviour in chloride solution	66
Discussion	68
Conclusions	71
Acknowledgements	71
References	72
5. Pre-treatment of AA6060 aluminium by selective removal of surface intermetallics.....	73
Abstract	73
Introduction	73
Experimental	75
Materials	75
Removal of surface intermetallics	75
Filiform corrosion testing	76
Results	77

Removal of particles from the surface of AA6060	77
FFC testing	82
Discussion	84
Conclusions	87
References	87
6. Pre-treatment of AA6060 aluminium for adhesive bonding.....	89
Abstract	89
Introduction	89
Experimental	90
Results and discussion	92
Surface characterisation of pre-treated surfaces	92
Electrochemical behaviour of pre-treated surfaces	99
Tensile strength of lap joints	100
Examination of fracture surfaces	102
Summary and conclusions	104
Acknowledgements	105
References	105
7. Effect of pre-treatment on the durability of epoxy-bonded AA6060 aluminium joints.....	107
Abstract	107
Introduction	107
Experimental	110
Materials	110
Surface treatment	110
Lap-shear testing	111
Wedge testing	111
Filiform corrosion testing	112
Surface characterisation	113
Results	113
Characterisation of pre-treated AA6060 surfaces	113
Single lap shear testing	117
Wedge testing	118
Examination of fracture surfaces	120
Filiform corrosion testing	123
Discussion	125
Wedge test	125
Filiform corrosion	127
Conclusions	128
Acknowledgements	129
References	129

8. Discussion.....	133
Formation and properties of the chemical conversion coatings	133
Durability of adhesive joints subjected to chemical pre-treatment	134
Corrosion of the substrate material	134
Loss of adhesion due to moisture	136
Pre-treatment by hot AC anodising	138
Comparison of pre-treatments employed in present work	140
Suggestions for future work	141
References	143
9. Conclusions.....	145

Summary

The increasing use of aluminium in automotive and transport applications is primarily driven by its high strength to weight ratio, enabling substantially improved fuel economy and reduced CO₂ emissions when substituted for heavier materials. However, the change of material presents new challenges with respect to design and methods of joining. Structural adhesive bonding offers several advantages compared with welding, but a major limitation is concern about the durability of joints in wet and corrosive environments. The pre-treatment of the aluminium surface prior to bonding is the key to long service life. Pre-treatments successfully employed by the aerospace industry cannot be used in automotive production, where cheaper and more environmentally friendly pre-treatments are required. Specifically, the use of chromates is unacceptable. Hence, there is a need to develop chromate-free pre-treatments that will consistently provide the required level of performance, while being acceptable both in terms of general engineering practice and economy. To accomplish this task, basic knowledge of the processes occurring on the aluminium surface during pre-treatment, properties of the modified surface, and mechanisms of joint degradation are necessary.

The purpose of the present work has therefore been to contribute to a better understanding of how the aluminium substrate affects the formation and properties of conversion coatings for adhesive bonding. In particular, a commercial chromate-free fluorotitanate/zirconate based process has been investigated and compared with conventional chromate treatment. The materials chosen for this work were commercially extruded AA6060-T6 aluminium and a structural single-part epoxy adhesive. To complement the studies of the commercial alloy, model analogues of the AA6060 aluminium matrix and -Al(Fe,Mn)Si phase particles present in the commercial alloy were also investigated.

It was observed that the -Al(Fe,Mn)Si particles played an essential role in the formation and properties of Ti-Zr oxide conversion coatings on AA6060 aluminium. The particles were significantly nobler than the aluminium matrix in the pre-treatment solution. An alkaline diffusion layer therefore developed around the particles during pre-treatment due to oxygen reduction and hydrogen evolution reactions. As Ti-Zr oxide precipitation was favoured at high pH, the conversion layers normally deposited at and in the vicinity of the cathodic particles. The conversion layers formed consequently exhibited considerable lateral variations in thickness. In addition to substrate

microstructure, bulk pH and agitation of the conversion bath were important factors controlling the extent of Ti-Zr oxide deposition and its distribution on the surface. On areas well away from the cathodic particles coverage was generally very poor, although a high density of small (<50 nm) oxide particles was deposited, presumably with a composition similar to the continuous conversion layer close to the β -Al(Fe,Mn)Si particles. The cathodic activity of the particles was only slightly reduced by formation of the Ti-Zr oxide conversion coating. In combination with poor coverage of the aluminium matrix, these conversion coatings are therefore not expected to improve the corrosion resistance of aluminium significantly.

In contrast to the above mechanism, the chromate conversion coating (CCC) formed by a *redox reaction* between chromate ions and aluminium. A relatively thick, porous chromium oxide layer developed over the aluminium matrix of AA6060, while a significantly thinner film was formed on the β -Al(Fe,Mn)Si particles. The morphology of the CCC covering the matrix was influenced by the hardening Mg_2Si phase, primarily by promoting nucleation of the CCC. Despite the thin film (<50 nm) formed on the β -Al(Fe,Mn)Si particles by chromating, the cathodic activity was significantly reduced. Inhibition of the cathodic reactivity at these particles is suggested as an important factor contributing to the high performance of chromate pre-treatments on aluminium.

Testing of epoxy-bonded AA6060 aluminium joints in humid environment showed that Ti-Zr based pre-treatment provided improved adhesion relative to alkaline etching and deoxidation only. However, Ti-Zr based pre-treatment was inferior to chromating. Rapid, interfacial crack growth during wedge testing was particularly observed for adherends with a relatively thick Ti-Zr oxide deposit, suggesting that excessive Ti-Zr oxide deposition should be avoided. Furthermore, as the substrate microstructure (*i.e.* type, area fraction and distribution of cathodic sites) strongly affected the Ti-Zr oxide deposition, the pre-treatment conditions should be adapted to the specific alloy in order to achieve optimum performance.

In the presence of chlorides, degradation of adhesive-bonded joints may be accelerated by a filiform corrosion (FFC) type of mechanism. The β -Al(Fe,Mn)Si particles in AA6060 played a crucial role in promoting FFC, as demonstrated by complete FFC immunity of the iron-free AA6060 model analogue alloy. Ti-Zr based pre-treatment provided less protection against FFC relative to chromate pre-treatment. The good FFC resistance of CCCs was partly attributed to a better inhibition of the cathodic activity at the β -Al(Fe,Mn)Si particles.

Summary

The cathodic γ -Al(Fe,Mn)Si particles present on the surface of AA6060 aluminium could be effectively removed by different etch treatments. However, selective removal of surface intermetallics did not prevent FFC because filament growth was supported by cathodic activity on particles that become exposed in the filament tail as a result of the corrosion process.

Based on lap shear testing, hot AC anodising in sulphuric acid to a film thickness of about 0.2 μm showed promise as another chromate-free pre-treatment for durable adhesive bonding. The performance was better than a conventional chromic-sulphuric acid based etch treatment. While hot AC anodising did not significantly inhibit the cathodic activity on the γ -Al(Fe,Mn)Si particles, good resistance against FFC was still obtained due to the oxide film covering the whole aluminium matrix. Based also on separate durability data recently available, hot AC anodising is considered as a robust alternative to chromating for adhesive bonding of aluminium in certain industrial applications.

Summary

1. Introduction

Background

The automotive industry is continuously working to accommodate the requirements of both environmental legislation and customer demands for higher performance and more luxury and safety features, by developing light-weight and hence more energy efficient vehicles. Substitution of aluminium for steel by construction of an aluminium space frame consisting of extruded components can be used to achieve a considerable weight reduction with no losses in strength and stiffness [1,2]. However, the change of material and body structure presents a significant challenge with respect to methods of joining to be used in body fabrication.

From a technical point of view, adhesive bonding offers several advantages [2-4] compared with other conventional joining methods such as welding and riveting. These include the possibility of joining dissimilar materials, ability to join thin sheets effectively and with improved joint stiffness and uniform stress distribution, and improved appearance of the finished structure. Another important factor is that adhesive bonding does not distort the components being joined as arc welding can do. Disadvantages of adhesive bonding include limited upper-service temperature compared with other joining methods, and low strength and toughness under the influence of tensile and peel stresses. However, the main limitation in the use of adhesive bonding for structural applications is concern about the durability of joints in wet and corrosive environments.

To attain a long service life under demanding conditions, pre-treatment of the aluminium before bonding is an extremely important factor [3]. The successful use of adhesive bonding in the aerospace industry [4-6] during the last fifty years shows that excellent durability can be obtained, even when the bonded structure is exposed to corrosive environments and dynamic fatigue loads. This requires use of complex and time-consuming pre-treatments. For automotive applications, simpler, cheaper and more environmentally friendly pre-treatments are necessary.

A large number of mechanical, chemical, electrochemical and other treatments specifically designed to modify the aluminium surface to enhance bond durability are available [7]. Among these, formation of a chromate conversion coating on aluminium represents a simple, versatile and effective

method. However, a recent EU directive (2000/53/EC) on “End-of-Life Vehicles” sets stringent requirements on manufacturers to ensure that the use of environmentally hazardous heavy metals is phased out. In particular, the use of lead, mercury, cadmium and hexavalent chromium should be prohibited.

Among the chromate-free alternatives, Ti and Zr based conversion coatings, often incorporating a polymeric constituent, seem to have gained acceptance to enhance the adhesion of aluminium to paints [8-10] and adhesives [11,12]. However, recent work has shown [13] that the formation and characteristics of Ti-Zr based conversion coatings are significantly affected by the microstructure of the aluminium substrate. Clearly, this raises questions concerning the ability of these pre-treatments in providing a consistent durability of bonded joints. In general, a better understanding of the formation, properties and performance of Ti-Zr based and other chromate-free conversion coatings is desirable, and probably necessary to increase the confidence in these pre-treatments for durable adhesive bonding.

Objective of the present work

The primary objective of this work is to obtain a better understanding of the microstructural factors influencing the formation and properties of conversion coatings for adhesive bonding of aluminium. In particular, a Ti-Zr based process was investigated and compared with conventional chromate treatment. Experimental methods employing combinations of electrochemical and surface characterisation as well as corrosion and adhesion testing were undertaken in order to obtain this objective.

The materials chosen for this work were extruded AA6060-T6 aluminium and a structural epoxy adhesive (XD4600), which are also being used in the production of aluminium space frames, e.g. for the Lotus Elise sports car. In addition to commercially produced AA6060, model analogues of the iron containing intermetallic particles and aluminium matrix of AA6060 were studied to assess the influence of microgalvanic factors on conversion layer formation and joint degradation.

Structure of the thesis

The following chapter gives a general introduction to the topic of adhesive bonding of aluminium, emphasising the role of pre-treatment to enhance joint

durability. The results presented in this thesis (chapters 3-7) are structured as a compilation of five separate technical papers intended for individual publication. Some repetition of experimental procedures has consequently been unavoidable. The formation and characteristics of a chromate conversion coating and Ti-Zr based conversion layers on AA6060 are studied in chapters 3 and 4, respectively, with emphasis on the role of Fe containing intermetallic particles present on the surface. Due to their cathodic nature, these particles are expected to increase the susceptibility to localised corrosion of aluminium, promoting filiform corrosion on coated surfaces [14]. The possibility of avoiding their detrimental effect by removal of the particles from the surface of AA6060 is examined in chapter 5.

Chapter 6 presents results from durability testing of lap joints subjected to various pre-treatments, including AC anodising in hot sulphuric acid, which appeared to be very promising as a rapid and environmentally friendly pre-treatment for adhesive bonding. This work has already been published [15]. In chapter 7, the effect of Ti-Zr based pre-treatment on durability of bonded joints is compared to a chromate treatment, using wedge adhesion and filiform corrosion tests to assess the durability. The discussion of experimental results in the individual chapters is generally limited to those presented within each chapter. An overall discussion of the results is therefore included in chapter 8.

References

1. D. Carle and G. Blount, *Materials and Design*, **20**, 267 (1999).
2. T. A. Barnes and I. R. Pashby, *Journal of Materials Processing Technology*, **99**, 72 (2000).
3. A. J. Kinloch, *Adhesion and Adhesives*, Chapman and Hall, London (1990).
4. A. J. Kinloch, *Proc. Instn.. Mech. Engrs.*, **211**, 307 (1997).
5. L. Kozma and I. Olefjord, *Materials Science and Technology*, **3**, 860 (1987).
6. W. Brockmann, O. D. Hennemann, H. Kollek and C. Matz, *Int. J. Adhesion and Adhesives*, **6**, 115 (1986).
7. G. W. Critchlow and D. M. Brewis, *Int. J. Adhesion and Adhesives*, **16**, 255 (1996).
8. P. D. Deck and D. W. Reichgott, *Metal Finishing*, **90**, 29 (1992).
9. T. Schram, G. Goeminne, H. Terryn, W. Vanhoolst and P. Van Espen, *Trans I. M. F.*, **73**, 91 (1995).

1. Introduction

10. P. D. Deck, M. Moon and R. J. Sujudak, *Progress in Organic Coatings*, **34**, 39 (1998).
11. G. Critchlow and D. M. Brewis, *J. Adhesion*, **61**, 213 (1997).
12. P. Briskham and G. Smith, *Int. J. Adhesion and Adhesives*, **20**, 33 (2000).
13. J. H. Nordlien, J. C. Walmsley, H. Østerberg and K. Nisancioglu, *Surface and Coatings Technology*, **153**, 72 (2002).
14. A. Afseth, J. H. Nordlien, G. M. Scamans and K. Nisancioglu, *Corros. Sci.*, **44**, 2491 (2002).
15. O. Lunder, B. Olsen and K. Nisancioglu, *Int. J. Adhesion and Adhesives*, **22**, 143 (2002).

2. Adhesive bonding of aluminium

The purpose of this chapter is to summarise some general aspects of adhesive bonding, particularly with respect to pre-treatment of the aluminium surface, which is the prime factor determining the durability of joints in wet environments. A large number of surface treatments are employed to enhance adhesion of paints and adhesives to aluminium, and reference is made to recent publications for more comprehensive reviews on the topic [1-3].

While many of the most successful treatments are based on the use of hexavalent chromium, a number of chromate-free processes are being developed due to environmental considerations. Available literature on chromate-free pre-treatments has also been reviewed in recent publications [4-6], and it is not considered necessary to repeat this task here. However, some common pre-treatments for aluminium employed in the aerospace and automotive industries are presented. The significance of the substrate material with respect to the durability of adhesive joints is discussed in the light of recent research on filiform corrosion (FFC) of painted aluminium, substantiating the motivation for the present work and choice of methods.

Intrinsic adhesion

Among different theories proposed to account for the phenomenon of adhesion the adsorption theory is the most widely accepted and of most relevance to adhesive bonding of metals [7]. Essentially, the theory states that if sufficiently intimate molecular contact is achieved between two materials, they will adhere due to interatomic and intermolecular forces established between the atoms and molecules in the surfaces of the two materials.

There are a variety of bond types that can occur, but the most common as far as adhesion technology is concerned are van der Waals bonds and hydrogen bonds, generally referred to as secondary bonds. These are relatively weak intermolecular forces, resulting from dipole-dipole interactions and attraction forces between oxygen and hydrogen atoms at the interface, respectively. In addition, formation of chemical bonds (chemisorption) may sometimes occur across the interface. These types of bonds, including covalent and ionic bonds, are generally referred to as primary bonds exhibiting bond energies of the order ten times stronger than the secondary bonds (Table 1).

While secondary force interactions are believed to be the dominant mechanism of adhesion of most adhesives, the environmental stability of adhesive bonds would be greatly improved by the presence of primary bonds across the substrate/adhesive interface. Various organosilanes are frequently applied as pre-treatment primers or adhesive additives in order to improve adhesion by formation of covalent Si-O-Al bonds. However, the exact bonding mechanisms are not well understood [8-10].

Table 1. Bond types and typical bond energies [7].

Type of bond		Bond energy (kJ/mol)
Primary	Ionic	600 - 1100
	Covalent	60 - 700
	Metallic	110 - 350
Secondary	Hydrogen bonds	10 - 40
	van der Waals bonds	1 - 20

If only secondary forces are acting across the adhesive/substrate interface, a thermodynamic work of adhesion (W_A) may be defined as

$$W_A = \gamma_s + \gamma_a - \gamma_{as} \quad (1)$$

where γ_s , γ_a and γ_{as} are the surface free energies of the substrate and adhesive, respectively, and γ_{as} is the interfacial energy. W_A simply represents the work required to separate the interface, and usually has a positive value, indicating thermodynamic stability of the interface. In the presence of a liquid the thermodynamic work of adhesion may become negative, indicating an unstable interface and loss of adhesion. Good correlation has been observed between calculations of W_A in different environments and interfacial debonding of unstressed joints [7]. However, while the sign of W_A can indicate whether a joint is thermodynamically stable or not, W_A provides no information on the kinetics of failure.

Measured strengths of adhesive joints are not readily correlated with the thermodynamic work of adhesion, even when the locus of joint failure is truly interfacial. This is because the test methods commonly employed for measuring the strength of joints includes viscoelastic and plastic energy losses in the adhesive and substrate, which completely obscure the influence of intrinsic adhesion forces on the measured joint strength. Surface roughening

is generally observed to increase the strength of joints. This effect can be attributed to increased interfacial area and more extensive energy dissipation being transferred to the adhesive near the interface, rather than a mechanical interlocking effect.

Objectives of the pre-treatment

Initially high joint strength can be obtained without any pre-treatment or by a simple degreasing of the aluminium surface before adhesive bonding. However, to maintain the integrity of bonded joints in wet environments some form of surface pre-treatment is always necessary, particularly if the joints are subjected to tensile stresses. The purpose of the pre-treatment is generally to modify the surface in order to achieve one or more of the following objectives [7]:

- Removal of weak boundary layers, including weak oxide layers formed by heat treatment or exposure to humid atmosphere, air-borne contamination and protective oils or greases.
- Enhancement of the degree of molecular contact between the adhesive and the substrate to promote formation of intrinsic adhesion forces exhibiting resistance to environmental attack by moisture.
- Generation of a specific surface morphology to increase the amount of energy dissipation to the adhesive.
- Creation of a continuous film on the surface, normally an oxide, which exhibits
 - high resistance against hydration
 - high stability over a wide pH range
 - protection against corrosion of the substrate
 - resistance to mechanical injury
- Protection of the surface prior to bonding. Pre-treated surfaces are influenced by humidity and contamination of the ambient atmosphere. Bonding is therefore normally performed within a limited time of the pre-treatment. Application of a primer, which is compatible with the adhesive, is often used to extend the shelf life and retain manufacturing flexibility.

Pre-treatments for structural bonding

Aerospace industry

Durability of adhesive joints is obviously of prime importance in aerospace applications, where the consequences of an adhesive failure can be catastrophic. Extensive use of high strength aluminium alloys exhibiting a relatively low corrosion resistance, demanding environments, and dynamic fatigue loads puts further requirements on the pre-treatments to be used.

The most successful and widely adopted pre-treatments used by American and European aerospace industry are multistage processes involving chromic acid anodising (CAA) or phosphoric acid anodising (PAA) [1,2]. The PAA procedure developed at Boeing Co. involves the use of 10 wt% phosphoric acid. Anodisation is performed at 10-15 V and a temperature of 21-24°C for 25 min. A porous oxide film is formed, about 0.5 µm in thickness. The composition of the oxide corresponds to non-hydrated Al₂O₃, and contains AlPO₄ in the outer part of the oxide film [11]. The PAA oxide has shown excellent stability in humid environments. Apparently, the phosphate is beneficial in suppressing the hydration of the aluminium oxide to form boehmite, AlOOH, and cohesively weak bayerite, Al(OH)₃. In addition, the porous nature of the oxide allows low viscosity adhesives to penetrate into the oxide structure, forming a “micro-composite” layer between the bulk adhesive and the aluminium metal. PAA surfaces treated with an epoxy-based primer to obtain such a structure showed superior performance in cyclic-fatigue tests in distilled water [12].

The CAA treatment is the preferred treatment of European aeroplane manufacturers. The typical surface oxide films formed by CAA consist essentially of Al₂O₃ and are significantly thicker (1-3 µm) and less porous than the PAA oxide films. The surface topography of the CAA oxide is relatively smooth, but the micro-roughness can be increased by use of a higher anodising temperature. Prior etching in chromic acid, or a subsequent immersion in phosphoric acid, is beneficial to long-term durability. In general, the CAA and PAA processes produce the most consistently good, durable bonds [2].

Various chromic-sulphuric acid etch treatments are in use, the most common being the process developed by the US Forest Products Laboratory. The FPL etch treatment is carried out in a sodium dichromate and sulphuric acid solution for 15-30 min at 65°C, giving a 5 nm thick oxide film with oxide protrusions extending 40 nm from the surface [1]. The oxide is amorphous, with a composition corresponding to Al₂O₃. Small concentrations (~0.5%) of

Cr and S have been detected in the oxide by XPS analysis [13]. The durability of bonds obtained by FPL etching alone is considered inferior to the CAA and PAA treatments. In the Boeing process the FPL etch is applied prior to PAA in order to produce a special oxide morphology on the surface.

As a result of the need for cheaper and more environmentally friendly etching procedures, alternative chromate-free etching solutions have been developed. The so-called P2 etch [14] is a patented sulphuric acid and ferric sulphate based treatment, producing oxide surfaces that are comparable to the FPL etch with respect to topography and adhesive bond strength. The STAB 3 (Surface Treatment for Aluminium Bonding) treatment [15] is an even cheaper method comprising a dip in a concentrated NaOH solution for 3-10 min at room temperature followed by a hard spray rinse. Due to the high pH of the etching solution, a Mg rich oxide is formed on AA2024-T3 aluminium. The treatment has shown durability results better than the FPL etch, but not as good as PAA.

Automotive industry

Pre-treatments employed in the automotive industry generally need to be simple and rapid in order to comply with the low cost and high manufacturing speeds required for automotive production. Pre-treatment systems utilised by Alcan International during their research into automotive bonding have been briefly described by Comrie [16]. One of these is a no-rinse chromic acid-silica suspension system that forms a silica-rich surface with a chromium-rich interfacial zone between the silica and the metal substrate [17]. The chromium-rich layer consists of a mixture of trivalent and hexavalent compounds, the latter providing enhanced corrosion protection of the underlying aluminium metal. The pre-treatment system is thought to enhance bond durability due to the surface topography arising from the presence of colloidal silica particulates. It is also possible that primary bonds can form between silanol groups in the hydrated silica surface and epoxide groups present within the adhesive [16].

Chromate-phosphate and some other chromate-based pre-treatments have been used for adhesive bonding of aluminium sheet to manufacture a range of experimental aluminium vehicles [3]. Durability trials have indicated that chromate-phosphate conversion coatings produce bonds comparable to PAA treatment, and that the prepared surface is capable of retaining its bondability for at least six months, in marked contrast with the FPL etch [2]. Moreover,

the phosphate component of the conversion coating would be expected to inhibit hydration of the oxide during exposure to water [18].

Anodising treatments for adhesive bonding are also employed by the automotive industry. Alcan has installed a high-speed cleaning and alternating current PAA line for continuous treatment of aluminium sheet [19] in Germany. The aluminium strip is passed through the electrolyte at 50-70°C, with a contact time of less than 6 s and a current density of 10-40 A/dm². The resulting oxide film is <0.2 µm thick and has large open pores, forming a very favourable substrate for lacquer, paint or adhesive. In the production of adhesive bonded aluminium space frames for the low volume Lotus Elise and Opel Speedster sports cars, Hydro Aluminium employs a sulphuric acid anodising (SAA) treatment prior to adhesive bonding of the AA6060 aluminium extrusions. For this application, an oxide film thickness of about 5 µm is used to provide both adhesion and good corrosion resistance of the uncoated structure.

A range of Ti and/or Zr based processes is also in use to enhance adhesion to paints [3,20,21] and adhesives [18,22]. The processing baths are based on fluorotitanate (H₂TiF₆) and fluorozirconate (H₂ZrF₆) solutions, and often contain organic acids or phosphate compounds to improve adhesion further [6]. The treatments are carried out by conventional immersion, spray or by no-rinse processes. The resulting oxide layers are very thin, typically only 10-50 nm [18,20,23] and their composition and structure depend on the specific bath composition used. The performance of these treatments for adhesive bonding seems to vary, but Zr based treatments have been observed to give durability results comparable to the FPL etch [2] and chromate-phosphate processes [18]. However, these treatments have not been tested over the wide range of environments in which chromate conversion coatings have proved effective [24].

Environmental degradation

The most important environmental factors determining the durability of adhesive bonded aluminium joints are humidity, temperature and mechanical stress [7,12,25]. Moderately increased temperature or mechanical stresses by themselves normally have no adverse effect on a structural joint. However, in the presence of water, increased temperatures may lead to accelerated degradation. Apparently, increased diffusion of water into the adhesive is an important factor. The rate of joint degradation by water is also increased if

the joint is subjected to stress. Cyclic loading seems to be more detrimental than a constant load [7,12].

Water may enter the bonded system by bulk diffusion through the adhesive, interfacial diffusion along the interface between the adhesive and substrate, and by capillary action through cracks or defects in the adhesive or conversion layer. Degradation of the joint may then occur by various mechanisms as illustrated in Figure 1. Water ingress may plasticize the adhesive itself [26], thereby lowering the glass transition temperature (T_g) of the adhesive and decreasing the load bearing capacity of the joint. Water may also cause true interfacial failure if only secondary molecular forces are acting across the oxide-polymer interface [7]. Furthermore, the presence of water can lead to weakening of the oxide layer covering the aluminium substrate. Aluminium oxides produced by most surface pre-treatments are not thermodynamically stable in moist environments and may react with water to form hydrated oxides [1,11,27] according to the reactions



It has been argued [28], based on electrochemical impedance spectroscopy (EIS) in combination with XPS measurements, that these hydration reactions can take place under an intact adhesive film. The hydrated oxides exhibit a relatively low cohesive strength [1], and if hydration occurs under an adhesive, the resulting increase in volume may induce high stresses and crack growth [28]. For epoxy-aluminium joints the failure path may be complex. However, for chromic acid etched and anodised adherends the locus of failure was determined by XPS to be largely in the oxide layer [29], indicating a mechanism involving hydration and weakening of the oxide. In general, the locus of failure must be identified by use of surface analytical techniques such as XPS or AES to determine the failure mechanism reliably.

The adhesive type may also influence the stability of the interfacial region due to reactions between water and components of the adhesive, forming products that leach out and react with the aluminium oxide. It is specifically believed [27] that an alkaline environment is formed in epoxies by reactions between water and curing agents such as dicyandiamide, causing attack of the aluminium oxide. In contrast, residues leaching from phenolic based adhesives are slightly acidic, which possibly contributes to the superior joint durability often shown by phenolic based adhesives [7].

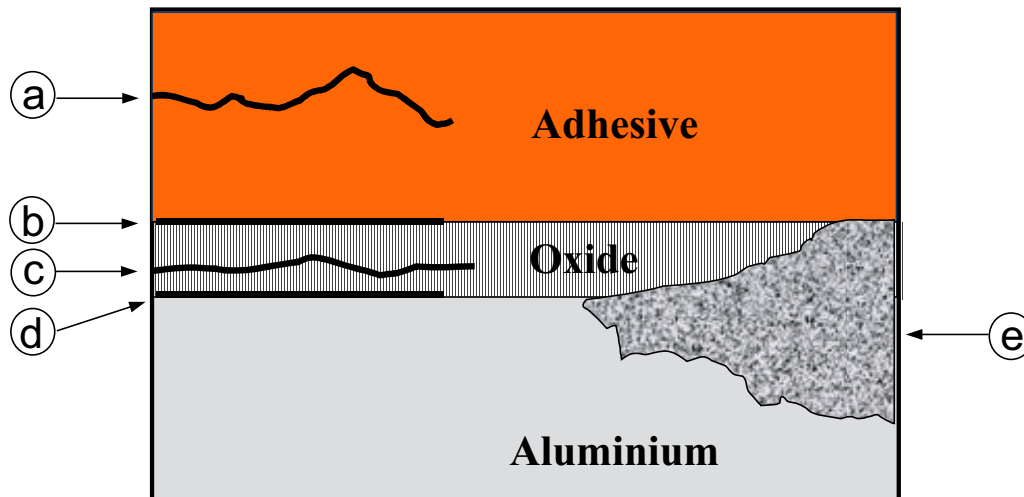


Figure 1. Schematic illustration of joint failure by a) cohesive fracture of the adhesive b) interfacial disbonding between oxide and adhesive c) cohesive fracture of oxide layer d) fracture at metal-oxide interface and e) corrosion of the aluminium substrate.

Corrosion of the substrate

In addition to the above factors, loss of adhesion will obviously occur if the substrate material is attacked by corrosion. Although corrosion of the adherend surface frequently takes place as a result of environmental failure by one of the other mechanisms, corrosion has been identified as the prime cause of environmental failure of clad aluminium joints [27]. The clad layer protects the electrochemically nobler substrate alloy against localised attack. However, undermining of the adhesive by preferential corrosion of the anodic clad layer is evidently undesirable in the context of adhesive bonding.

Relatively little information is available in the published literature on the role of corrosion in the degradation of aluminium-adhesive joints. Environmental testing is typically performed in humid atmosphere or in distilled water at temperatures up to 70°C [11-13,15,22,28,29]. One exception is a work by Horton and Spinks [30], who studied the role of chlorides on durability of adhesive bonded AA5251 aluminium. Interestingly, stressed lap shear and wedge tests showed that 0.5% NaCl solution was more detrimental to bond durability than both 5% NaCl solution and distilled water. The role of aluminium corrosion in the bond degradation mechanism was not established.

Degradation of adhesive bonded aluminium by corrosion of the substrate material would be expected to resemble the processes occurring during corrosion of painted aluminium. Extensive research during recent years have brought to attention the significant role of metallurgical factors in controlling filiform corrosion (FFC) of painted aluminium sheet materials [31-33]. The near surface microstructure of rolled aluminium becomes distinctly different from the bulk structure as a result of high shear and elevated temperatures during processing. The surface layer, typically $< 1 \mu\text{m}$ in thickness, is generally characterised by a refined grain structure with rolled-in oxide particles and a very fine distribution of secondary intermetallics [33]. Moreover, heat treatment at temperatures above 400°C may cause electrochemical activation of the surface due to enrichment of Pb, even when present in trace amounts [34], making the material susceptible to superficial corrosion attack such as FFC. Clearly, the presence of electrochemically active surface layers are expected to have a detrimental effect also on adhesive joints, analogous to the previously reported behaviour of clad aluminium joints [27].

The necessity of presence of cathodic second phase particles for FFC to occur on aluminium was demonstrated by use of binary model alloys [35]. While a single phase, solid solution Al-Fe alloy did not support FFC, heat treatment to precipitate cathodic Al_3Fe particles resulted in extensive FFC. However, the FFC resistance of an Al-Mn alloy was not impaired by heat treatment to form Al_6Mn particles, as this phase has electrochemical properties similar to that of the aluminium matrix.

Unpublished work [36] examining the degradation of unstressed epoxy-bonded AA6060 joints showed that exposure to conditions promoting FFC (DIN EN 3665) was more detrimental to joint strength than exposure in an acidified synthetic sea water fog (SWAAT test). Inspection of the adhesively fractured surfaces indicated that the aluminium adherends corroded by a FFC type of mechanism. Hence, the results demonstrated that degradation of adhesive joints by FFC is indeed possible, at least under accelerated test conditions. Since the lap joints in these tests were manufactured from extruded AA6060 material, no disturbed surface layer similar to that observed for rolled sheet was present. However, intermetallic -Al(Fe,Mn)Si phase [37] particles are present in AA6060 due to impurity iron. These particles are cathodic to the aluminium matrix [38,39]. In general, commercial aluminium alloys always contain iron impurities in the form of various cathodic phases, fulfilling one of the basic requirements for FFC to occur.

Discussion

Chemical pre-treatment

Many of the chromate-free pre-treatments available for paint and adhesive application produce conversion films or deposits that are detected only by surface analyses. It is therefore likely that the composition, morphology and uniformity of conversion coatings resulting from such chemical pre-treatments are significantly influenced by surface heterogeneities of the aluminium substrate, particularly different types of intermetallic phases. Although advanced surface analytical methods have been used to study the modification of aluminium surfaces by various pre-treatments, relatively little attention has been paid to the role of the heterogeneous substrate material with respect to conversion coating formation and performance. This could partly be due to limitations in the lateral resolution of some of the most commonly used techniques, *e.g.* XPS.

Chromate-free titanium and zirconium based processes are being increasingly used to prepare aluminium surfaces prior to painting and adhesive bonding. The conversion coatings may be applied by dipping, spraying or no-rinse processes. Recent work showed [40] that the formation of a Ti-Zr based conversion layer on AA6060 aluminium by dipping was largely controlled by the intermetallic -Al(Fe,Mn)Si particles present on the alloy surface, resulting in conversion layers with considerable variations in thickness. Similarly, the thickness and coverage of organosilanes adsorbed on AA2024 aluminium were strongly affected by the distribution of second-phase particles on the alloy surface [41]. These examples show that the intermetallic particles can have a significant effect on the formation and properties of the films deposited. There is obviously a need to better understand the role of intermetallic particles in the deposition mechanism of different chromate-free pre-treatments, and how the conversion layers formed affect the performance of bonded joints. Even in the case of chromate conversion coatings, most of the fundamental work has been limited to high purity aluminium and AA2024 alloy, which are not relevant for use in automotive applications.

On this background, the present study aims to obtain more knowledge of how the substrate microstructure influences the deposition and properties of conversion coatings for adhesive bonding. A Ti-Zr based process is particularly studied and compared with conventional chromate treatment in terms of conversion coating formation, characteristics and performance. The substrate material chosen for this study is an AA6060-T6 aluminium alloy since

extruded aluminium alloys in the 6000 series are extensively used in light-weight car manufacturing.

Apparently, the -Al(Fe,Mn)Si particles in AA6060 play an important role in the formation of the Ti-Zr based conversion coatings due to their cathodic nature relative to the aluminium matrix. Macroscopic synthesised crystals with composition similar to the -Al(Fe,Mn)Si phase and an iron-free AA6060 model analogue alloy, simulating the aluminium matrix of the commercial alloy, are therefore included to assess the magnitude of micro-galvanic reactions occurring on the surface during pre-treatment. Field emission SEM and Auger electron spectroscopy are among the surface analytical techniques used, because high lateral resolution is necessary to characterise the pre-treated surfaces reliably.

Anodising

Experience has shown that the most durable bonds are obtained by anodising pre-treatments employed by the aerospace industry. The superior performance is apparently due to the relatively thick oxide film, which resists hydration and protects the substrate better against corrosion than the thin oxide layers formed by etch pre-treatments. While the aerospace procedures are not acceptable in automotive production due to environmental and cost considerations, continuous AC anodising of aluminium sheet in phosphoric acid (PAA) [19] and sulphuric acid (SAA) are in use for coil coating applications. The use of alternating current and elevated temperatures makes degreasing of the aluminium strip unnecessary, as effective cleaning is obtained by hydrogen evolved from the surface during the cathodic cycle of the AC current. Furthermore, relatively high current densities can be used at elevated temperature, allowing very short anodising times.

While anodising at low temperature produces hard and brittle oxide films, it is known that by using higher temperatures softer and more ductile films are obtained [42-44]. Such thin film anodising is utilised in the production of lacquered aluminium strip for packaging applications, involving forming operations of the coated surface. However, the ductile oxide films formed by high temperature anodising should be attractive also for structural adhesive bonding as these oxides would provide an intermediate stiffness between the metal substrate and the adhesive. The graded stiffness of the interface region reduces local stress concentrations and should thus enhance the durability of joints, particularly under dynamic loads [12].

No information about the performance of structural adhesive joints pre-treated by elevated temperature AC anodising is available in the scientific literature, despite the rapid and chromate-free processing characterising this type of treatment. Introductory experiments are therefore conducted in this work to assess whether hot AC anodising should be exploited further for structural adhesive bonding of aluminium in automotive applications.

Environmental degradation

As discussed above, the presence of various intermetallic phases can have a crucial effect on the corrosion behaviour of aluminium alloys by forming microgalvanic couples promoting FFC [33,35] and other types of localised attack of the aluminium matrix [45]. Apart from the problems associated with clad aluminium alloys, corrosion has not been observed to be one of the most common mechanisms of environmental attack on adhesive joints in aerospace applications [7]. Possibly, the extensive use of sealants to protect the edges of joints reduces the probability of corrosion effectively. Hydration of the aluminium oxide may still occur, since all organic sealants are permeable to water and moisture will eventually reach the interfacial region.

Little long-term experience is yet available about the degradation mechanisms of adhesive bonded aluminium joints in automotive applications. However, preliminary conclusions from the European Aluminium Association (EAA) working group on general test procedures for aluminium bonding in automobile production [46] imply that the use of chlorides in accelerated tests is essential to obtain correlation with outdoor exposure results. Thus, it seems that the corrosion protection afforded by the pre-treatment is an important factor affecting the adhesive bond durability, unless the joints are coated to prevent access of chlorides to the interface.

No single, universally accepted accelerated test method exists to assess the durability of bonded joints in corrosive environment. While corrosion testing of bonded joints may be useful for ranking purposes, the mechanism of joint degradation would be difficult to determine from such tests. It is therefore desirable to separate between loss of adhesion due to subtle changes in the nature of the oxide layer caused by moisture, and failure caused by corrosion of the substrate material.

In the present work, corrosion resistance of the adhesive-substrate interface is assessed by testing of surfaces coated with a thin layer (about 0.2 mm) of adhesive. The adhesive used throughout this work is a single part structural

epoxy adhesive as epoxy adhesives represent the most common structural adhesives and have gained wide acceptance in many industries. Standard FFC testing of the coated surfaces is employed to rank the pre-treatments with respect to corrosion. This test is observed to be much more reliable than commonly used salt spray tests in evaluating outdoor performance of coated aluminium [47]. Degradation of bonded aluminium-to-aluminium joints in humid atmosphere is studied using conventional lap shear and wedge samples.

References

1. L. Kozma and I. Olefjord, *Materials Science and Technology*, **3**, 860 (1987).
2. G. W. Critchlow and D. M. Brewis, *Int. J. Adhesion and Adhesives*, **16**, 255 (1996).
3. P. G. Sheasby and R. Pinner, *The Surface Treatment and Finishing of Aluminium and Its Alloys*, 6th Ed., Vol. 1, ASM International, Metals Park, Ohio (2001).
4. S. M. Cohen, *Corrosion*, **51**, 71 (1995).
5. G. W. Critchlow, *Trans IMF*, **76** (1), B6 (1998).
6. A. Nylund, *Aluminium Transactions*, **2**, 121 (2000).
7. A. J. Kinloch, *Adhesion and Adhesives*, Chapman and Hall, London (1990).
8. J. Fang, B. J. Flynn, Y. L. Leung, P. C. Wong, K. A. R. Mitchell and T. Foster, *Journal of Materials Science Letters*, **16**, 1675 (1997).
9. N. G. Cave and A. J. Kinloch, *Polymer*, **33**, 1162 (1992).
10. R. P. Digby and S. J. Shaw, *Int. J. Adhesion and Adhesives*, **18**, 261 (1998).
11. A. J. Kinloch, H. E. Bishop and N. R. Smart, *J. Adhesion*, **14**, 105 (1982).
12. A. J. Kinloch, M. S. G. Little and J. F. Watts, *Acta Mater.*, **48**, 4543 (2000).
13. P. Poole and J. F. Watts, *Int. J. Adhesion and Adhesives*, **5**, 33 (1985).
14. W. J. Russell and E. A. Garnis, US Patent No. 4,212,701, 15 July 1980.
15. T. Smith, *J. Adhesion*, **14**, 145 (1982).
16. R. Comrie, Dielectric Studies of the Durability of Aluminium/Epoxy Bonded Systems, Thesis, University of Strathclyde, Scotland (1998).
17. J. A. Treverton and A. Bosland, *Corrosion Science*, **37**, 723 (1995).
18. G. W. Critchlow and D. M. Brewis, *J. Adhesion*, **61**, 213 (1997).

19. J. Ball, P. K. F. Limbach and J. D. B. Sharman, Proceedings of 1st International Symposium on *Aluminium Surface Science and Technology*, Antwerp, Belgium, 12-15 May 1997.
20. P. D. Deck and D. W. Reichgott, *Metal Finishing*, **90**, 29 (1992).
21. P. D. Deck, M. Moon and R. J. Sujdak, *Progress in Organic Coatings*, **34**, 39 (1998).
22. P. Briskham and G. Smith, *Int. J. Adhesion and Adhesives*, **20**, 33 (2000).
23. T. Schram, G. Goeminne, H. Terry, W. Vanhoolst and P. Van Espen, *Trans IMF*, **73** (3), 91 (1995).
24. B. R. W. Hinton, *Metal Finishing*, **89** (9), 55 (1991) and **89** (10), 15 (1991).
25. D. M. Brewis, *Materials Science and Technology*, **2**, 761 (1986).
26. J. W. Wylde and J. K. Spelt, *Int. J. Adhesion and Adhesives*, **18**, 237 (1998).
27. W. Brockmann, O. D. Hennemann, H. Kollek and C. Matz, *Int. J. Adhesion and Adhesives*, **6**, 115 (1986).
28. G. D. Davis, P. L. Whisnant and J. D. Venables, *J. Adhesion Sci. Technol.*, **9**, 433 (1995).
29. A. J. Kinloch, L. S. Welch and H. E. Bishop, *J. Adhesion*, **16**, 165 (1984).
30. T. Horton and G. M. Spinks, *Polymer International*, **28**, 9 (1992).
31. H. Leth-Olsen and K. Nisancioglu, *Corrosion Science*, **40**, 1179 (1998).
32. K. Nisancioglu, J. H. Nordlien, A. Afseth and G. M. Scamans, *Materials Science Forum Vols. 331-337*, 111, Trans Tech Publications Ltd., Switzerland (2000).
33. A. Afseth, J. H. Nordlien, G. M. Scamans and K. Nisancioglu, *Corrosion Science*, **44**, 2491 (2002).
34. J. T. B. Gundersen, *Dissertation*, NTNU 2002:17, Norwegian University of Science and Technology, Trondheim, Norway (2002).
35. A. Afseth, J. H. Nordlien, G. M. Scamans and K. Nisancioglu, *Corrosion Science*, **44**, 2529 (2002).
36. H. Laugen, M.Sc. Thesis (in Norwegian), Department of Materials Technology, Norwegian University of Science and Technology, Trondheim, Norway (1998).
37. L. F. Mondolfo, *Aluminium Alloys: Structure and Properties*, Butterworths, London (1976).
38. E. Mattson, L. O. Gullman, L. Knutsson, R. Sundberg and B. Thundal, *British Corrosion Journal*, **6**, 73 (1971).
39. K. Nisancioglu, *J. Electrochem. Soc.*, **137**, 69 (1990).
40. J. H. Nordlien, J. C. Walmsley, H. Østerberg and K. Nisancioglu, *Surface and Coatings Technology*, **153**, 72 (2002).

2. Adhesive bonding of aluminium

41. D. Susac, X. Sun and K. A. R. Mitchell, *Applied Surface Science*, **207**, 40 (2003).
42. E. A. Wootton, *Sheet Met. Ind.*, **53**, 297 (1976).
43. A. P. Gruar and D. R. Gabe, *Trans Inst. Met. Finish.*, **63**, 1 (1985).
44. A. Strawbridge, D. R. Gabe and A. J. Dowell, *Trans Inst. Met. Finish.*, **68**, 69 (1990).
45. K. Nisancioglu, Proceedings of *The 3rd International Conference on Aluminium Alloys: Their Physical and Mechanical Properties*, Trondheim, Norway, **3**, 239 (1992).
46. J. Hunter, T. Luksepp, M. Benmalek and J. Vrenken, EAA Working Group 4, General test Procedures: "Progress in the harmonisation of test procedures for aluminium bonding", Adhesive Bonding in Automobile Production, Bad Neuheim, 21-22 Nov 2001.
47. H. Leth-Olsen, *Dissertation*, NTNU 1996:85, Norwegian University of Science and Technology, Trondheim, Norway (1996).

2. Adhesive bonding of aluminium

3. Formation and characterisation of a chromate conversion coating on AA6060 aluminium

O. Lunder^{1,2}, J. Walmsley¹, P. Mack³ and K. Nisancioglu²

¹ SINTEF Materials Technology, N-7465, Trondheim, Norway

² Norwegian University of Science and Technology,
N-7491, Trondheim, Norway

³ Thermo VG Scientific, East Grinstead, United Kingdom

ABSTRACT

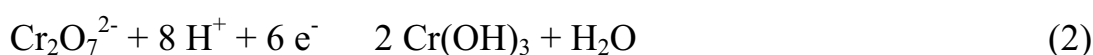
AA6060-T6, an AlMg0.5Si0.4 model alloy and γ -Al(Fe,Mn)Si phase electrodes have been subjected to chromate treatment in a commercial chromate-fluoride based solution. The coated surfaces were subsequently examined by use of field emission SEM, TEM, AES and electrochemical measurements in 0.1 M NaCl solution in order to study the effect of substrate microstructure on coating formation and properties. Non-uniform growth of the chromate conversion coating (CCC) on AA6060-T6 resulted in a porous morphology, with cracks extending down to the base metal. Poor coverage was particularly observed at the grain boundaries. The thickness of the CCC after completed treatment was about 150-200 nm, while significantly thinner films were formed on the γ -Al(Fe,Mn)Si particles. AlMg0.5Si0.4 in the artificially aged (T6) condition exhibited a coating morphology similar to AA6060-T6, while CCC formation on homogenised AlMg0.5Si0.4 was characterised by growth of localised oxide particles and filaments, resulting in poor coverage. These observations indicated that precipitation of Mg₂Si particles due to heat treatment promoted nucleation of the CCC. Chromate treatment caused a significant reduction of cathodic activity on AA6060 during subsequent polarisation in chloride solution. This was attributed to rapid formation of a thin chromium oxide film on the γ -Al(Fe,Mn)Si particles during the chromate treatment, resulting in significant cathodic passivation of the phase. Inhibition of the oxygen reduction reaction at cathodic inter-metallic particles is suggested as an important factor contributing to the high performance of chromate pre-treatments on aluminium.

INTRODUCTION

Chromate conversion coatings (CCC) on aluminium effectively protect against localised corrosion and promote excellent adhesion to paints and adhesives. Due to health and environmental considerations recent legislation imposes strong limitations in future use of chromates, *e.g.* in the automotive industry. A number of alternatives have been developed in recent years. However, none of these seem to match the performance and versatility of the chromate based processes. Fundamental knowledge of how the CCCs are formed and work may assist in developing more environmentally friendly pre-treatments for different applications.

The performance of the CCCs has been attributed to several factors, *e.g.*, providing barrier protection of the aluminium matrix due to their hydrophobic character and stability over a wide pH range [1]. In addition, the coatings appear to be self-healing due to storage and release of Cr^{VI} species that diffuse to the defect and react with the bare aluminium to form a hydrated Cr^{III} oxide which prevents pit initiation [1-4].

Formation of a CCC on aluminium requires presence of fluoride to thin the oxide on the surface [5], allowing the charge transfer reactions to proceed. Anodic dissolution of aluminium and reduction of soluble chromate to insoluble hydrated chromium oxide can then take place according to the reactions



Chromate is incorporated into the hydrated Cr^{III} oxide forming covalent Cr^{VI}-O-Cr^{III} linkages and resulting in a yellow Cr^{III}-Cr^{VI} mixed oxide [3,6].

In order to promote coating growth, K₃Fe(CN)₆ is often added as an accelerator. Recent research indicates that both Fe(CN)₆³⁻ (ferricyanide) and Fe(CN)₆⁴⁻ (ferrocyanide) become incorporated in the CCC. The Fe^{III}/Fe^{II} couple is believed to act as a catalyst whereby Fe^{III} is reduced to Fe^{II} by oxidation of Al. Fe^{II} is then oxidised back to Fe^{III} by reduction of the chromate [6].

The CCCs are largely amorphous, with composition and structure affected by the preceding chemical treatment and composition of the conversion bath [5,7,8]. The heterogeneous microstructure of aluminium alloys is another

factor that complicates the understanding of coating formation and growth. In recent studies the influence of alloy metallurgy in the formation of CCCs on aluminium has been addressed, particularly for the high-strength AA2024-T3 alloy [9-13]. It appears that coating nucleation and growth on AA2024-T3 is influenced strongly by the size, shape and composition of the intermetallic particles present as well as the composition of the neighbouring matrix region. In general, it is observed that the final coating thickness on Cu- and Fe containing particles is significantly thinner than on the aluminium matrix [6,11,13]. However, initial stages of CCC growth on a clean and fresh AA2024-T3 surface prepared by use of an ultramicrotome, were shown to take place at coarse $Al_6(Cu,Fe,Mn)$ particles and over an outer lying matrix region surrounding the particles [12]. Coating growth was supported by anodic dissolution of aluminium from a copper depleted matrix zone immediately adjacent to the particles.

The imperfections in the CCCs caused by the presence of various intermetallic phases in the surface are expected to reduce the corrosion protection afforded by these coatings [6,14]. Nevertheless, the CCC films have been found to significantly reduce the activity of both cathodic and anodic sites on the alloy surface. The inhibition of the oxygen reduction reaction at cathodic intermetallic particles appears to be an important part of the corrosion inhibition mechanism of chromate conversion coatings [3,15].

The purpose of the present study is to investigate the role of microstructure in the formation of a chromate conversion coating on extruded AA6060 aluminium. This alloy is commonly used in automotive and architectural applications due to a favourable combination of extrudability, mechanical strength and corrosion resistance. The surfaces were given a conventional surface treatment, involving alkaline etching and deoxidation prior to treatment in a commercial chromate solution (Alodine C6100). Specifically, the influence of Fe impurities in the alloy, present in the form of $-Al(Fe,Mn)Si$ particles was examined. In addition, the effect of Mg_2Si phase precipitation was studied by comparing the morphology of coatings formed on solution heat-treated and artificially aged substrates. Field emission SEM, TEM and AES measurements were used to characterise the conversion coatings. Potentiodynamic polarisation experiments in aerated 0.1 M NaCl solution were also conducted to assess the reduction in cathodic activity on the AA6060 surface as a result of chromate treatment.

EXPERIMENTAL

Materials

The test material was commercially produced AA6060-T6 extrusions, 2 x 110 mm² in cross-section. At the exit from the die the profiles were air cooled from 520°C to below 200°C in less than 4 min. Ageing to T6 temper was achieved by heat treatment at 195°C for 3.25 h. A ternary AlMg0.5Si0.4 alloy, with Mg and Si concentrations close to the AA6060 alloy, was made from super purity aluminium and pure alloying elements. The alloy was cast into extrusion billets about 100 mm in diameter. After solidification the billets were homogenised at 575°C for 4 h, followed by water quenching to prevent precipitation of Mg₂Si phase. The billets were then machined to a diameter of 95 mm and preheated to 470°C before direct extrusion to profiles with a cross-sectional area of 3.2 x 60 mm². The profiles were water quenched immediately after the exit from the die to keep the Mg and Si in solid solution. Some of the specimens were artificially aged to T6 temper by heat treatment at 195°C for 3.25 h.

Large γ -Al(Fe,Mn)Si crystals were synthetically produced by controlled solidification of melts made from high purity components. An aluminium melt containing 7.5% Si, 3.0% Fe and < 0.2% Mn was heated to 800°C in an alumina crucible under argon atmosphere, and the melt was stirred with a graphite rod to ensure complete dissolution. The melt was solidified and then reheated to 750°C in argon atmosphere, cooled to 710°C and kept at this temperature for one hour before cooling to 630°C over a period of 20 h (4°C/h). The melt was maintained at this temperature for 30 h to promote further growth of the intermetallic particles formed, followed by rapid cooling to room temperature.

Quantitative electron probe microanalysis showed that the laboratory made γ -Al(Fe,Mn)Si particles were homogeneous. The composition corresponded with the predominant type of Fe-rich particles expected to be present in AA6060 [16]. The chemical composition of the materials is given in Table 1. Working electrodes for electrochemical characterisation of the γ -Al(Fe,Mn)Si particles were prepared according to a method described elsewhere [17]. The electrode area was determined by image analysis.

Table 1. Composition of materials (wt%, bal. Al).

Material	Si	Fe	Mg	Mn	Cu	Zn	Ti	Cr	Zr
AA6060	0.43	0.18	0.51	0.020	0.0022	0.0123	0.0097	0.0017	0.0013
AlMg0.5Si0.4	0.38	<0.001	0.47	0.001	0.0012	0.0015	0.0005	0.0009	0.0002
-Al(Fe,Mn)Si	9.2	33.1	-	0.13	-	-	-	-	-

Chromating procedure

The following procedure was used to produce the chromate conversion layers on AA6060 and the ternary model alloy:

1. Degrease in acetone
2. Alkaline etch in 100g/l NaOH solution, 60°C, 50 s
3. Rinse with tap water
4. Deoxidise in fluoride/sulphuric/phosphoric acid based solution (4% Alfideox 73, 25°C, 1 min)
5. Rinse with tap and distilled water
6. Chromate treatment in 15 ml/l Alodine C6100, pH 2, 25°C, 10-180 s
7. Rinse with tap and distilled water
8. Dry in hot air stream

The alkaline etch resulted in about 5-6 μm of metal removed from the surface of AA6060, while 2-3 μm was removed from the surface of the ternary AlMg0.5Si0.4 alloy under similar conditions. A slight etching of the AA6060 surface (about 0.1 μm) was observed due to the subsequent deoxidation. Distilled water was used to prepare all the solutions.

Synthetically prepared -Al(Fe,Mn)Si phase electrodes were also chromated. In this case, the exposed particles, embedded in an epoxy resin [17], were gently wet ground on grit 2400 SiC paper instead of etching in the hot NaOH solution to avoid cracking at the particle-epoxy interface. Subsequent preparation of the -Al(Fe,Mn)Si phase electrodes was carried out as described above in steps 3 - 8.

Electrochemical measurements

The electrochemical cell consisted of a 1 litre PVC beaker with the electrolytes (Alodine C6100 and 0.1 M NaCl solution, respectively) open to ambient

laboratory air. Temperature was maintained at $25 \pm 1^\circ\text{C}$ in all experiments, and a graded mechanical stirrer was used to keep a constant agitation. The saturated calomel electrode (SCE) was used as reference in all experiments. Measurements were made by use of a Gill AC potentiostat connected to a PC with software from ACM Instruments. AA6060 and AlMg0.5Si0.4 alloy specimens were cut to a size of about $20 \times 20 \text{ mm}^2$, etched and deoxidised as described above and then mounted in a special PTFE specimen holder revealing an exposed circular area of 1.33 cm^2 . The area of $\gamma\text{-Al(Fe,Mn)Si}$ phase working electrodes was typically about 1 mm^2 .

Corrosion potentials of the test materials during chromating in 15 ml/l Alodine C6100 solution were recorded as a function of time up to 3 min. Potentiodynamic polarisation of chromated and non-chromated test materials were conducted in an 0.1 M NaCl solution made from reagent grade chemicals and distilled water. The potential sweeps were started immediately after exposure to the solution at -1150 mV and were terminated at -250 mV . The sweep rate was 30 mV/min . The reproducibility of the polarisation curves was generally very good as long as identical stirring conditions were maintained.

Surface characterisation

The morphology of the conversion coatings were studied in a field emission SEM (Hitachi S4300 SE) with X-ray EDS capability. TEM characterisation was carried out in cross-section geometry on ion etched thin foil specimens on a Phillips CM30 equipped with an X-ray EDS analytical system. Auger electron spectroscopy (AES) was performed on a Thermo VG Scientific Microlab 350 instrument. The spectra were acquired at an accelerating voltage of 10 keV and a primary electron beam current of 13 nA .

RESULTS

Microstructure of the test materials

Light microscopy of polished and anodised specimens showed that the AA6060 and AlMg0.5Si0.4 alloys both exhibited fully recrystallised microstructures (Figure 1 a, c). However, AA6060 had a significantly smaller grain size than AlMg0.5Si0.4. Moreover, the presence of 0.18% Fe in AA6060 caused formation of $\gamma\text{-Al(Fe,Mn)Si}$ particles, seen as the bright phase in

3. Formation and characterisation of a chromate conversion coating on AA6060 aluminium

Figure 1 b. This phase was virtually absent in AlMg0.5Si0.4 (Figure 1 d) due to its very low Fe concentration.

The hardness of AA6060 and as extruded AlMg0.5Si0.4 was determined to be 72 HV (Hardness Vickers, 10 N load) and 55 HV, respectively. By artificial ageing of the as extruded AlMg0.5Si0.4 alloy, the hardness increased to 76 HV due to precipitation of Mg₂Si phase particles [16]. The higher quench rate after extrusion of the AlMg0.5Si0.4 alloy probably explains why the hardness exceeded that of AA6060.

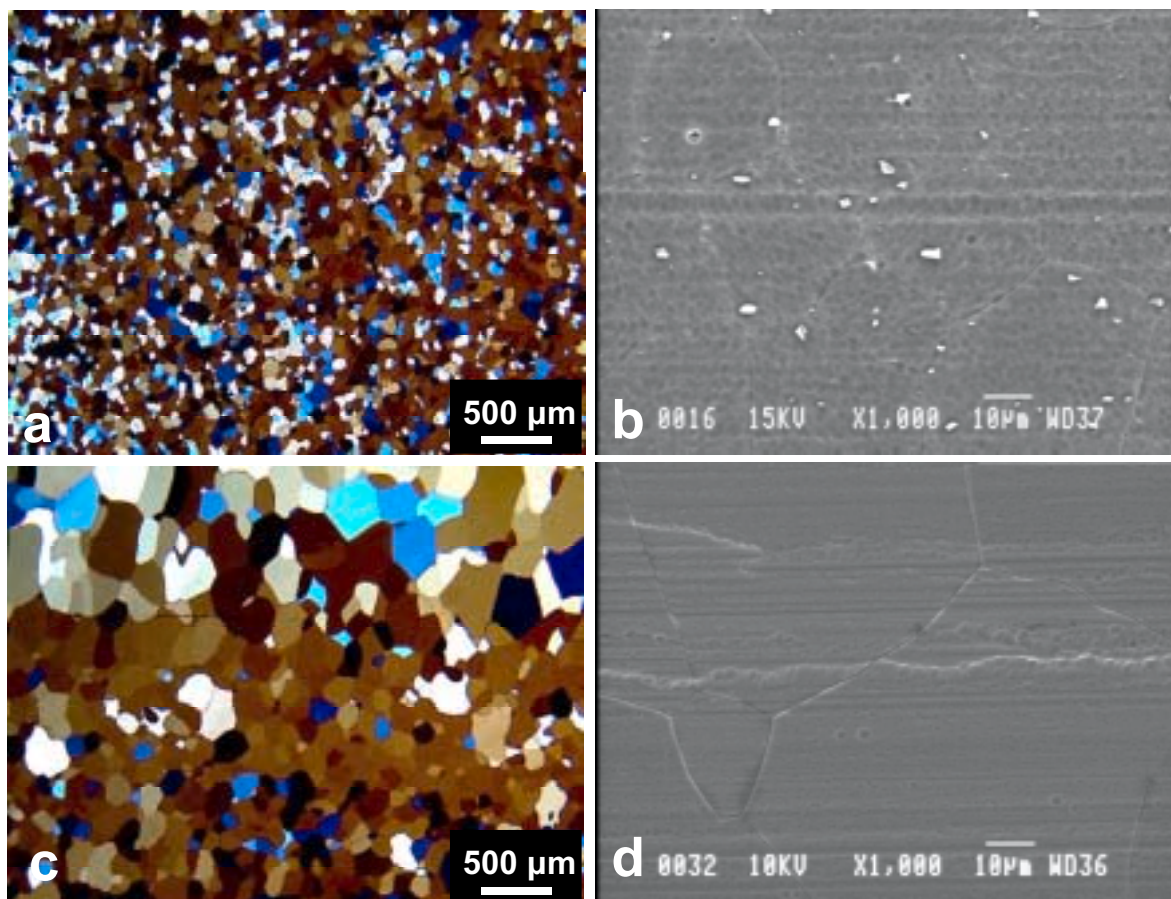


Figure 1. Microstructure of AA6060 (a, b) and ternary AlMg0.5Si0.4 alloy (c, d) in plan view. Light microscopy images (a, c) show that AA6060 exhibits a smaller grain size than the AlMg0.5Si0.4 alloy. SEM image of AA6060 (b) shows the distribution of bright -Al(Fe,Mn)Si phase particles on the etched and deoxidised surface.

Electrochemical behaviour during CCC formation

Figure 2 shows the corrosion potential of the test materials as a function of time during chromating. The α -Al(Fe,Mn)Si phase electrode exhibited a fairly constant and reproducible potential of about -280 mV during immersion in the chromate solution. AA6060 and as extruded AlMg0.5Si0.4 both showed initial potentials of about -620 mV, increasing to a stable value of about -600 mV after 20 - 30 s of immersion, *i.e.* similar to the open circuit potentials typically observed during chromating of aluminium [10,18-20]. While the AlMg0.5Si0.4 alloy showed a fairly stable potential during the 3 min immersion period, the potential on AA6060 was characterised by oscillations around the “steady-state” potential. Occurrence of similar potential oscillations during chromate treatment of an AA6063 alloy has been reported previously [20].

Potentiostatic polarisation of the α -Al(Fe,Mn)Si phase electrodes at -600 mV, corresponding to the potential exhibited by the AA6060 alloy during chromating, resulted in a nearly constant cathodic current density of about 0.5 - 1 mA/cm² (data not shown). Thus, a certain cathodic activity on the α -Al(Fe,Mn)Si phase would be expected during the entire time of immersion in the chromate solution.

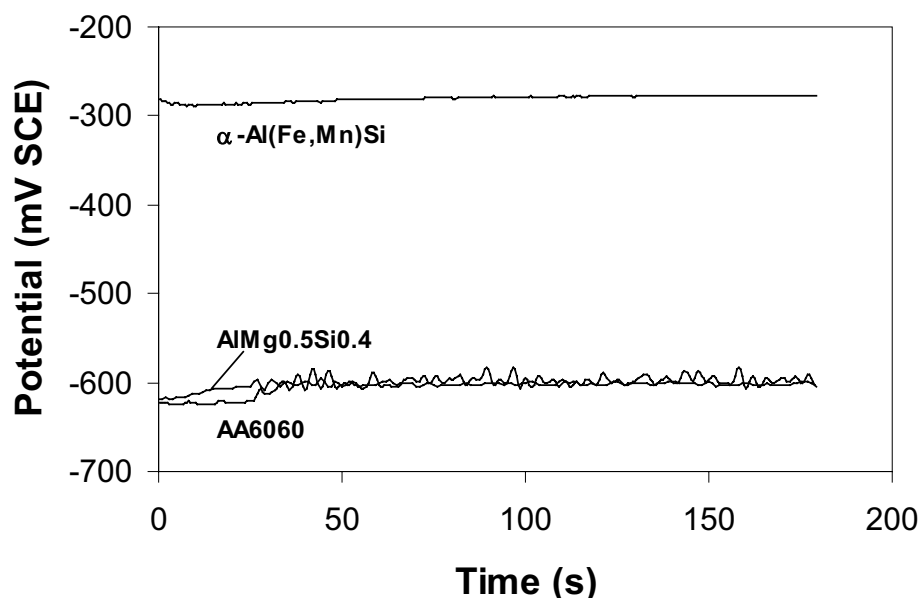


Figure 2. Corrosion potential of AA6060, as extruded AlMg0.5Si0.4 and α -Al(Fe,Mn)Si phase during chromate conversion coating.

Surface characterisation of AA6060

AA6060 specimens chromated for 10 s, 30 s and 3 min were studied in field emission SEM in order to have an impression of the CCC growth as a function of time. Typical examples of the morphology of the coating are shown in Figure 3. Before chromate treatment, the etched and deoxidised surface (Figure 3 a) exhibited a scalloped topography, formed during the alkaline etching step. The sub-micron size crystallographic pits at the grain boundaries were formed during deoxidation.

After 10 s of immersion in the conversion solution nucleation of the CCC was visible and small pits appeared over the whole surface (Figure 3 b). Preferential nucleation of the CCC occurred both at pre-existing metal ridges and along certain features within the grain bodies, corresponding to the bright areas in Figure 3 c. A number of spherical shaped oxide particles of the order 50 nm in diameter were observed in the intervening areas. Also after 30 s of immersion the influence of substrate microstructure and topography on the CCC morphology was seen, as shown in Figure 3 d. The coating exhibited a porous morphology with incomplete coverage of the surface, particularly at the grain boundaries. Nucleation of the conversion coating did not seem to occur at the grain boundaries. However, bridging of the conversion coating across the grain boundaries took place at some locations during coating growth (Figure 3 d).

The CCC obtained after 3 min of immersion, shown in Figure 3 e, also had a porous appearance and incomplete coverage of the grain boundaries. The grain boundaries thus acted as anodic areas supporting CCC deposition on the grain bodies according to the reactions (1) and (2), respectively. Dissolution of aluminium during coating growth probably also occurred locally at defects or pores in the conversion coating covering the aluminium matrix. Film formation on the -Al(Fe,Mn)Si particles present on the AA6060 surface was very limited, and the particles appeared to be more or less unaffected by the chromate treatment when observed in plan view in the SEM (Figure 3 f).

3. Formation and characterisation of a chromate conversion coating on AA6060 aluminium

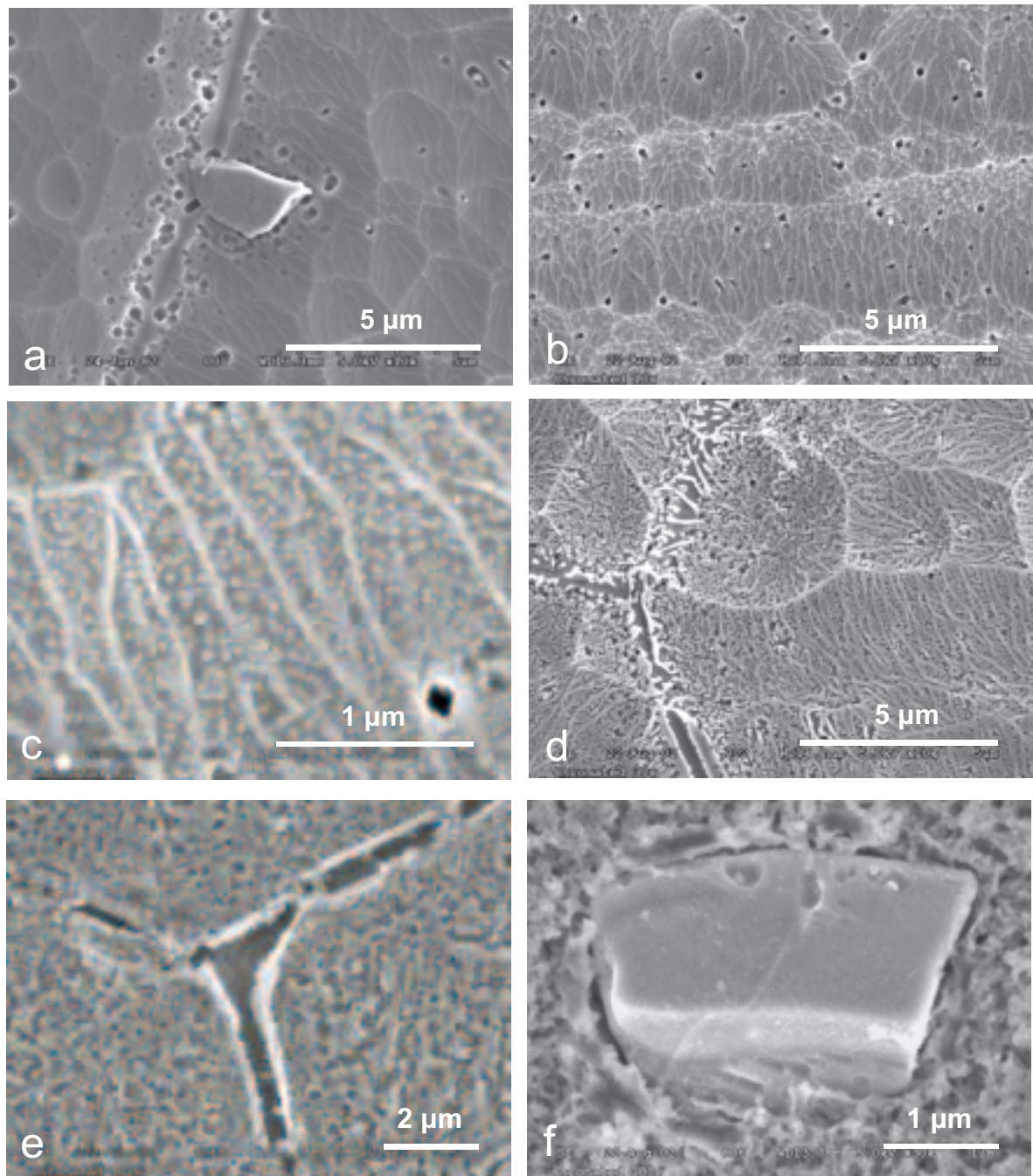


Figure 3. SEM images of AA6060 surface before chromating (a) and after immersion in chromating solution for 10 s (b, c), 30 s (d) and 3 min (e, f). The chromate conversion coating is characterised by a porous morphology and incomplete coverage at grain boundaries (d, e). Film formed on the -Al(Fe,Mn)Si particles after chromating (f) is too thin to be seen in a plan view SEM image.

3. Formation and characterisation of a chromate conversion coating on AA6060 aluminium

Closer examination of an equivalent surface in TEM revealed more information about the CCC formed after 3 min of immersion. The cross-section in Figure 4 a shows that there were indeed a number of defects in the conversion coating, extending down to the aluminium substrate. The thickness of the CCC on the aluminium matrix was typically 150-200 nm. Figure 4 b shows an -Al(Fe,Mn)Si particle standing in relief on the aluminium matrix as a result of its lower etch rate during alkaline etching before the chromate treatment. A thin film with an estimated thickness of about 40 nm was present on the particle. However, the composition of the film could not be determined by X-ray EDS analysis as reduction of the spot size to a diameter of about 40 nm dramatically reduced the intensity of emitted X-rays.

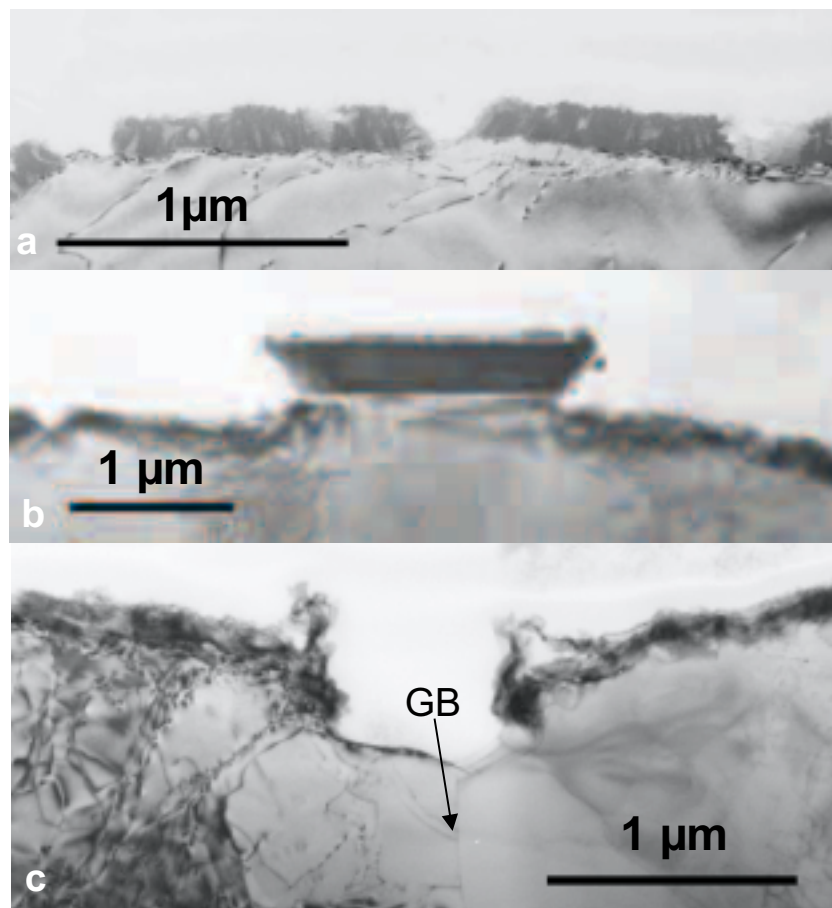


Figure 4. TEM cross-sections of AA6060 specimen after immersion in chromating solution for 3 min, showing a) incomplete coating coverage on the aluminium matrix, b) presence of a very thin CCC on intermetallic particle and c) (b) and apparent absence of a CCC at grain boundary zone.

Furthermore, the absence of a CCC at the grain boundaries was confirmed (Figure 4 c). The depression of the surface in the grain boundary (GB) zone indicated that preferential metal dissolution occurred in this location, not only during coating growth, but also during alkaline etching before the chromate treatment, as indicated by Figure 3 a.

AES survey spectra were acquired from various points and small areas (less than $5 \mu\text{m}^2$) on an AA6060 surface chromated for 30 s. Cr and O were detected at every location, also when measurements were restricted to the surface of the -Al(Fe,Mn)Si particles (Figure 5 a, b). Al was detected in small quantities on the surface of all the analysed particles, while F and Fe were observed on some of the particles. Analysis of area 2 in Figure 5 a, representing the CCC covered aluminium matrix, also gave a weak Al signal. This was attributed to a certain porosity of the CCC, as no Al signal was observed by point analysis of the coating itself (spectrum not shown here). The relatively higher Al and F levels detected on the surface of intermetallic particles are in line with recent work investigating the deposition of CCCs on Fe- and Cu based intermetallic phases [13]. Moreover, a fairly strong C peak was generally observed due to adventitious surface carbon, which is almost always observed in AES or XPS analyses [13]. Some of the intermetallic particles were particularly carbonaceous, but the exact source of the carbon could not be reliably determined.

Higher energy resolution spectra acquired from an -Al(Fe,Mn)Si particle and the CCC covered aluminium matrix (shown in Figure 5 c) were recorded across the overlapping regions of the Cr LMM and O KLL peaks. The spectra are shown in integrated form in Figure 5 d together with the spectrum of a Cr metal reference. The shapes of the spectra obtained from both areas 1 and 2 were significantly different from the envelope of the Cr metal reference spectrum. The peak at 570 eV appeared to be split into two components, indicative of two chromium states in the CCC. Earlier work [1,2,4,21] has shown that Cr^{VI} constitutes typically 20-30% of the total Cr in a CCC, whereas a significantly lower Cr^{VI} to Cr^{III} ratio was recently reported for thin conversion layers formed on intermetallic Al_2Cu analogues [22]. However, a closer determination of the chemical state of Cr in the conversion coatings formed on the particles and the matrix of AA6060 was beyond the scope of the present work.

3. Formation and characterisation of a chromate conversion coating on AA6060 aluminium

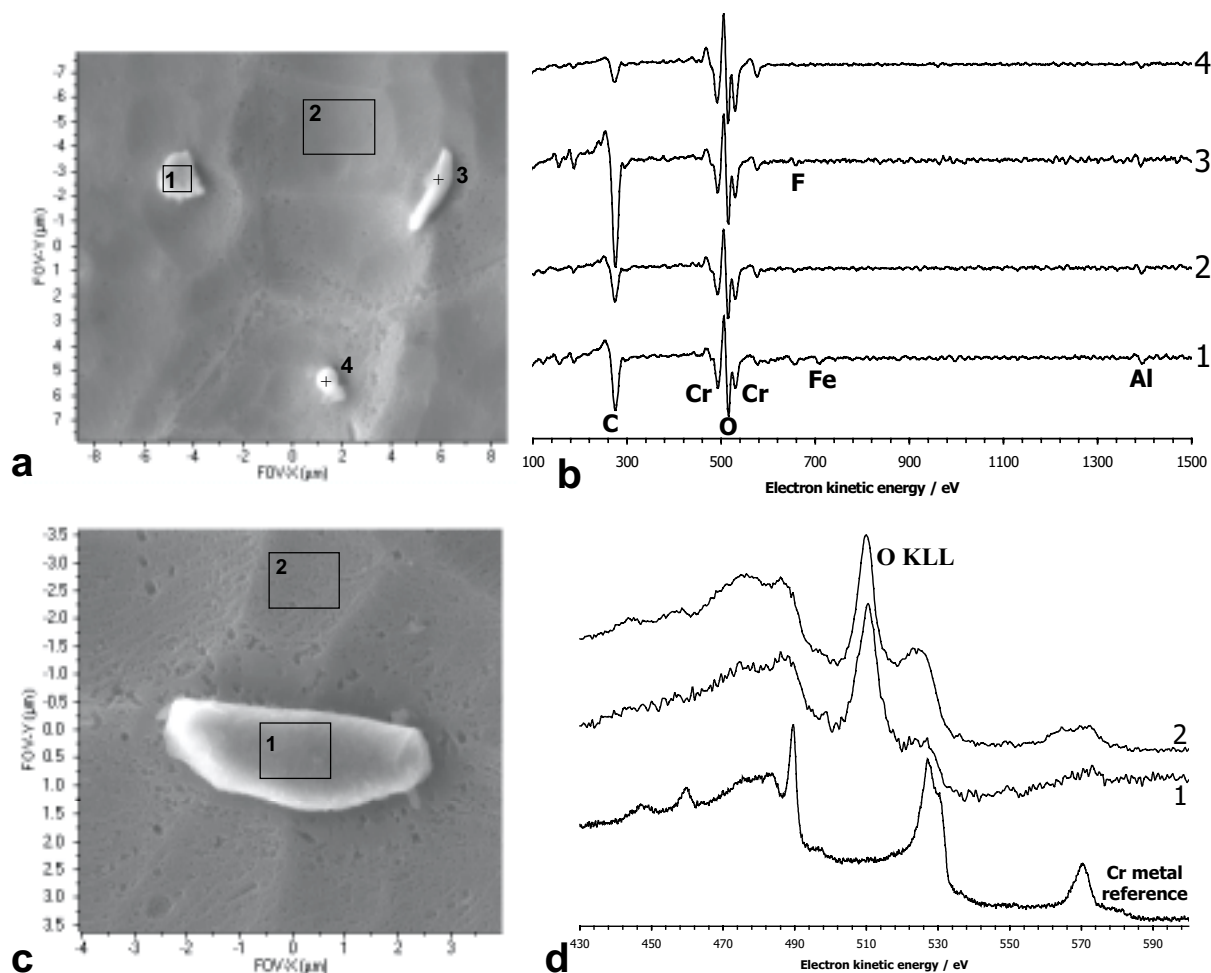


Figure 5. a) SEM image of AA6060 surface after 30 s of immersion in chromating solution. b) Differentiated Auger survey spectra acquired from intermetallic particles (area 1 and points 3 and 4) and aluminium matrix (area 2) marked on SEM image in a). c) SEM image of another location on the same sample and d) High energy resolution spectra of the Cr LMM and O KLL region, acquired from particle (area 1) and CCC covered aluminium matrix (area 2) marked on SEM image in c) and a Cr metal reference.

Growth of CCC on AlMg0.5Si0.4

To determine whether the discontinuities in the CCCs at grain boundaries were promoted by artificial ageing, AlMg0.5Si0.4 specimens in both as extruded (Mg and Si in solid solution) and artificially aged tempers were chromated for up to 3 min and subsequently examined in SEM. Examples of surface morphologies on the artificially aged material are shown in Figure 6. After 30 s of immersion in the conversion bath (Figure 6 a) a nearly continuous CCC was formed. Close inspection at high magnification indicated that a zone along the grain boundaries, approximately 150 nm in width, remained uncoated. Continued immersion in the chromate bath for up to 3 min caused the CCC to grow in thickness, resulting in a weight gain of about 2 mg/dm². The morphology of the CCC (Figure 6 b) closely resembled the porous appearance of AA6060 after equivalent treatment, see Figure 3 e. Moreover, the width of the non-coated zone along the grain boundaries increased to about 500 nm after 3 min of immersion, similar to what was observed for AA6060.

SEM images of the as extruded AlMg0.5Si0.4 alloy, chromated for 30 s and 3 min and shown at the same magnification as in Figure 6, are presented in Figure 7. The “conversion coating” in this case took the form of individual, branched filaments growing in a direction controlled by the crystallographic orientation of the grains, since all the filaments tended to grow in the same direction within one single grain. There was also an increased tendency to nucleation of these chromium oxide filaments along certain topographical features parallel with the extrusion direction (horizontal in Figure 7 a). Relatively few new filaments were nucleated in the time interval from 30 s to 3 min, but the initially formed filaments clearly became thicker during this period. Contrary to the artificially aged material, the grain boundaries were coated, while a considerable area fraction of the total surface remained non-coated even after 3 min of immersion. However, the coating weights (determined by stripping of the CCCs in concentrated nitric acid for 15 min) on as extruded and aged materials were similar, about 4 mg/dm².

The large difference in the morphology and thickness of the conversion coatings formed for the two tempers was also reflected in the visual appearance on a macroscopic scale. While samples of the artificially aged material exhibited a uniform golden brown colour similar to that obtained for AA6060, the as extruded AlMg0.5Si0.4 showed a non-uniform appearance with shades that varied from nearly colourless to golden brown.

3. Formation and characterisation of a chromate conversion coating on AA6060 aluminium

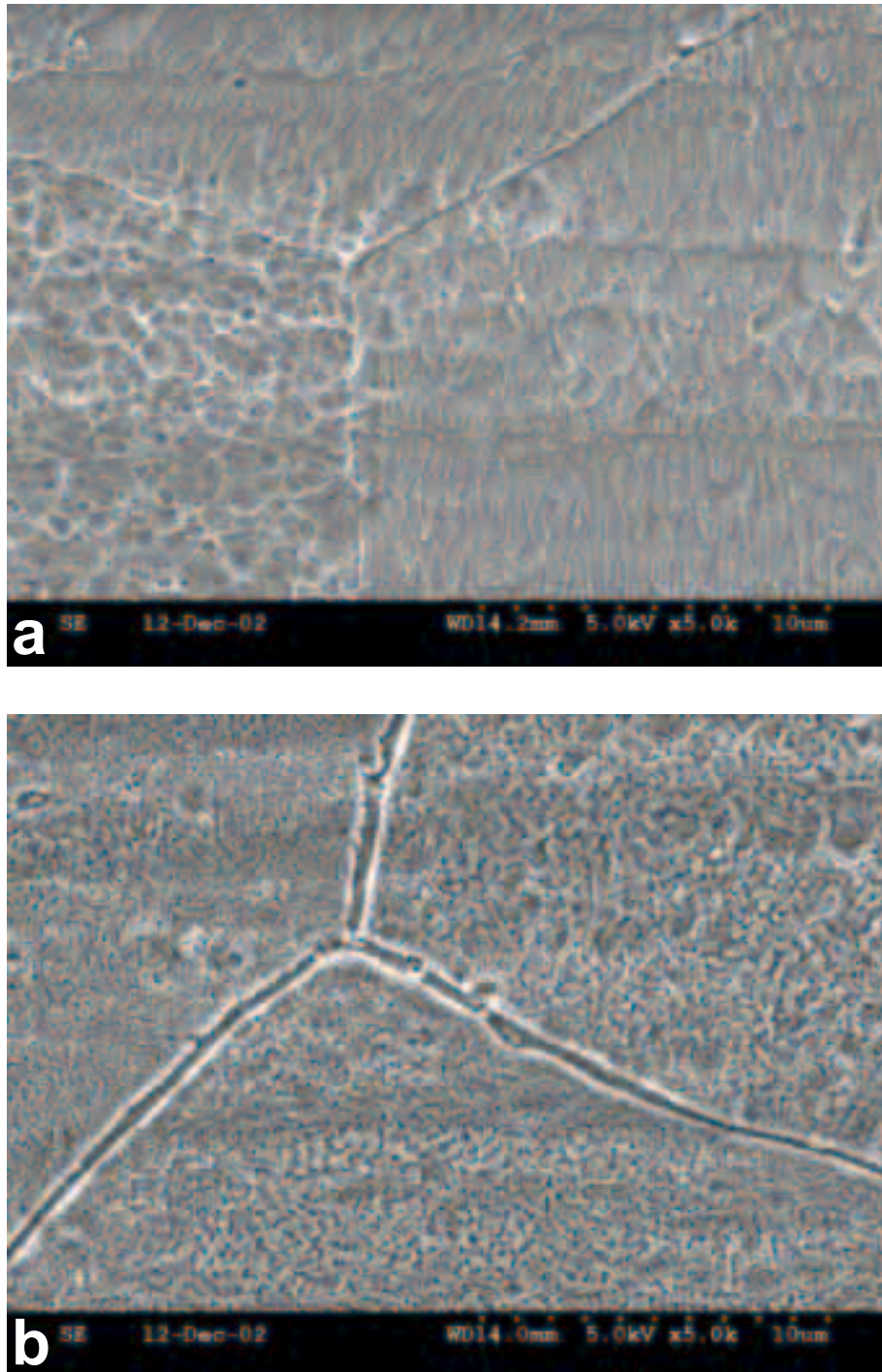


Figure 6. SEM images of artificially aged AlMg_{0.5}Si_{0.4} alloy after immersion in chromating solution for a) 30 s and b) 3 min.

3. Formation and characterisation of a chromate conversion coating on AA6060 aluminium

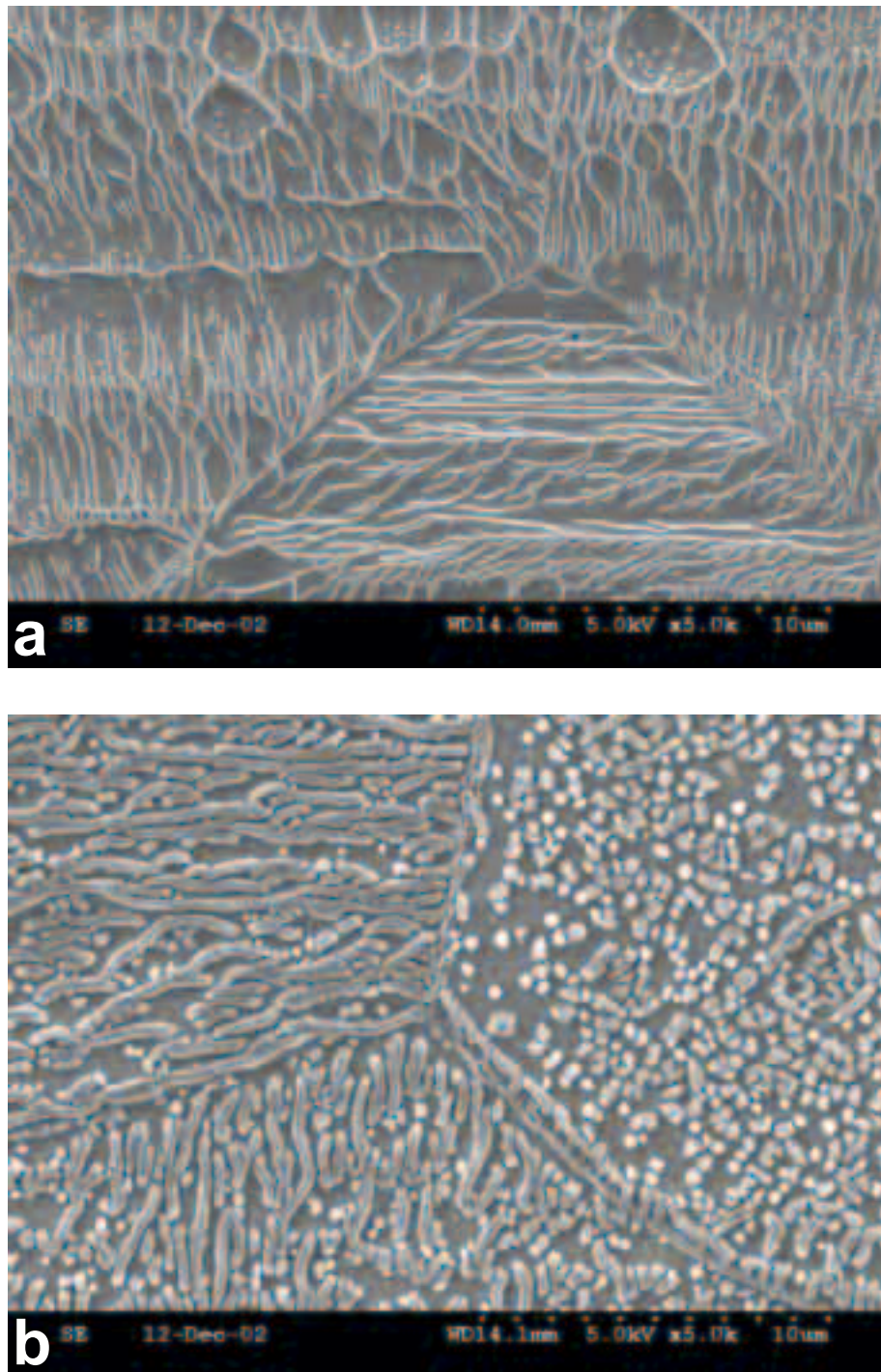


Figure 7. SEM images of as extruded AlMg_{0.5}Si_{0.4} alloy after immersion in chromating solution for a) 30 s and b) 3 min.

Electrochemical behaviour in chloride solution

Polarisation curves obtained for uncoated AlMg0.5Si0.4 and AA6060 in 0.1 M NaCl solution are shown in Figure 8. The cathodic curves were steep and typical of conditions dominated by oxygen reduction reaction. Significantly lower cathodic current densities were observed for the AlMg0.5Si0.4 variants relative to AA6060. Evidently, the cathodic behaviour of AA6060 was largely controlled by the γ -Al(Fe,Mn)Si particles present on the surface of this material. Comparison of the two AlMg0.5Si0.4 variants further showed that heat treatment by artificial ageing to peak strength had a significant, but much smaller effect than the γ -Al(Fe,Mn)Si particles on cathodic activity. The slight ennoblement observed by heat treatment was probably related to the reduction of Mg in solid solution with the aluminium matrix as a result of Mg₂Si precipitation.

AlMg0.5Si0.4 and AA6060 also showed differences in anodic behaviour. The former material exhibited a sudden increase in the anodic current at potentials around -550 mV, while the current density of AA6060 increased steadily by anodic polarisation from the corrosion potential at about -670 mV. Hence, presence of γ -Al(Fe,Mn)Si particles seemed to lower the effective pitting potential in chloride solution measured at a sweep rate of 30 mV/min.

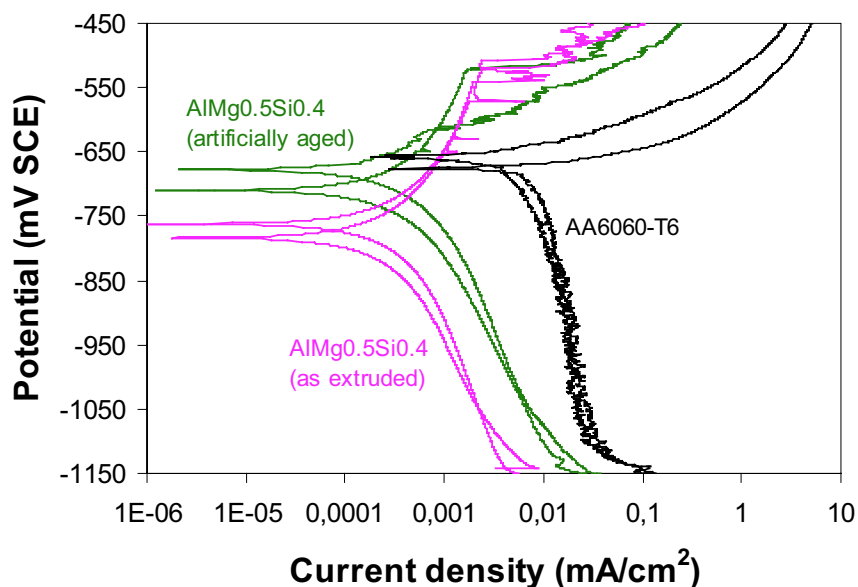


Figure 8. Duplicate polarisation curves for NaOH etched and deoxidised AlMg0.5Si0.4 and AA6060 alloys in 0.1 M NaCl solution.

Figure 9 shows potentiodynamic polarisation curves for chromated (treatment time 10 s and 3 min) and etched AA6060. The chromated surfaces exhibited significantly lower cathodic current densities and a shift of the corrosion potential in the negative direction relative to the etched surface. In terms of electrochemical behaviour, the surfaces chromated for 10 s and 3 min were remarkably similar despite the large difference in total amount of coating deposited. At a potential of about -670 mV the anodic current density on chromated surfaces increased rapidly and followed the curve obtained for the etched and deoxidised surface.

Polarisation curves for deoxidised and chromated α -Al(Fe,Mn)Si phase electrodes showed that the cathodic activity was reduced significantly by the chromate treatment (Figure 10). As observed for the AA6060 alloy, the electrochemical behaviour of the α -Al(Fe,Mn)Si phase in chloride solution was practically independent of the pre-immersion time in the chromate solution. Furthermore, no colour change of the α -Al(Fe,Mn)Si phase was observed as a result of chromate treatment. These results indicated that a very thin and passivating film was immediately formed on the α -Al(Fe,Mn)Si phase by exposure to the chromate solution. Galvanic coupling of the α -Al(Fe,Mn)Si phase electrode (~ 1 mm²) to AlMg0.5Si0.4 (133 mm²) during chromate treatment, simulating the microgalvanic effect between the particles and matrix on AA6060, gave surfaces which exhibited electrochemical behaviour similar to the results shown in Figure 10.

Polarisation curves of the chromated AA6060 surfaces in Figure 8 were recorded about 2 h after immersion in the chromate solution. Polarisation curves for samples stored for 18 h and 90 h in laboratory air (Figure 11) indicated that the cathodic current density remained unaffected by ageing, while the corrosion potential moved in positive direction towards the pitting potential of the bare surface. Again, the difference in the behaviour of specimens treated for 10 s and 3 min was negligible, apart from a small reduction in the anodic current for the samples treated for 3 min. The relatively thick CCC on the samples treated for 3 min resulted in very localised pitting attacks by anodic polarisation, whereas samples chromated for 10 s and uncoated samples were locally etched over significantly larger surface areas.

3. Formation and characterisation of a chromate conversion coating on AA6060 aluminium

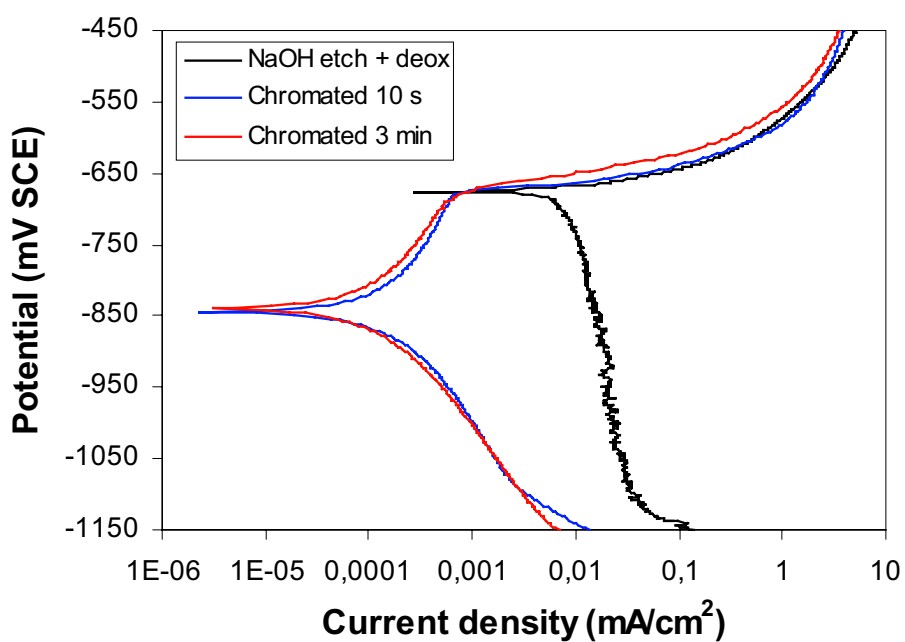


Figure 9. Polarisation curves for etched and chromated AA6060 in 0.1 M NaCl solution. Polarisation curves were recorded approximately 2 h after the chromating treatments.

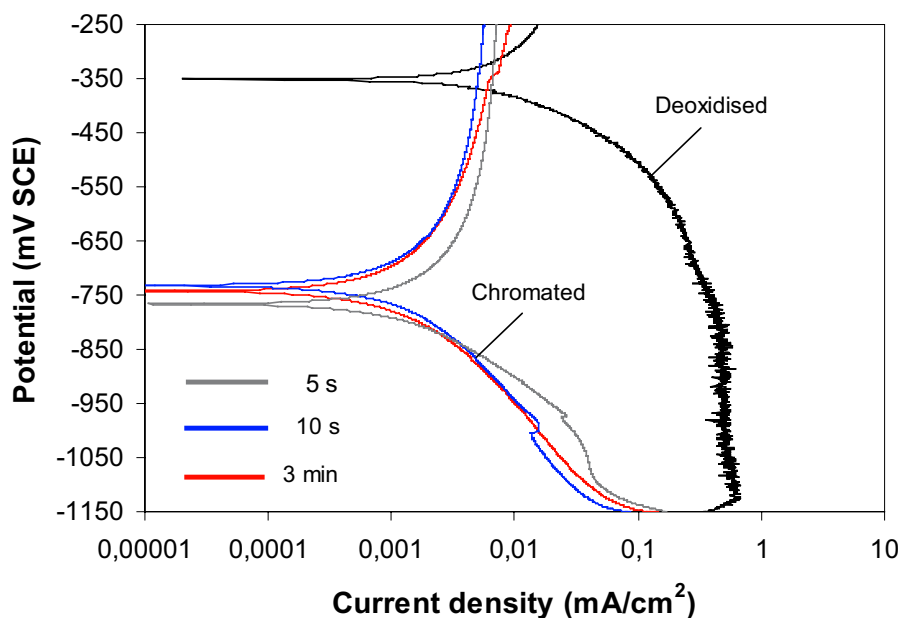


Figure 10. Polarisation curves for deoxidised and chromated γ -Al(Fe,Mn)Si phase electrodes in 0.1 M NaCl solution.

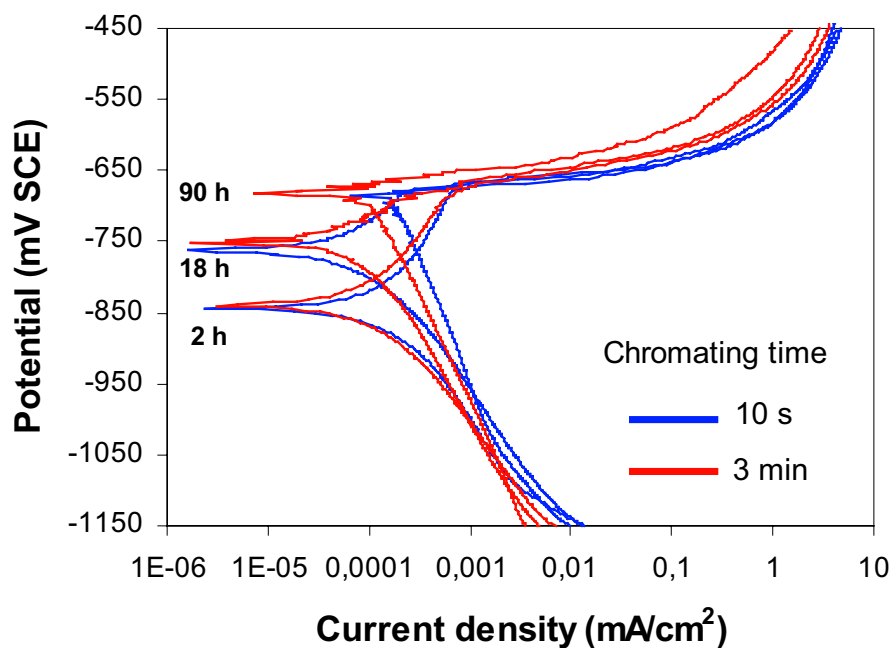


Figure 11. Polarisation curves for chromated AA6060 in 0.1 M NaCl solution, recorded after 2, 18 and 90 h of storage in laboratory air after chromating.

DISCUSSION

Morphology of the conversion coatings

Present observations indicated that the formation and growth of a chromate conversion coating on AA6060 does not take place uniformly over the alloy surface, but is strongly affected by the alloy microstructure. Specifically, the coating formed on the γ -Al(Fe,Mn)Si particles was much thinner than that formed over the aluminium matrix, in general agreement with earlier observations [6,11,13]. However, these particles are expected to become coated first by the reduction of chromate since these are cathodic with respect to the aluminium matrix (Figure 2). Previous work has shown that nucleation of a CCC on 99.99% Al occurred preferentially along grain or cellular boundaries associated with cathodic impurity segregation [9]. In a more recent study by Brown and Kobayashi [12] coating nucleation was observed to take place at cathodic $\text{Al}_6(\text{Cu,Fe,Mn})$ particles on AA2024-T3. Thus, it appears that rapid film formation can occur on the γ -Al(Fe,Mn)Si particles during early stages, while growth of this film must be relatively slow since the

thickness obtained after completed treatment is small compared to the overall CCC thickness.

On AA2024-T3, the inhibition of CCC growth on intermetallic phases was attributed to interactions between ferricyanide accelerators and the Cu containing intermetallics to form insoluble deposits, which limit the CCC formation [6,11]. This explanation is not directly applicable for the present results, since the substrate employed is Cu free and a molybdate-based accelerator is used instead of cyanide in the Alodine C6100 solution. However, AES analyses showing F and Al on the $-\text{Al}(\text{Fe},\text{Mn})\text{Si}$ particles resembled recent results obtained by Juffs and co-workers [13], who proposed that higher levels of fluoride and thin aluminium oxides detected on FeAl_3 phase particles indicated that areas of the surface oxide was continually undergoing dissolution. Simultaneous generation of aluminium oxide was thought to be enhanced by oxygen reduction reactions on the cathodic particles, which makes the surface conditions more alkaline and suitable for formation of hydrated aluminium oxides [13].

The striking difference in coating morphology between as extruded (homogenised) and artificially aged AlMg0.5Si0.4 substrates must somehow be related to the precipitation of a fine dispersion of Mg_2Si phases particles in the latter. Heat treatment makes the alloy more heterogeneous from an electrochemical point of view, as the Mg_2Si particles are electrochemically more active than the aluminium matrix [16] due to the relatively high Mg concentration. In the work by Brown and Kobayashi [12] CCC nucleation was observed not only at cathodic $\text{Al}_6(\text{Cu},\text{Fe},\text{Mn})$ particles, but also in association with S-phase Al_2CuMg particles exhibiting anodic activity relative to the surrounding matrix. Upon immersion in the coating bath, the S-phase particles underwent dissolution by selective dealloying of the Mg component. The anodic dissolution of the particles in turn supported the reduction of chromate to hydrated chromium oxide over the matrix region surrounding the particles. As the level of Cu enrichment was increased, the particles were transformed to effective cathodes for the reduction of chromate ions and hydrogen evolution, promoting local matrix dissolution [12].

A similar mechanism involving dealloying of Mg from Mg_2Si phase particles supporting chromate reduction and nucleation of a hydrated chromium oxide in their vicinity may well occur also during initial stages of CCC formation on AA6060-T6. However, Si enrichment caused by Mg dealloying would not be expected to result in the formation of effective cathodes. Anyway, the present and earlier results indicate that numerous particles in the surface, whether anodic or cathodic with respect to the surrounding matrix, may enhance the

nucleation and growth of a CCC on aluminium. The large number of Mg_2Si particles present on artificially aged $AlMg_{0.5}Si_{0.4}$ may therefore have promoted formation of a large number of chromium oxide nuclei that grew and rapidly merged to form a porous but reasonably homogeneous CCC. In contrast, the homogenised $AlMg_{0.5}Si_{0.4}$ material exhibited relatively few nucleation sites under similar chromating conditions. Film growth in this case occurred by growth of the chromium oxide nuclei, forming large particles and filaments and resulting in poor coating coverage (Figure 7).

The CCC morphologies observed presently are different from the typical “mud cracked” films often reported in the literature [23,24]. In addition to substrate microstructure, preceding chemical treatment and formulation of the conversion bath may significantly affect the coating structure. Even on 99.99% aluminium, formation of films exhibiting uniform thickness during growth [25] as well as precipitation of spherical particles, which merged and formed successive layers, were reported [19].

Exposure of bare aluminium and its oxidation in contact with the chromate bath appears to be necessary for coating growth to occur [5,25]. Present SEM and TEM observations indicated that the CCC on AA6060 exhibited numerous pores and cracks providing pathways from the bulk solution towards the aluminium substrate. In addition, grain boundaries appeared to be particularly active. Formation of precipitate free zones (PFZ) along the grain boundaries of artificially aged materials probably rendered CCC nucleation more difficult in these zones. Moreover, the increasing width of the uncoated zone at the grain boundaries with time (Figure 6) implied increased aluminium dissolution from these areas. As progressively larger areas of the surface were covered the total area available for aluminium dissolution was restricted. The grain boundaries apparently became preferred anodic sites during the late stages of coating growth. Similar behaviour was observed for artificially aged $AlMg_{0.5}Si_{0.4}$, while no preferential anodic activity was observed at the grain boundaries of the as extruded $AlMg_{0.5}Si_{0.4}$ alloy. The poor coating coverage of this material left abundant areas available for aluminium dissolution, supporting sustained coating growth.

Poor CCC coverage of the aluminium matrix does not necessarily imply a poor filiform corrosion (FFC) resistance of coated materials. Recent work [26] provided strong evidence that FFC is largely controlled by microgalvanic coupling between the aluminium matrix and nobler second phase particles. Thus, efficient inhibition of cathodic activity on intermetallic particles is probably much more important than complete coverage of the aluminum

matrix as far as FFC resistance is concerned. Since the AlMg0.5Si0.4 model alloy employed in this work is virtually free from cathodic phases, this material is expected to possess an inherently high resistance against FFC. Poor CCC coverage may, however, cause reduced adhesion to paints and adhesives because the aluminium oxide/polymer interface areas would exhibit a lower hydrolytic stability than the CCC/polymer interface. It has been reported [27] that paint adhesion increased continuously and rapidly when the coating weight of a chromate-phosphate conversion coating was increased from zero up to 10 mg/dm².

Behaviour of coated surfaces in chloride solution

Comparison of the polarisation curves obtained for AA6060 and AlMg0.5Si0.4 (Figure 8) indicates that the cathodic activity on AA6060 was largely determined by the intermetallic β -Al(Fe,Mn)Si particles. TEM and AES analyses showed that a very thin chromium oxide film was formed on these particles as a result of chromate treatment, accompanied by significantly reduced cathodic activity during subsequent polarisation in 0.1 M NaCl solution (Figures 9 and 10). Independence of treatment time (from 10 s to 3 min) on the cathodic behaviour of AA6060 and β -Al(Fe,Mn)Si phase electrodes indicated rapid film formation on the particles. Rapid passivation of intermetallic phases on AA2024-T3 was recently observed also as a result of addition of small concentrations of chromate to chloride solutions [1,28]. In general, chromate treatment appears to be particularly useful for Cu containing alloys, since passivation of both anodic and cathodic sites inhibits dealloying of the particles and consequently surface enrichment of Cu [28]. By analogy, chromates may inhibit Fe enrichment caused by dealloying of Al from AlFeMnSi phases [17].

According to Figure 9, the measured pitting potential of about -670 mV on AA6060 was not much affected by the presence of a CCC on its surface. A similar result was obtained for pure aluminium in 0.5 M NaCl solution [29], while presence of a CCC on AA2024-T3 caused only a small positive shift of the pitting potential in 3.5% NaCl solution [29]. Since coating breakdown and pitting are dominated by surface defects, pit initiation is enhanced by β -Al(Fe,Mn)Si particles in the surface, as illustrated by Figure 8. Removal of cathodic AlFeSi particles on AA1230 (used to clad AA2024-T3) by means of acid pickling before chromate treatment produced CCCs with greater uniformity and less defects [14].

Chromate conversion coatings are known to age during storage in air, which may lead to immobilisation of the Cr^{VI} , dehydration and possible structural changes in the coatings [4,22,30]. These phenomena may affect the electrochemistry of coated surfaces, as shown in Figure 11 by a shift of the corrosion potential in the positive direction with time. However, the cathodic currents measured on coated AA6060 surfaces remained low relative to the etched surface, which indicated that the cathodic inhibition provided by the CCC was not reduced significantly by ageing. Similar experiments [30] on AA2024-T3 showed a considerable increase in cathodic activity after storage of the coated surfaces in air for 165 h. This was attributed to development of flaws in the coating, revealing a Cu rich substrate. In conclusion, these results demonstrate that ageing of the CCCs is a factor that must be considered in electrochemical testing of chromate conversion coated surfaces.

High degree of micro-roughness of the CCCs was suggested [23] to cause efficient wetting and contact between the surface and an organic coating or adhesive. Indeed, an increased interfacial area implies that more interfacial bonds must be broken before loss of adhesion occurs. However, there are a number of other factors that influence the adhesion of organic coatings and adhesives to metal surfaces [31]. To produce durable bonds, the stability of the conversion coating and its ability to protect the substrate in wet and corrosive environments are essential factors. Testing of wet adhesion and resistance against filiform corrosion of painted surfaces and adhesive bonded joints is therefore required to assess the performance of CCCs and chromate-free replacements used in pre-treatment of aluminium.

CONCLUSIONS

- The chromate conversion coating formed on extruded AA6060-T6 was significantly affected by the microstructure of the substrate. The deposited chromium oxide was characterised by a porous morphology, with cracks extending down to the base metal. Poor coverage was particularly observed at the grain boundaries. The overall thickness of the CCC after 3 min of treatment was about 150-200 nm, while significantly thinner films were formed on the intermetallic $-\text{Al}(\text{Fe},\text{Mn})\text{Si}$ particles.
- An artificially aged AlMg0.5Si0.4 model alloy exhibited a coating morphology similar to AA6060-T6. However, on homogenised AlMg0.5Si0.4 material, formation of the CCC was characterised by nucleation and growth of oxide particles and filaments, resulting in a coarse structure and poor coverage. These observations indicated that the

precipitation of Mg₂Si particles due to heat treatment promoted nucleation of the CCC, giving a more homogeneous coating on a macroscopic scale.

- Chromate treatment, even for only 10 s, resulted in a significant reduction in the cathodic activity on AA6060 in 0.1 M NaCl solution. This was attributed to rapid formation of a thin oxide film on the -Al(Fe,Mn)Si particles during the chromate treatment. Effective suppression of the cathodic reactivity of intermetallic particles should be very beneficial to improve the filiform corrosion resistance of coated aluminium.

ACKNOWLEDGEMENTS

C. Simensen and S. O. Olsen, SINTEF Materials Technology and M. Raanes, Norwegian University of Science and Technology are acknowledged for the preparation and chemical analyses of -Al(Fe,Mn)Si crystals, respectively.

REFERENCES

1. M. Kendig, S. Jeanjaquet, R. Addison and J. Waldrop, *Surface and Coatings Technology*, **140**, 58 (2001).
2. M. W. Kendig, A. J. Davenport and H. S. Isaacs, *Corrosion Science*, **34**, 41 (1993).
3. G. S. Frankel and R. L. McCreery, *Interface*, **10**, (4), 34 (2001).
4. J. Zhao, L. Xia, A. Sehgal, D. Lu, R. L. McCreery and G. S. Frankel, *Surface and Coatings Technology*, **140**, 51 (2001).
5. M. F. Abd Rabbo, J. A. Richardson and G. C. Wood, *Corrosion Science*, **18**, 117 (1978).
6. W. R. McGovern, P. Schmutz, R. G. Buchheit and R. L. McCreery, *J. Electrochem. Soc.*, **147**, 4494-4501 (2000).
7. J. A. Treverton and N. C. Davies, *Metals technology*, Oct., 480 (1977).
8. H. A. Katzman, G. M. Malouf, R. Bauer and G. W. Stupian, *Applications of Surface Science*, **2**, 416 (1979).
9. G. M. Brown, K. Shimizu, K. Kobayashi, G. E. Thompson and G. C. Wood, *Corrosion Science*, **33**, 1371 (1992).
10. G. M. Brown, K. Shimizu, K. Kobayashi, G. E. Thompson and G. C. Wood, *Corrosion Science*, **34**, 1045 (1993).
11. P. L. Hagans and C. M. Haas, *Surface and Interface Analysis*, **21**, 65 (1994).
12. G. M. Brown and K. Kobayashi, *J. Electrochem. Soc.*, **148**, B457-B466 (2001).

3. Formation and characterisation of a chromate conversion coating on AA6060 aluminium

13. L. Juffs, A. E. Hughes, S. Furman and P. J. K. Paterson, *Corrosion Science*, **44**, 1755 (2002).
14. P. Campestrini, E. P. M. van Westing and J. H. W. de Wit, *Electrochimica Acta*, **46**, 2553 (2001).
15. G. O. Ilevbare and J. R. Scully, *J. Electrochem. Soc.*, **148**, B196-B207 (2001).
16. L. F. Mondolfo, *Aluminium Alloys: Structure and Properties*, Butterworths, London (1976).
17. K. Nisancioglu, *J. Electrochem. Soc.*, **137**, 69 (1990).
18. P. Campestrini, *Microstructure-related Quality of Conversion Coatings on Aluminium Alloys*, Ph.D. Thesis, Delft University of Technology, The Netherlands (2002).
19. D. J. Arrowsmith, J. K. Dennis and P. R. Sliwinski, *Trans. Inst. Met. Finish.*, **62**, 117 (1984).
20. A. Hovestad, Th. Zuidwijk, A. J. Bosch, E. P. M. Van Westing and G. M. Ferrari, *Proceedings of 2nd International Symposium on Aluminium Surface Science and Technology*, p. 187, Manchester, 21-25 May 2000.
21. L. Xia and R. L. McCreery, *J. Electrochem. Soc.*, **145**, 3083 (1998).
22. M. Jaime Vasquez, G. P. Halada and C. R. Clayton, *Electrochimica Acta*, **47**, 3105 (2002).
23. J. A. Treverton and M. P. Amor, *Journal of Materials Science*, **23**, 3706 (1988).
24. F. W. Lytle, R. B. Greigor, G. L. Bibbins, K. Y. Blohowiak, R. E. Smith and G. D. Tuss, *Corrosion Science*, **37**, 349 (1995).
25. R. C. Furneaux, G. E. Thompson and G. C. Wood, *Corrosion Science*, **19**, 63 (1979).
26. A. Afseth, J. H. Nordlien, G. M. Scamans and K. Nisancioglu, *Corros. Sci.*, **44**, 2491 (2002).
27. P. G. Sheasby and R. Pinner, in *The Surface Treatment and Finishing of Aluminium and Its Alloys*, 6th Ed., Vol. 1, ASM International, Metals Park, Ohio (2001).
28. A. Kolics, A. S. Besing and A. Wieckowski, *J. Electrochem. Soc.*, **148**, B322 (2001).
29. W. Zhang, B. Hurley and R. G. Buchheit, *J. Electrochem. Soc.*, **149**, B357 (2002).
30. A. E. Hughes, R. J. Taylor and B. R. W. Hinton, *Surface and Interface Analysis*, **25**, 223 (1997).
31. A. J. Kinloch, *Adhesion and Adhesives*, Chapman and Hall, London (1990).

4. Formation and characterisation of Ti-Zr based conversion layers on AA6060 aluminium

O. Lunder^{1,2}, C. Simensen¹, Y. Yu² and K. Nisancioglu²

¹ SINTEF Materials Technology, N-7465, Trondheim, Norway

² Norwegian University of Science and Technology, N-7491, Trondheim, Norway

ABSTRACT

Formation of a Ti-Zr based conversion layer on AA6060 aluminium has been studied electrochemically and by use of various surface analytical methods. Measurements show that the -Al(Fe,Mn)Si particles present in AA6060 are cathodic to the aluminium matrix in a fluorotitanate-zirconate (H_2TiF_6 - H_2ZrF_6) based solution, and reduction reactions occur predominantly on the particles. The alkaline diffusion layer thus formed causes preferential deposition of a hydrated Ti and Zr oxide covering the particles and surrounding areas, eventually leading to a conversion layer with significant variations in thickness. In addition to substrate metallurgy, agitation and pH of the conversion bath are factors that significantly control the conversion layer deposition. The conversion layers formed cause only a small reduction in the cathodic activity of the -Al(Fe,Mn)Si particles and do not impart improved corrosion resistance of the AA6060 alloy in chloride solution.

INTRODUCTION

Chromate conversion coatings have been applied successfully on aluminium for a long time to improve the corrosion resistance and adhesion to organic coatings and adhesives. However, the need for more environmentally friendly processes, e.g. in the automotive industry, has led to the development of various chromate-free alternatives. The majority of alternative chemical conversion coatings currently in use are Ti and/or Zr oxide based and sometimes also incorporates a polymer to promote adhesion.

The formation of a chemical conversion coating and hence the corrosion behaviour may be significantly affected by the presence of intermetallic

phases on the surface of commercial purity aluminium alloys. Limited information is available on the relationship between substrate metallurgy and formation of Ti-Zr based conversion coatings. However, recent work [1] has shown that the formation of a conversion coating on AA6060 aluminium in a hexafluorozirconic-hexafluorotitanic-polyacrylic acid based solution (Alodine 2840) was greatly influenced by intermetallic particles present on the substrate material. Preferential nucleation of the Ti-Zr based conversion layer and its growth occurred on and around the intermetallic -Al(Fe,Mn)Si particles, but a complete coverage could not be obtained even after prolonged immersion in the conversion bath [1]. It was proposed that the localised oxide deposition is associated with a local increase in pH resulting from cathodic activity of the particles during the conversion process. The conversion layer deposition was assumed to rapidly reduce the cathodic activity of the particles, thereby limiting the growth of the conversion layer and resulting in incomplete coating coverage.

The work referred to above [1] was emphasising surface characterisation of the Ti-Zr based conversion layers by use of SEM, TEM and GDOES analyses. In the present work, another fluorotitanate-zirconate based system (Gardobond X4707, no polymeric component added) was investigated. The purpose was to examine Ti-Zr based conversion layer formation and characteristics on AA6060 aluminium in more detail by including also electrochemical measurements during the conversion treatment. In addition to the commercial AA6060 material, electrodes of synthetically prepared -Al(Fe,Mn)Si particles and a particle-free AA6060 matrix alloy (AlMg0.5Si0.4) were made in order to obtain further insight into the mechanism of the conversion layer formation.

EXPERIMENTAL

Materials

Studies were conducted on commercially produced AA6060 alloy extrusions that were about $2 \times 110 \text{ mm}^2$ in cross-sectional area, air cooled after extrusion and aged to T6 temper by heat treatment at 195°C for 3.25 h. The ternary AlMg0.5Si0.4 alloy was made from super purity aluminium and pure alloying elements and cast into extrusion billets about 100 mm in diameter. After solidification the billets were homogenised at 575°C for 4 h, water quenched to prevent precipitation of Mg_2Si phase, machined to a diameter of 95 mm and preheated to 470°C before direct extrusion to profiles with a cross-

sectional area of 3.2 x 60 mm². The profiles were water quenched immediately after the exit from the die to keep the Mg and Si in solid solution. Some of the specimens were artificially aged to T6 temper by heat treatment at 195°C for 3.25 h. The chemical composition of the test materials is given in Table 1.

Table 1. Composition of materials (wt%, bal. Al).

Material	Si	Fe	Mg	Mn	Cu	Zn	Ti	Cr	Zr
AA6060	0.43	0.18	0.51	0.020	0.0022	0.0123	0.0097	0.0017	0.0013
AlMg0.5Si0.4	0.38	<0.001	0.47	0.001	0.0012	0.0015	0.0005	0.0009	0.0002
-Al(Fe,Mn)Si	9.2	33.1	-	0.13	-	-	-	-	-

Large (of the order 1 mm) -Al(Fe,Mn)Si particles were grown by controlled solidification of melts made from high purity components. An aluminium melt containing 7.5% Si, 3.0% Fe and < 0.2% Mn was heated to 800°C in an alumina crucible under argon atmosphere and the melt stirred with a graphite rod to ensure complete dissolution. The melt was solidified and then reheated to 750°C in argon atmosphere, cooled to 710°C and kept at this temperature for one hour before cooling to 630°C over a period of 20 h (4°C/h). The melt was maintained at this temperature for 30 h to promote further growth of the intermetallic particles formed, followed by rapid cooling to room temperature.

Quantitative electron probe microanalysis showed that the laboratory made -Al(Fe,Mn)Si particles were homogeneous and had a composition corresponding well within the predominant type of Fe-rich compounds formed in an alloy like AA6060 according to Mondolfo [2]. Energy dispersive X-ray analysis of about 70 particles in AA6060 showed an average Fe/Si atomic ratio similar to that of the synthetically prepared -Al(Fe,Mn)Si phase, but with a somewhat higher Mn concentration (0.3 ± 0.2 %).

Working electrodes for electrochemical characterisation of the -Al(Fe,Mn)Si particles were prepared according to a method described in earlier work [3]. An image of a typical particle, approximately 1 mm in diameter, and sketch of a multi-crystalline electrode are shown in Figure 1. The area of exposed particles was determined by image analysis.

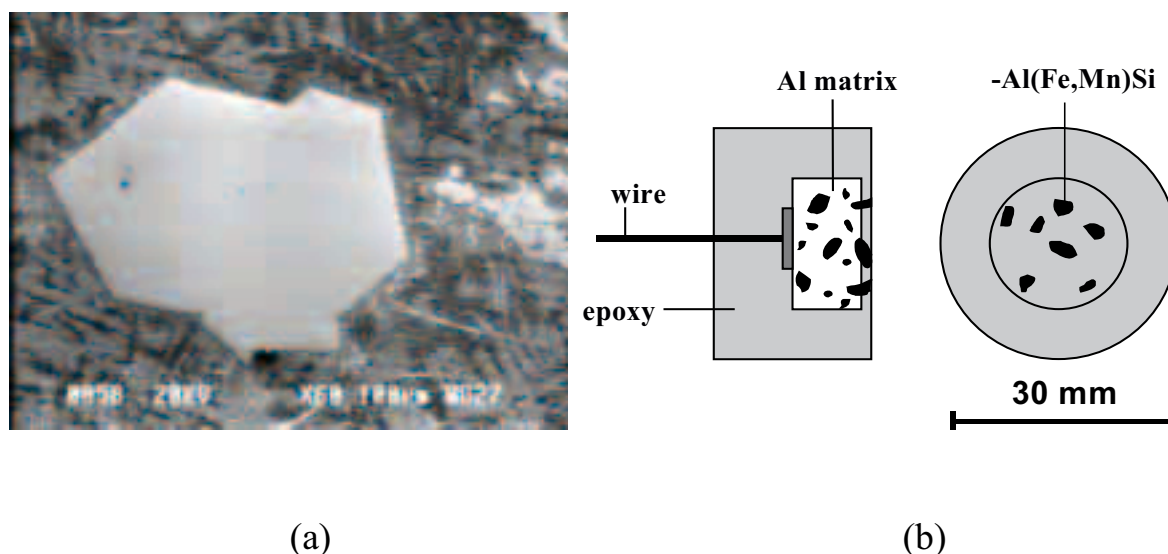


Figure 1. SEM image of large $-\text{Al}(\text{Fe},\text{Mn})\text{Si}$ phase particle (a) and sketch of multicrystalline electrode (b) used for electrochemical characterisation. The aluminium matrix was preferentially etched and the surface re-coated with epoxy and gently re-ground on grit 2400 SiC paper such that only the intermetallic particles were exposed, while the aluminium matrix provided electrical contact to the external circuit.

Pre-treatment procedure

The following general procedure was used to produce the conversion layers:

1. Degrease in acetone
2. Alkaline etch in 100g/l NaOH solution, 60°C, 50s
3. Rinse with tap water
4. Deoxidise in fluoride/sulphuric/phosphoric acid based solution (4% Alfideox 73, 25°C, 1 min)
5. Rinse with tap and distilled water
6. Conversion coating in fluorotitanate/zirconate acid based solution (4% Gardobond X4707, 25°C, pH 2.9-4.0, adjusted by use of Gardolene 6800)
7. Rinse with tap and distilled water
8. Dry in hot air stream

During alkaline etching about 5-6 μm of metal was removed from the surface of AA6060, while 2-3 μm was removed from the surface of the ternary $\text{AlMg}_{0.5}\text{Si}_{0.4}$ alloy under the same conditions. The deoxidising solution also

had a slight etching effect; about 0.1 μm of the AA6060 surface was etched away during treatment.

Surface characterisation

The morphology and near surface structure and chemistry of selected specimens were investigated using different techniques. SEM characterisation was performed in plan view on a JEOL 840A with an X-ray EDS analytical system. Specimens were also examined in a field emission SEM (Hitachi S4300 SE), allowing high resolution imaging of the oxide covered surfaces. TEM characterisation was carried out in cross-section geometry on ultramicrotomed (UM) specimens on a Phillips CM30 equipped with an X-ray EDS analytical system. The ultramicrotomed thin foils were prepared by use of the procedure described in reference [4].

Quantitative element depth profiles were obtained by use of glow discharge optical emission spectroscopy (GDOES). Similar specimens were analysed by X-ray photoelectron spectroscopy (XPS) in a VG MicroLab III instrument by use of an aluminium X-ray source. Auger electron spectroscopy (AES) analysis was performed on a Thermo VG Scientific Microlab 350 instrument. The Auger spectra were acquired at a beam energy of 10 keV with a primary beam current of 13 nA.

Electrochemical measurements

AA6060 and AlMg0.5Si0.4 alloy specimens for electrochemical measurements were cut to a size of about 20 x 20 mm² and placed in a special PTFE specimen holder revealing an exposed circular area of 1.33 cm² while providing electrical contact to the back of the specimen. The electrochemical cell consisted of a 1 litre PVC beaker with the conversion bath open to ambient laboratory air. Temperature was maintained at 25 \pm 1°C in all experiments, and a graded mechanical stirrer was used to control the agitation of the solution. Positioning of the stirrer and electrodes was kept constant throughout this work in order to maintain similar convection conditions. The saturated calomel electrode (SCE) was used as reference in all experiments. All measurements were made by use of a Gill AC potentiostat connected to a PC with software provided by ACM Instruments.

After etching and deoxidation according to steps 1 through 5 in the coating procedure, corrosion potentials of the test materials were recorded as a

function of time during conversion coating in fluorotitanate/zirconate solutions adjusted to pH 2.9 and 4.0, respectively. Potentiostatic polarisation of γ -Al(Fe,Mn)Si phase particles was performed in similar solutions. Specimens were polarised at the desired potential immediately after immersion in the electrolyte.

Potentiodynamic polarisation measurements were conducted in aerated 0.1 M NaCl solution in order to assess the degree of inhibition of the cathodic reactions as a result of the pre-treatments. A similar approach has been employed earlier to assess the degree of passivation caused by surface preparation of AA2024 aluminium for conversion coating [5]. The electrolyte was made from reagent grade chemicals and distilled water. The potential sweep rate was 30 mV/min and measurements were started immediately after exposure to the solution. The reproducibility of the electrochemical measurements was generally very good as long as identical stirring conditions were maintained.

RESULTS

SEM, EPMA and TEM observations

For relatively thick conversion layers the distribution of the Ti-Zr deposition was readily visible in SEM. X-ray EDS analyses detected Ti and Zr particularly on top of the γ -Al(Fe,Mn)Si particles and in a dark zone surrounding the particles, as shown in Figure 2. The contrast between bright and dark areas is apparently due to a lower secondary electron emission yield in the regions where the conversion layer was relatively thick. Thus, secondary electron images were useful in mapping the conversion layer distribution on different substrates and under various coating conditions.

The strong influence of γ -Al(Fe,Mn)Si particles in promoting formation of Ti-Zr based conversion layers on AA6060 is clearly illustrated in Figure 3. Identical treatment of the particle-free AlMg0.5Si0.4 alloy and AA6060 (Figure 3 a and b, respectively) in stagnant pH 4.0 solution resulted in no visible conversion layer formation on the AlMg0.5Si0.4 alloy, while the dark zones surrounding the intermetallic particles on AA6060 indicated significant layer formation. Moreover, a significant effect of convection in the solution was evident by comparing Figures 3 b, c and d. By increasing the stirring during conversion coating, the layer deposition could be reduced to the extent that only the γ -Al(Fe,Mn)Si particles themselves were covered (Figure 3 d).

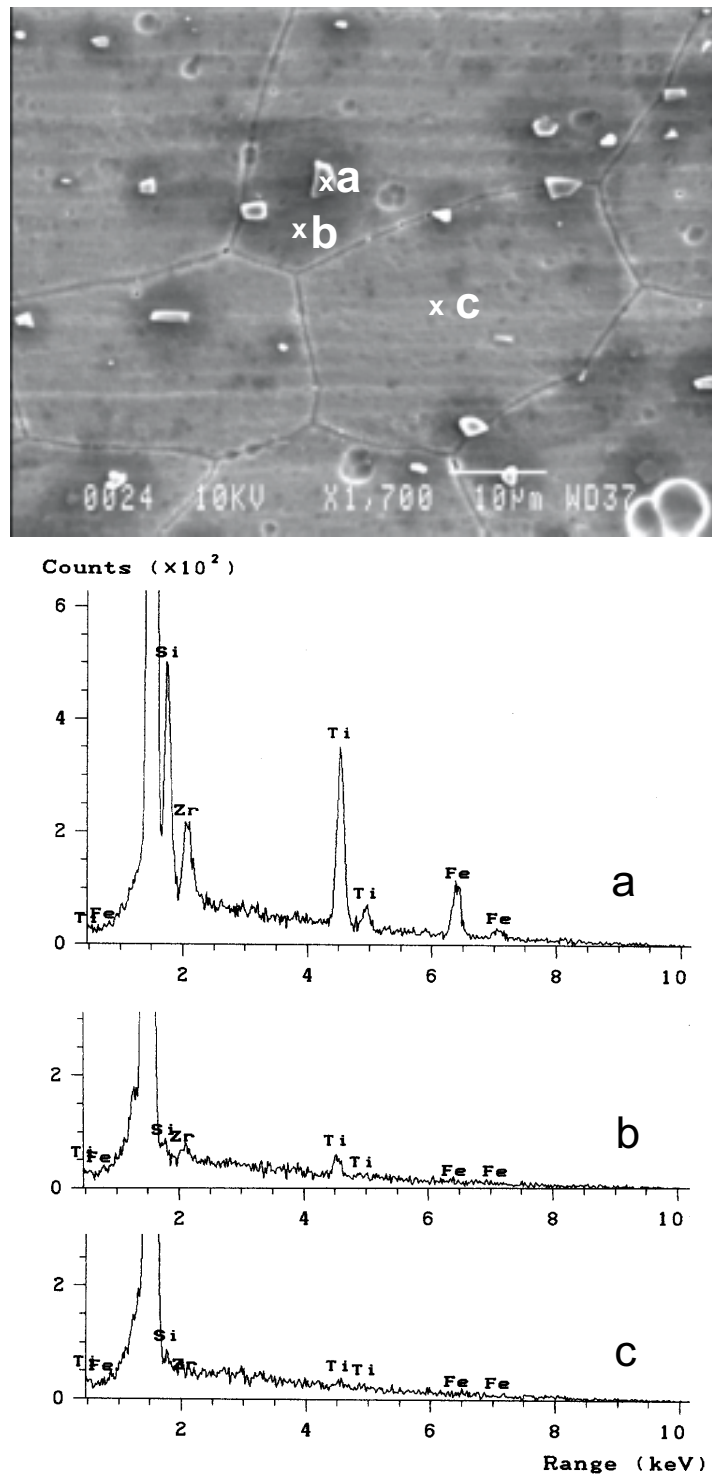


Figure 2. SEM image of AA6060 with relatively thick conversion layer. X-ray EDS analysis on particle (location a) showed strong Ti and Zr signal. Ti and Zr were also detected in dark areas surrounding the particles (location b), but not in the brighter areas at some distance from the particles (location c).

SEM examination of treated AA6060 surfaces further showed that increasing the pH of the conversion bath greatly enhanced the coating deposition (Figure 4). Under stirring conditions resulting in incomplete coverage of the Al(Fe,Mn)Si particles in a pH 2.9 solution (Figure 4 b), equivalent treatment in a pH 4.0 solution resulted in formation of a thick layer on the particles and its surroundings (Figure 4 d). It was observed, however, that extensive (non-uniform) layer deposition occurred even in the pH 2.9 solution under stagnant conditions, causing a slight discoloration of the surface.

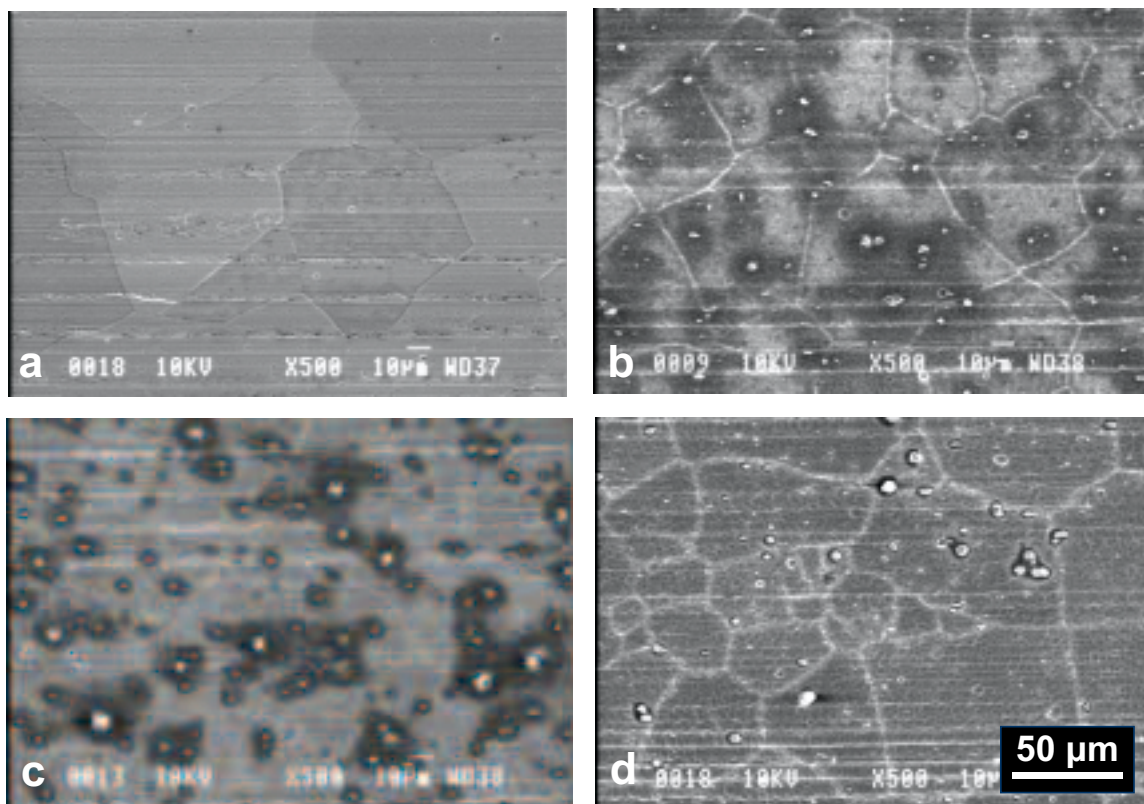


Figure 3. SEM images of surfaces after conversion treatment at pH 4.0 for 3 min. a) $\text{AlMg}_{0.5}\text{Si}_{0.4}$, stagnant solution b) AA6060, stagnant solution c) AA6060, mildly stirred solution d) AA6060, vigorously stirred solution. The Ti-Zr based conversion layer was deposited (dark areas) around the intermetallic particles on AA6060 in b) and c). The conversion layer was confined to the particles in vigorously stirred solution (d). No layer deposition seemed to occur in the absence of cathodic particles in the surface (a).

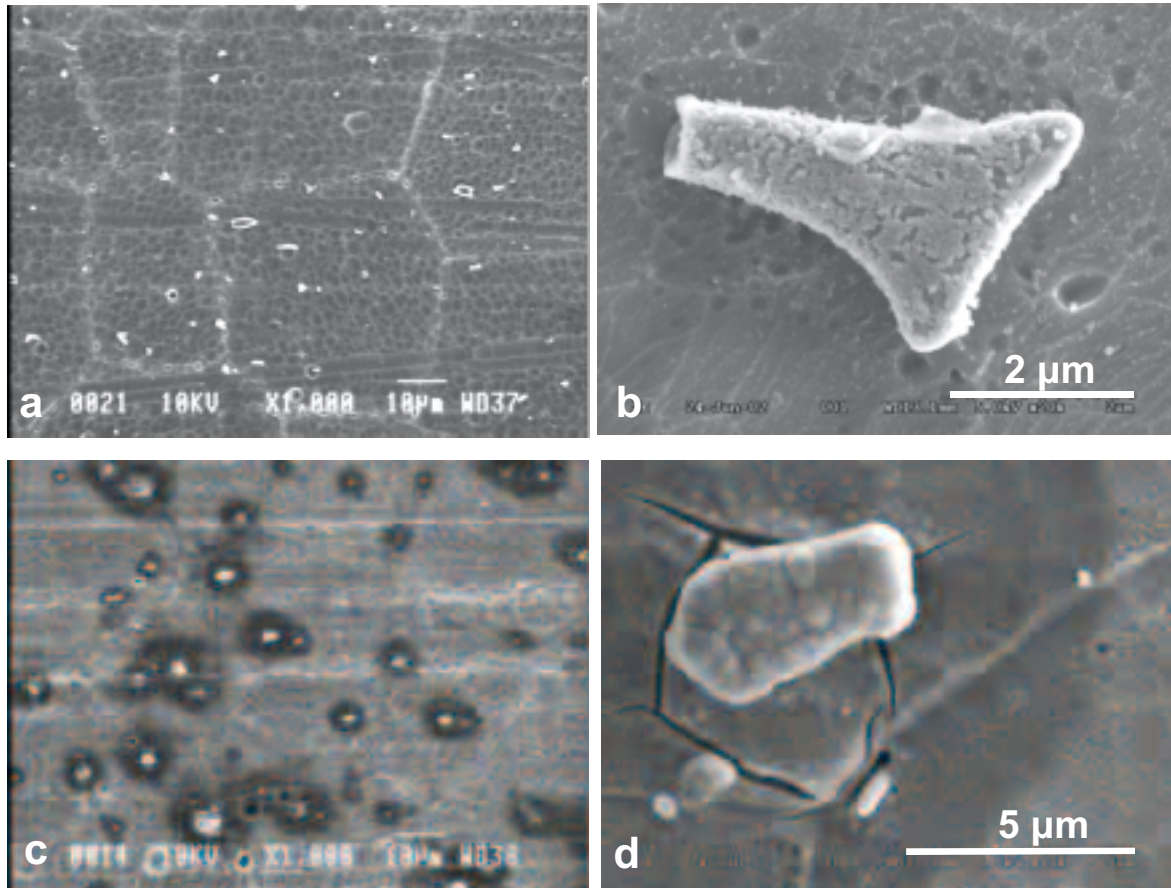


Figure 4. SEM images of AA6060 after 90 s of immersion in mildly stirred conversion solution of pH 2.9 (a, b) and pH 4.0 (c, d), showing incomplete coverage of -Al(Fe,Mn)Si particles by the conversion layer at pH 2.9 (b) and a thick layer at pH 4.0 (d). Cracking of conversion layer in d) may be due to dehydration in high vacuum of the SEM.

The nucleation of a conversion layer at the -Al(Fe,Mn)Si particles was also visualised by electron probe microanalysis (EPMA), see Figure 5. No F was detected in the Ti-rich oxide film covering the intermetallic particles. The Zr signal observed at these areas was weak (not shown in Figure 5), indicating that the oxide deposited is a mixed Ti and Zr oxide with relatively high Ti/Zr ratio.

Closer examination of apparently un-coated areas on AA6060 in field emission SEM showed that instead of a continuous conversion layer, these regions exhibited a high density of small particles, about 50 nm in diameter (Figure 6 a, b). The particles formed were too small to be analysed in the SEM, but it is reasonable to assume that the composition was similar to the

layer formed in the vicinity of the -Al(Fe,Mn)Si particles, *i.e.* essentially a Ti-rich oxide. The particulate “coating” was also formed on the AlMg0.5Si0.4 alloy (both in T4 and T6 temper), despite the absence of -Al(Fe,Mn)Si particles in this material (Figure 6 c, d). However, aluminium surfaces are never completely homogeneous, even at high purity. It is therefore possible that the oxide particles deposited on the surface were associated with small, cathodic sites due to impurity segregation [6]. A particulate type of structure has also been observed previously [7] on fluorotitanate and fluorozirconate treated AA6063 surfaces.

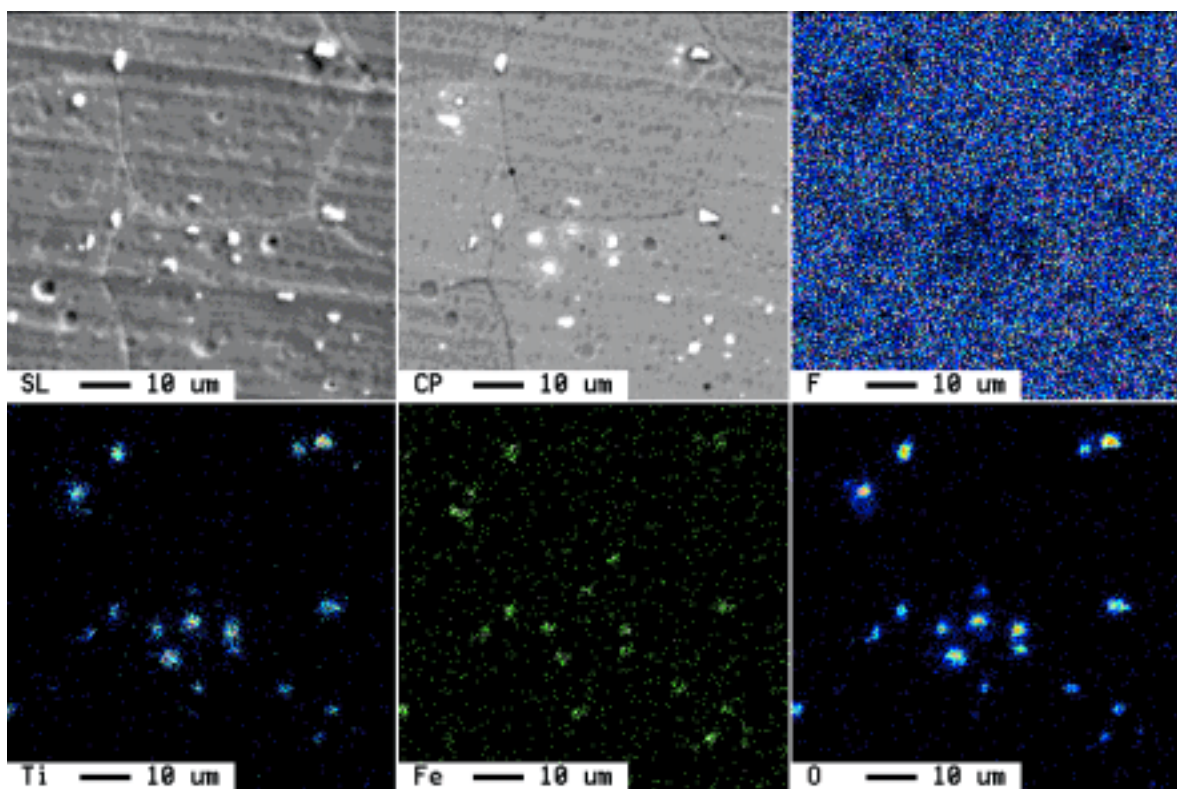


Figure 5. EPMA mapping of elements F, Ti, Fe and O on AA6060 surface after pre-treatment for 30 s in conversion bath, pH 4.0. A fluorine-free Ti oxide was formed on the Fe-rich intermetallics shown in the secondary and backscatter electron images (top left and middle, respectively).

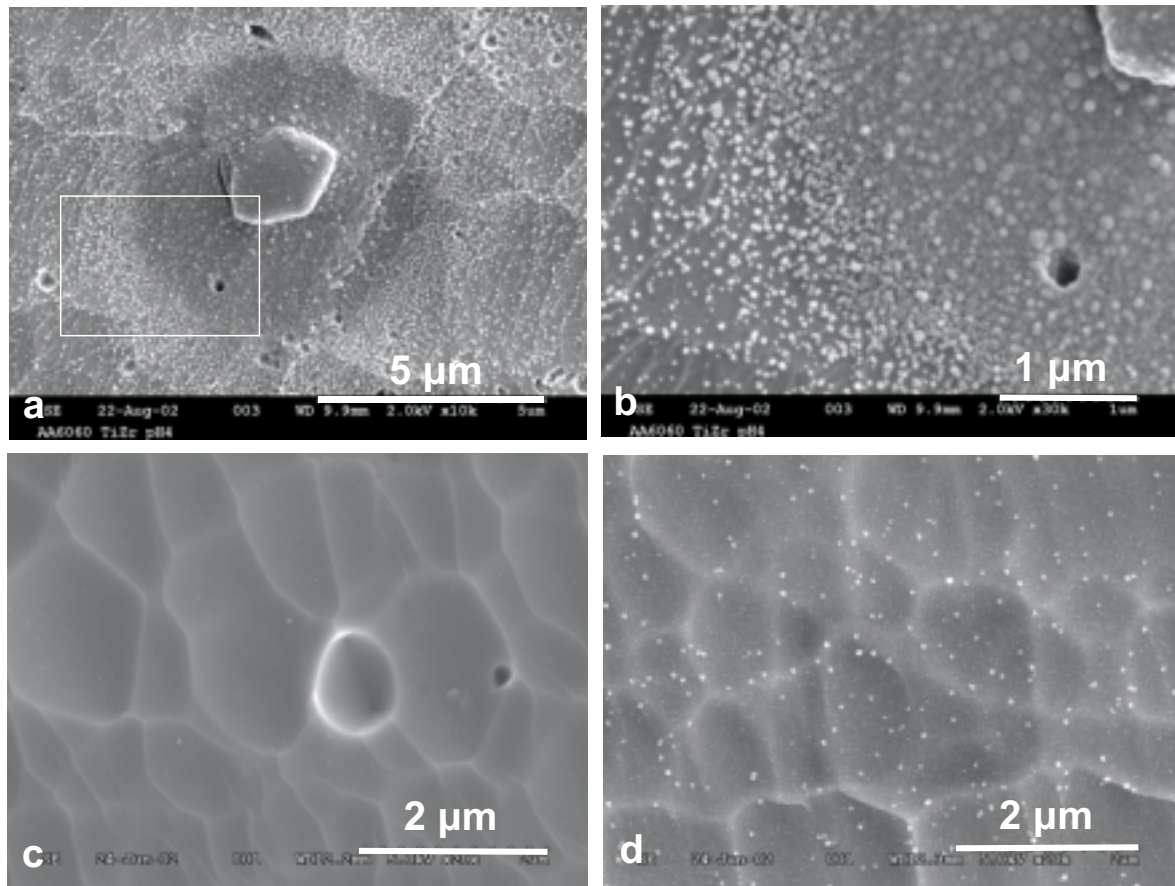


Figure 6. Field emission SEM images of AA6060 surface (a, b) after conversion treatment at pH 4.0 for 90 s, showing transition from a continuous to a particulate type of structure at some distance from intermetallic particle. Etched and deoxidised ternary AlMg0.5Si0.4 alloy (c) also exhibited a particulate type of “conversion coating” after similar treatment (d).

TEM studies of ultramicrotomed specimens equivalent to those examined in SEM (Figure 2) confirmed the large variation in the thickness of the conversion layer, as illustrated in Figure 7. Above the $-Al(Fe,Mn)Si$ particles the layer sometimes exceeded 150 nm in thickness, while the surface appeared to be without any coating in other locations on the same specimen. Electron diffraction proved the layer to be amorphous. X-ray EDS analyses at different locations did not reveal any significant changes in the composition of the layer across the thickness, apart from a slight tendency for a higher Ti/Zr ratio towards the oxide/metal interface.

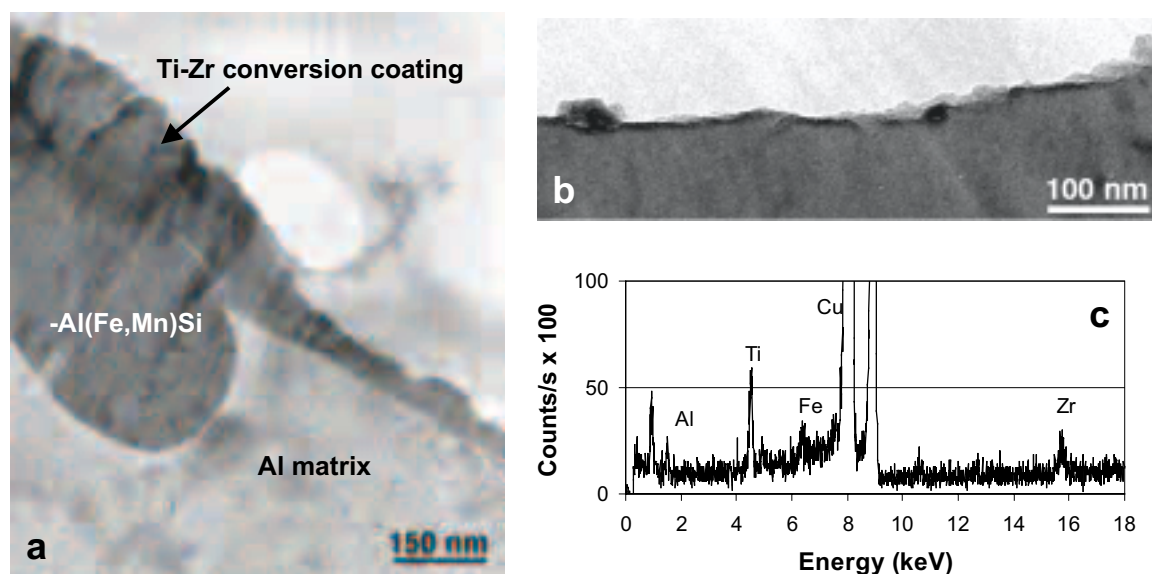


Figure 7. TEM of ultramicrotomed section of AA6060 surface exhibiting a thick conversion layer on $-Al(Fe,Mn)Si$ particle (a) and very thin layer in a particle-free region (b). X-ray EDS analyses of the conversion layer (c) showed characteristic peaks for Al, Ti, Fe, Cu and Zr. Characteristic energies of F and O were too low to be detected in the equipment used. Strong Cu signal originated from the Cu grid on which the thin foil specimen rested.

Surface analyses

The XPS spectrum of a treated AA6060 surface showed characteristic peaks for Al, O, Ti and F, while Zr was barely detectable (Figure 8). Binding energies of 458.3 eV and 463.78 eV for the Ti $2p_{3/2}$ and Ti $2p_{1/2}$ peaks, respectively, indicate that Ti was most likely in Ti^{4+} state. Estimated Ti/Zr atomic ratios ranging from 3.8 to 7.0 corresponded well with a Ti/Zr atomic ratio of 4.7 determined from ICP analysis of the conversion solution.

From quantitative GDOES depth profiles of an equivalent specimen (Figure 9) the conversion film thickness was estimated to be of the order 10-20 nm, *i.e.*, in the same range as reported in other studies [8-11]. However, the GDOES data represented an *average* analysis over an area 4 mm in diameter. The fact that Ti could be detected even after sputtering to a depth of more than 100 nm is explained by surface roughness as well as large variations in the conversion film thickness, as shown by the SEM and TEM studies. Hydrogen was detected throughout the depth profile in Figure 9 and a fairly constant O/H ratio of 20-26 was assessed from the GDOES results, indicating presence of a hydrated oxide.

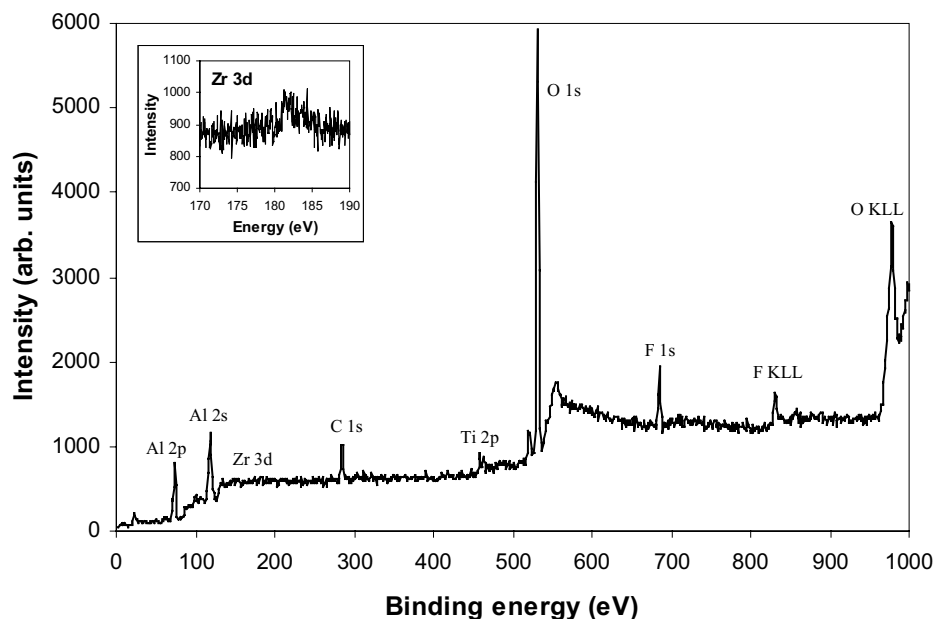


Figure 8. XPS survey spectrum of AA6060 surface after conversion coating in the fluotitanic/zirconic acid based conversion solution for 90 s, pH 2.9, 25°C. Semi-quantitative analyses obtained from high-resolution spectra indicated a Ti/Zr atomic ratio of 5.1 ± 1.4 . The Zr 3d peak at 182 eV (inserted) was only detected in the high-resolution scans.

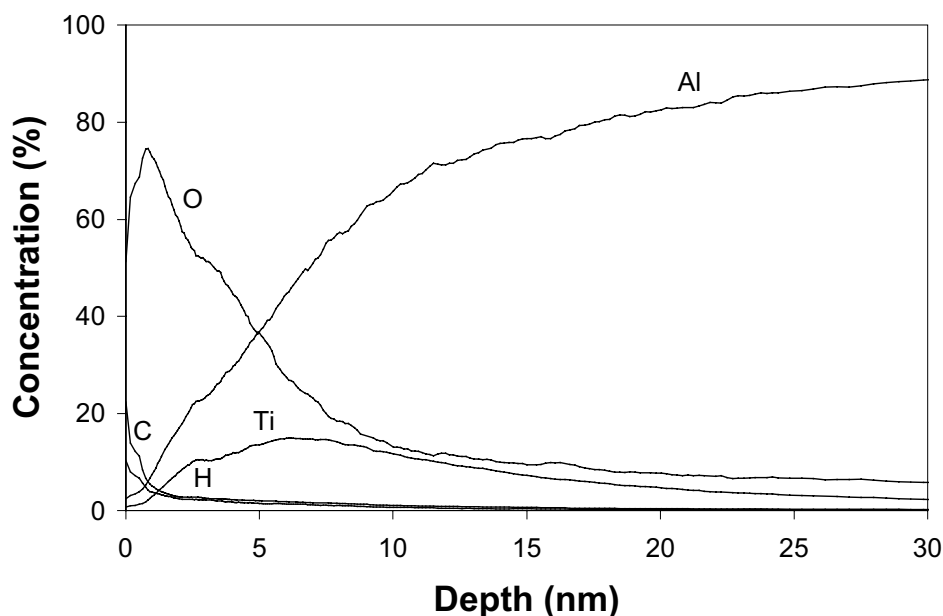


Figure 9. GDOES depth profiles of elements Al, O, Ti, H and C (wt%) on AA6060 surface after conversion coating in the fluotitanic/zirconic acid based conversion solution for 90 s, pH 2.9, 25°C. Data are normalised to 100%. Zr and F are omitted due to lack of reference specimens for quantification. Zr followed the Ti profile on a qualitative intensity vs. time plot (not shown).

Auger analysis of a similar sample was performed as this technique provides both high lateral resolution and surface sensitivity. Spectra acquired from small areas ($< 0.2 \mu\text{m}^2$) on and immediately next to an -Al(Fe,Mn)Si particle are shown in Figure 10. Strong Ti and relatively weak Zr signals were observed in areas 1 and 2, but not in area 3 at some distance from the particle, supporting the earlier observation [1] that preferential deposition of the Ti-Zr film occurs on and around cathodic intermetallic particles. The absence of characteristic Fe LMM peaks at 600-700 eV in the spectrum acquired from the particle (area 1) shows that the film must be thicker than the sampling depth, which is typically a few nm in AES analysis.

The AES analyses further indicated that the Al concentration in the Ti-Zr conversion coating was very low and that F was not present in concentrations high enough to be detected. However, F was detected in the virtually uncoated part of the surface (area 3), possibly in the form of AlOF [11,12]. This could not be confirmed based on the present analyses due to the limited chemical state information obtained by AES.

Electrochemical behaviour of AA6060 and its phases in the conversion bath

After an initial potential transient the corrosion potential of AA6060 during conversion coating attained a steady state potential of about -1300 mV in the conversion bath at pH 2.9, as shown in Figure 11. Under similar conditions the ternary $\text{AlMg}_{0.5}\text{Si}_{0.4}$ alloy, corresponding to the matrix of AA6060, exhibited a potential that was typically 50-100 mV more negative, while the potential of the -Al(Fe,Mn)Si phase was about -850 mV. Increasing the pH of the conversion solution (in the range 2.9-4.0) caused the steady state potential of the alloys and the -Al(Fe,Mn)Si phase to shift about 50 mV and 10 mV, respectively, in the positive direction. Increased stirring of the solution also generally shifted the potential in the positive direction.

The potential measurements indicate that the -Al(Fe,Mn)Si particles act as local cathodes on the AA6060 aluminium surface during conversion coating. The area fraction of -Al(Fe,Mn)Si phase in the AA6060 alloy was determined to be 0.64% based on image analysis of polished surfaces. For a similar cathode/anode area ratio, the galvanic current density on an -Al(Fe,Mn)Si electrode (0.92 mm^2) when coupled to the $\text{AlMg}_{0.5}\text{Si}_{0.4}$ “matrix” alloy (133 mm^2) typically increased during the first 30 s and then attained a steady-state of about 3-5 mA/cm^2 , as shown in Figure 12 a. The potential transient of the macroscopic galvanic couple (Figure 12 b) was

similar to that of AA6060 shown in Figure 11, indicating that the macroscopic galvanic couple simulated the time dependence of processes occurring on a microscopic scale on AA6060 during conversion coating.

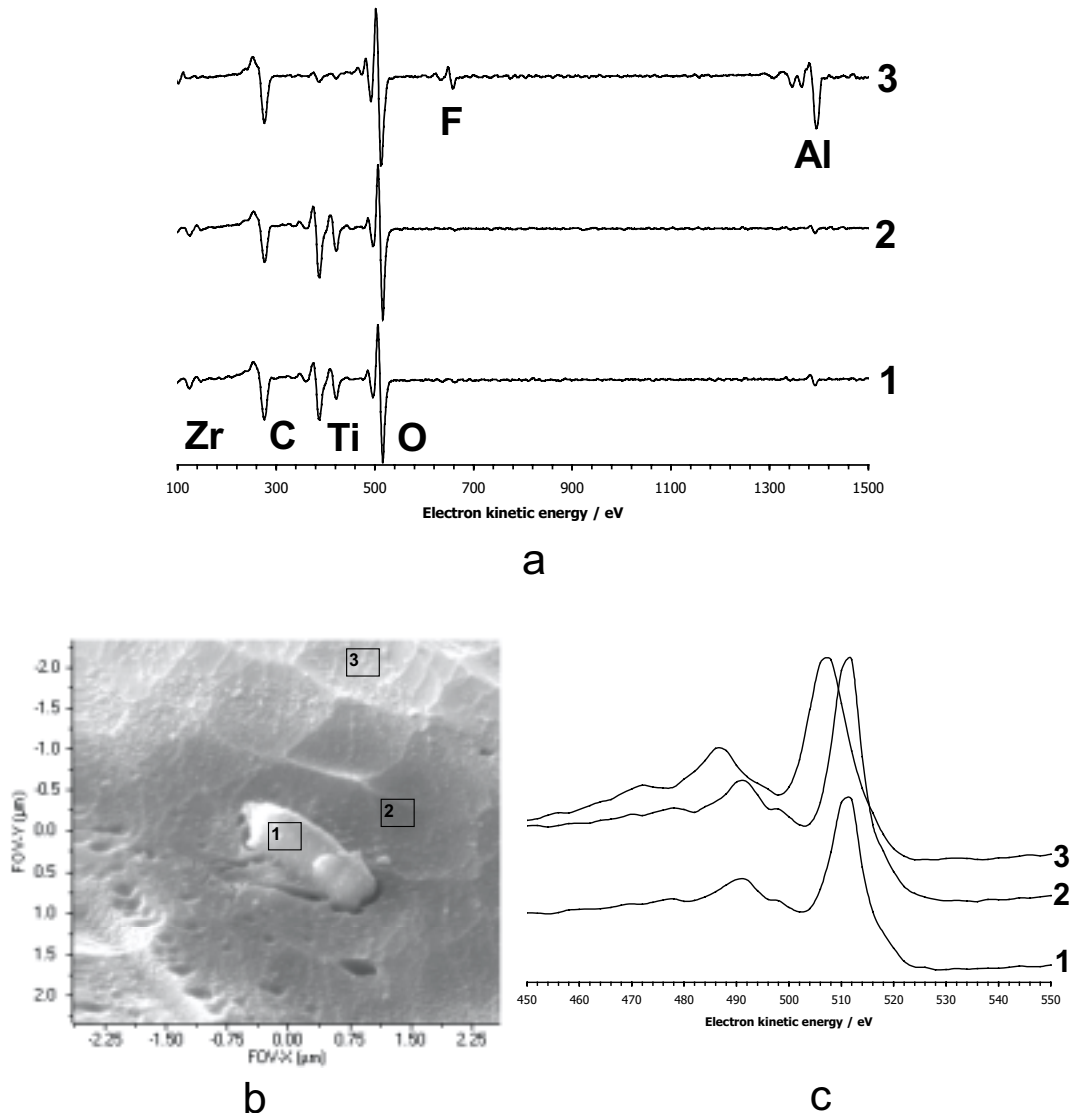


Figure 10. Differentiated survey Auger spectra obtained from AA6060 after pre-treatment in pH 4.0 conversion solution for 90 s (a). The spectra, corresponding to areas marked in SEM image (b) show strong Ti and weak Zr signals on the - Al(Fe,Mn)Si particle (area 1) and immediately next to it (area 2), but not well away from the particle (area 3), where strong Al and F signals were observed. The O KLL regions of the spectra in integrated form (c) show that the principal oxygen peak acquired from area 3 is located at 508 eV, as expected for oxygen in Al oxide. The peaks at 511 eV (areas 1 and 2) may be assigned to oxygen in Ti or Zr oxide.

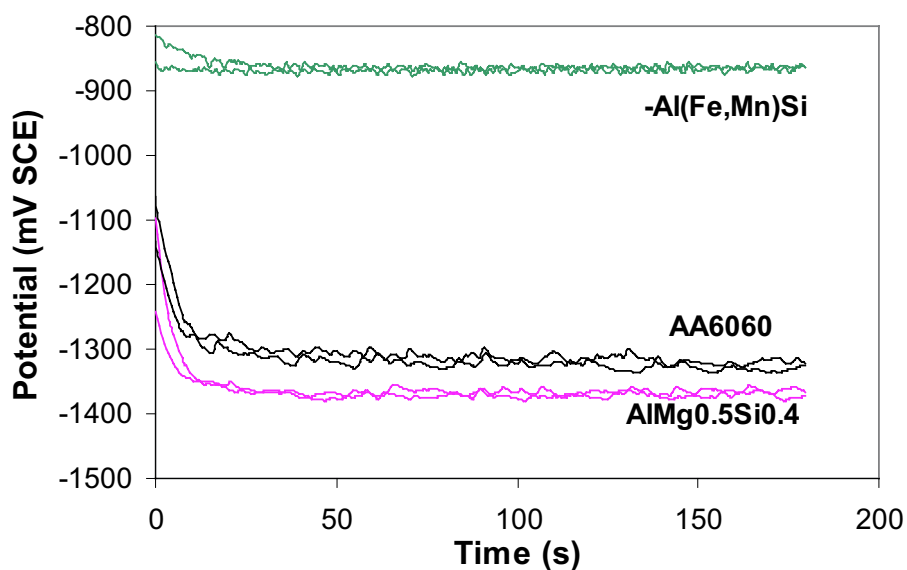


Figure 11. Corrosion potential of AA6060, AlMg0.5Si0.4 matrix alloy and -Al(Fe,Mn)Si phase in moderately stirred fluorotitanate/zirconate based conversion bath, pH 2.9, 25°C.

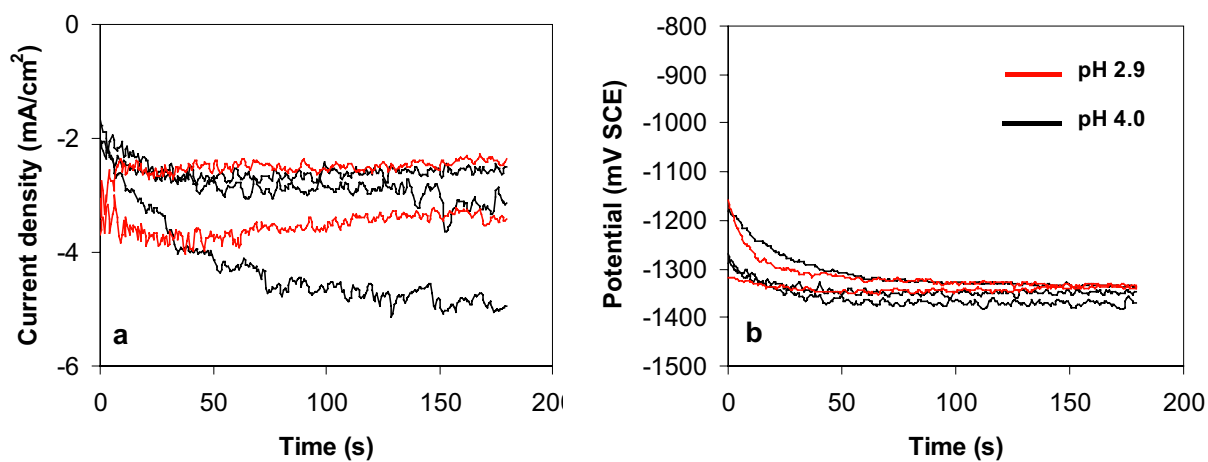


Figure 12. a) Galvanic current density on -Al(Fe,Mn)Si phase as a result of galvanic coupling to AlMg0.5Si0.4 in conversion solutions of pH 2.9 and pH 4.0, b) Potential development of the galvanic couples. The cathode area was about 0.7% of the anode area.

Potentiostatic polarisation of γ -Al(Fe,Mn)Si phase electrodes at applied potentials in the range -900 mV to -1400 mV showed no or only a slight decrease in current density with time, as shown in Figure 13. Interference colours due to film formation were seen during subsequent examination of the electrode surfaces under a stereo microscope. The surface appearance was potential dependent. In solutions of pH 2.9 and pH 4.0, no colour change was visible after polarisation at -900 mV, whereas a golden brown colour was obtained after polarisation at -1000 mV and -1100 mV, indicating a film thickness of the order 100 nm. Surfaces polarised at -1200 mV and -1300 mV exhibited a number of interference colours, indicative of films with a variable thickness. Polarisation at -1400 mV resulted in no colour change, suggesting that any film present must be very thin. At a still lower potential of -1500 mV etching of the γ -Al(Fe,Mn)Si phase took place and formation of gas bubbles, probably due to hydrogen evolution, could be observed. The cathodic current fluctuated and tended to increase with time under these conditions, possibly as a result of surface roughening or ennobling caused by selective dissolution of aluminium from the surface [13].

The reduction in cathodic current with time during potentiostatic polarisation of the γ -Al(Fe,Mn)Si phase (Figure 13) must be associated with the observed film formation. Cross-plotting of the potentiostatic data corresponding to 0 and 180 s into a potential-log(current density) diagram (Figure 14) shows that the largest relative reduction in current density occurred at potentials between -1000 mV to -1300 mV, *i.e.* corresponding to the potential range where a visible film was formed. As stated above, the observed reduction in cathodic current density with time was rather small, indicating that the cathodic activity on the γ -Al(Fe,Mn)Si particles of an AA6060 aluminium surface remained fairly constant during the conversion treatment.

The cathodic current density measured during potentiostatic polarisation of the γ -Al(Fe,Mn)Si phase increased with increased agitation of the conversion bath. Conversely, nitrogen bubbling of the solution to remove most of the dissolved oxygen resulted in a small reduction in the cathodic current density. The effects of stirring and nitrogen bubbling tended to decrease with time, apparently as the oxide film on the γ -Al(Fe,Mn)Si surface increased in thickness. The film then controlled the passage of charge, as the effect of convective transport in the solution became limited.

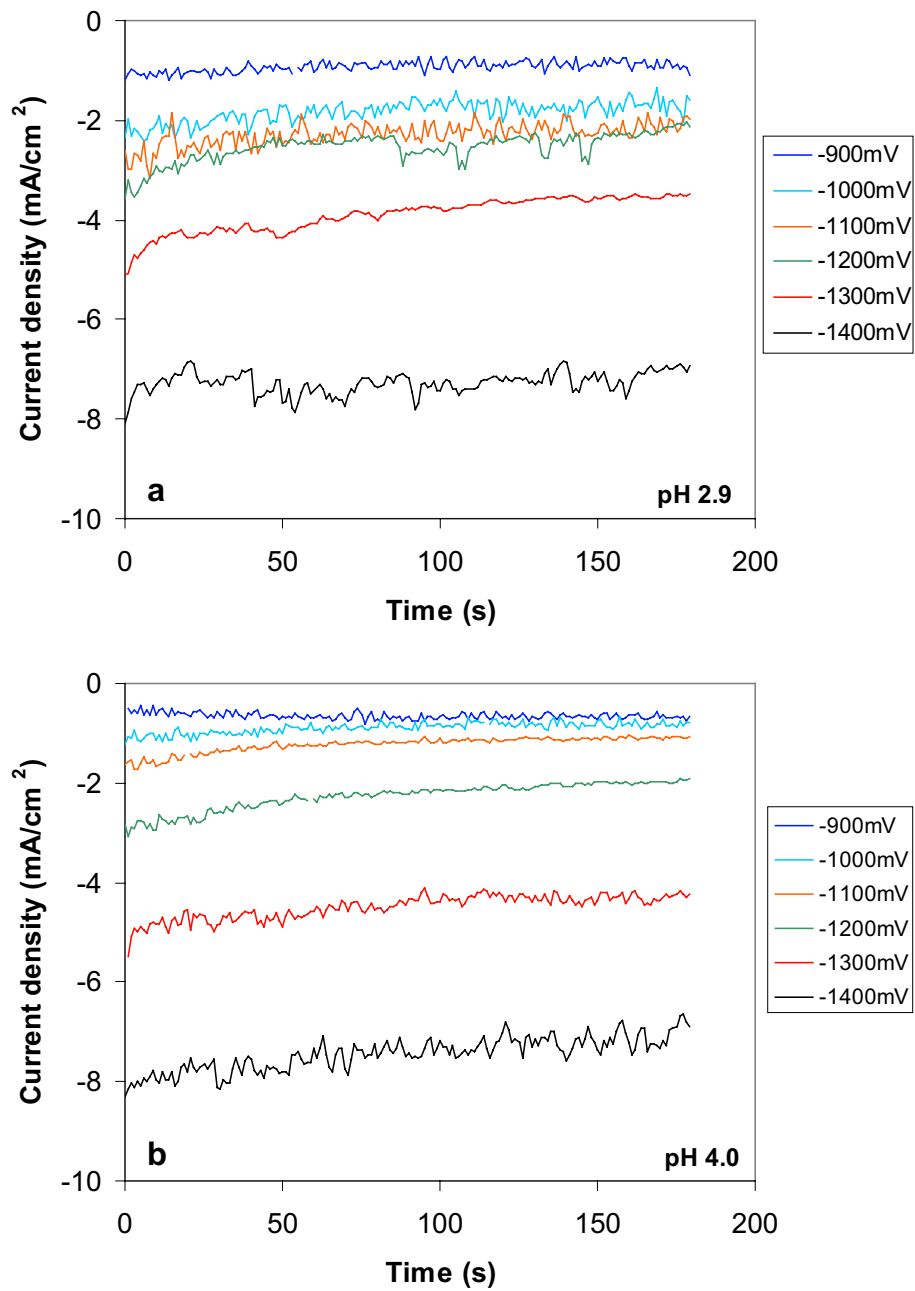


Figure 13. Potentiostatic polarisation of -Al(Fe,Mn)Si phase in mildly stirred fluorotitanate/zirconate conversion solution of pH 2.9 (a) and pH 4.0 (b).

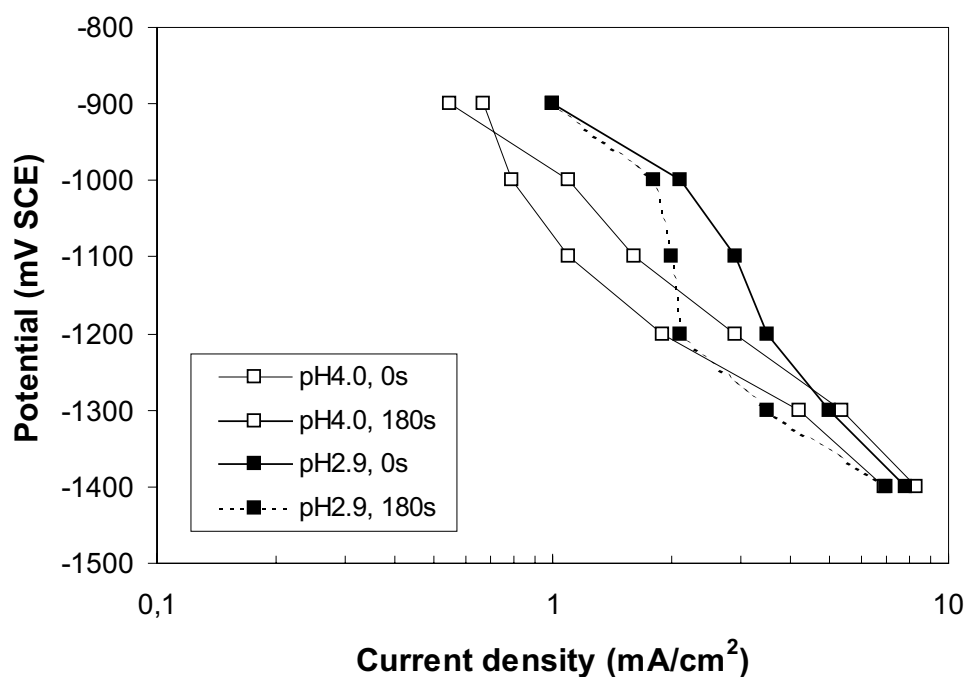


Figure 14. Cathodic polarisation curves of $-Al(Fe,Mn)Si$ phase in conversion solution, plotted on the basis of initial and final (after 180 s) current densities shown in Figure 13.

The AA6060 alloy investigated in this work was artificially aged and hence contained a high density of hardening Mg_2Si particles. This phase is reported to be electrochemically more active than the aluminium matrix due to its high Mg content, especially in acid solution [2,14,15]. Rapid and preferential corrosion of the Mg_2Si particles in the surface was therefore expected already during deoxidation of the AA6060 alloy, although this was not easily visualised due to the small size of the particles. However, by use of available Mg_2Si crystals from an earlier work [15] the corrosion potential of the Mg_2Si phase was measured to be about -1850 ± 50 mV in the presently studied conversion baths, i.e. about 500 mV more active than the potential of the $AlMg_{0.5}Si_{0.4}$ matrix (Figure 11).

Precipitation of Mg_2Si due to artificial ageing has generally only a negligible effect on the corrosion potential of 6000 series alloys [14]. In the present system, ageing to T6 temper resulted in corrosion potentials about 10-20 mV nobler than the corresponding solution heat-treated (T4) materials. The electrochemical results and microscopic examination indicated that the Mg_2Si

phase particles did not play any essential role in the formation of Ti-Zr based conversion layers.

Effect of pre-treatment on electrochemical behaviour in chloride solution

Polarisation curves of AA6060 after various pre-treatments are presented in Figure 15. Results show that conversion treatment at pH 2.9 had practically no effect on corrosion potential and cathodic reaction rate in the chloride solution. In fact, a slight increase in the cathodic current was observed relative to the etched and deoxidised surface at potentials below about -800 mV. In contrast, the surfaces pre-treated at pH 4.0 exhibited a significant decrease in cathodic reaction rate with increasing exposure time in the Ti-Zr conversion bath. The corrosion potential was shifted only by about 10 mV in the negative direction.

The anodic part of the polarisation curves showed no significant difference between the etched/deoxidised and the conversion coated surfaces. Hence, pre-treatment at pH 2.9 appeared to have a negligible effect on the corrosion behaviour of the bare metal, while cathodic inhibition was observed as a result of pre-treatment in the pH 4.0 conversion bath. This reduction in cathodic activity on AA6060 was attributed to a weak passivation of the intermetallic β -Al(Fe,Mn)Si particles in the alloy surface, which could be deduced also from the following experiments:

Galvanically coupled β -Al(Fe,Mn)Si and AlMg0.5Si0.4 electrodes with an area ratio as in AA6060 were immersed in the pH 4.0 conversion bath for up to 180 s in order to separate the anodic and cathodic processes occurring on the AA6060 surface during conversion coating. As shown in Figure 12, this resulted in galvanic current densities of about 3-5 mA/cm² on the β -Al(Fe,Mn)Si phase. The β -Al(Fe,Mn)Si electrodes were subsequently rinsed, dried and subjected to potentiodynamic polarisation in 0.1 M NaCl solution. Results obtained for β -Al(Fe,Mn)Si electrodes prepared in this manner are shown in Figure 16. The cathodic activity was clearly reduced with increasing time in the conversion bath. Subsequent examination of the electrodes under stereo microscope indicated that this resulted from thickening of an oxide film formed on the β -Al(Fe,Mn)Si surface during treatment in the conversion bath.

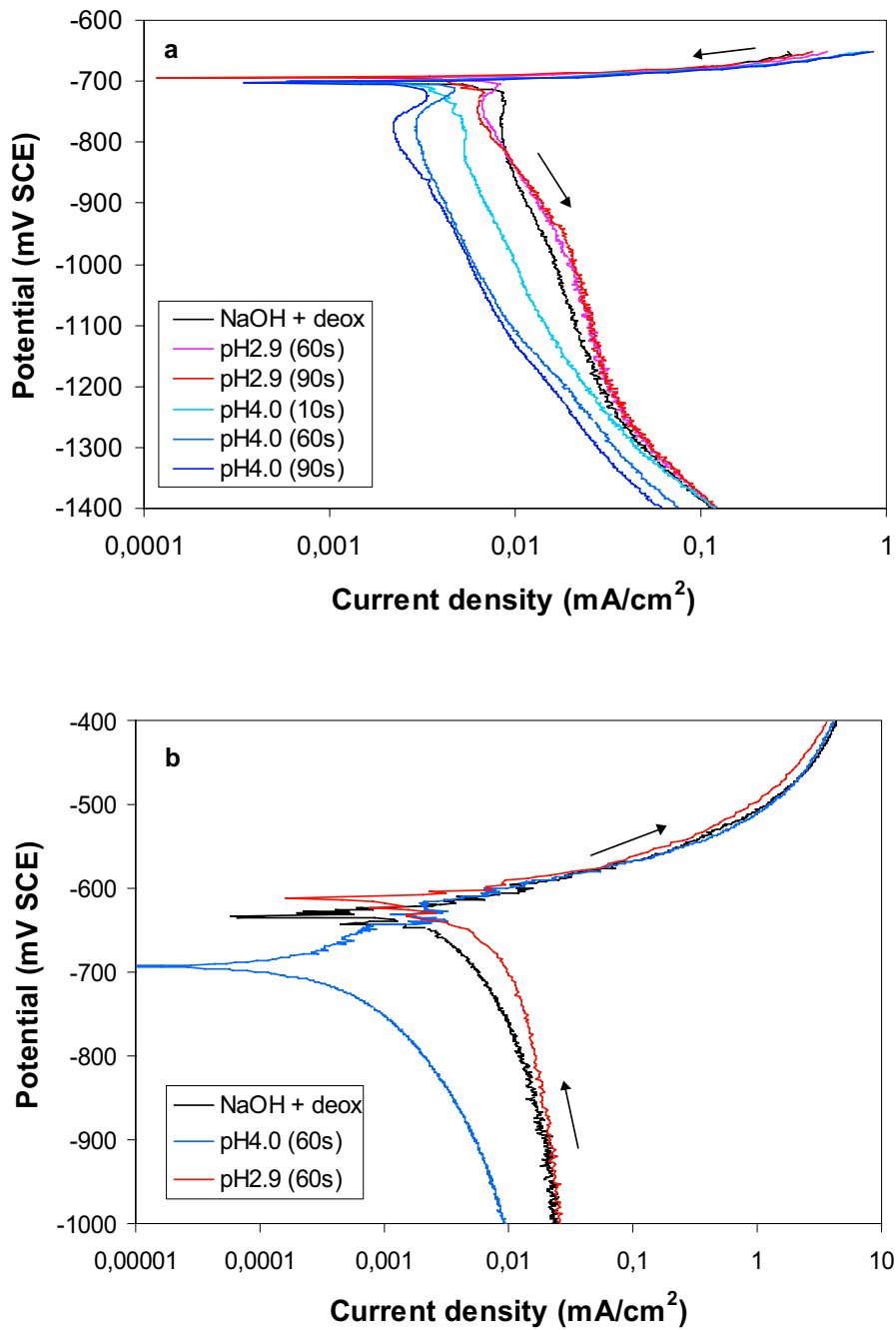


Figure 15. Potentiodynamic polarisation curves for AA6060 in aerated 0.1 M NaCl solution. a) Potential sweep in negative direction, showing reduction in cathodic activity after pre-treatment at pH 4.0 and negligible effect of pre-treatment at pH 2.9. b) Potential sweep in positive direction, showing no effect of the Ti-Zr based pre-treatments on anodic behaviour.

Pre-treatment of the γ -Al(Fe,Mn)Si electrode in the conversion bath under open circuit conditions resulted in no visible film formation and no reduction in cathodic activity (curve 2 in Figure 16). Hence, it can be concluded that reduction in cathodic activity of the γ -Al(Fe,Mn)Si phase in chloride solution is related to the deposition of an oxide film on its surface, formed under cathodic polarisation in the conversion bath.

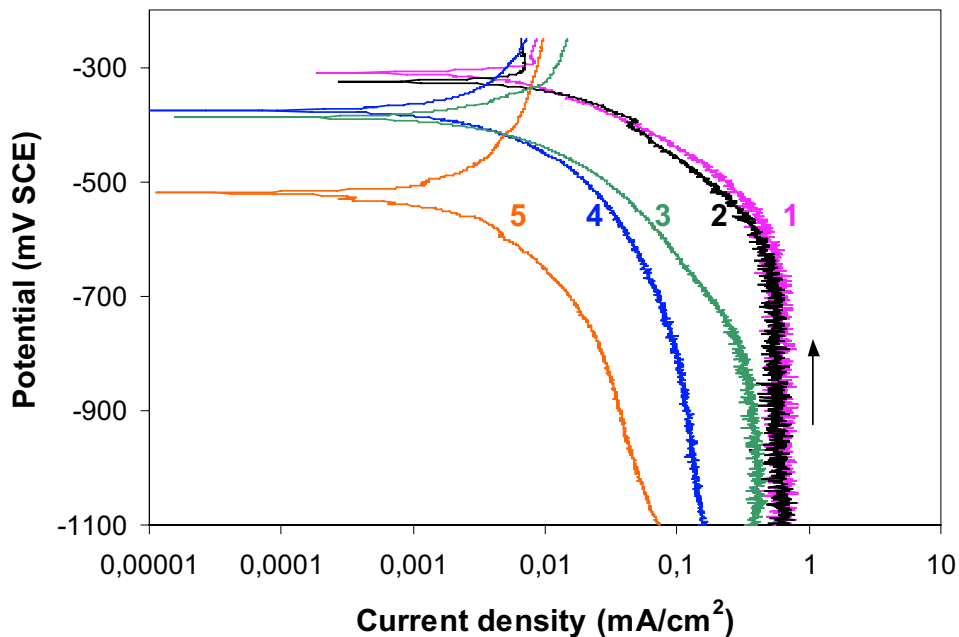


Figure 16. Cathodic polarisation curves for γ -Al(Fe,Mn)Si phase in aerated 0.1 M NaCl solution. Treatment of electrodes before potential sweep: deoxidised only (1), immersed at open circuit potential in conversion bath at pH 4.0 for 90 s (2), galvanically coupled to AlMg0.5Si0.4 alloy while immersed in conversion bath at pH 4.0 for 45 s (3), 90 s (4) and 180 s (5).

DISCUSSION

The present results confirm previous work [1] showing that Ti-Zr based conversion layers formed on AA6060 are highly non-uniform and affected by the cathodic γ -Al(Fe,Mn)Si particles on the surface. During film formation, presence of free fluoride ions will dissolve the native aluminium oxide, accompanied by an initial shift of the corrosion potential in the negative

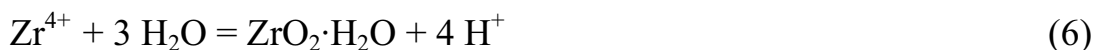
direction, and cause Al metal dissolution and formation of complexes as represented by the following reactions



The cathodic reactions, occurring predominantly on the $-\text{Al}(\text{Fe},\text{Mn})\text{Si}$ particles, are oxygen reduction and hydrogen evolution:



The alkaline diffusion layer formed adjacent to the $-\text{Al}(\text{Fe},\text{Mn})\text{Si}$ particles as a result of reactions (3) and (4) favours precipitation of a Ti and Zr containing oxide conversion film, *e.g.* according to the scheme



Both TiO_2 and $\text{TiO}_2 \cdot \text{H}_2\text{O}$ are stable in the presence of water [16]. However, the presence of a hydrated oxide as indicated in the above equations is more likely and in good agreement with the O/H ratio determined by the GDOES analysis.

The absence of fluorine and aluminium in the deposited oxide film contrasts findings in an earlier study of a no-rinse fluorotitanate based process [11]. This apparent discrepancy may be explained by the fact that, in no-rinse processing, a thin layer of solution is applied to the substrate, which is then dried without any rinsing to reduce the amount of effluent. Thus, all chemicals and reaction products remain on the surface in some form, including significant amounts of oxidised Al and F-containing compounds [11].

Since the conversion layer formation in the present process is controlled by local pH variations on the aluminium surface, the thickness and distribution of the deposit must be affected by stirring of the electrolyte. Increased stirring reduces the alkaline diffusion layer around the $-\text{Al}(\text{Fe},\text{Mn})\text{Si}$ particles, thereby restricting the zone where the pH is high enough to allow deposition of a continuous conversion layer, as shown in Figure 3. Increasing the pH of

the conversion bath from 2.9 to 4.0 has the opposite effect, as increased bulk pH of the conversion solution facilitates the build-up of an alkaline diffusion layer around the particles. The resulting oxide deposition on the - Al(Fe,Mn)Si particles appears to have only a limited inhibiting effect on the cathodic activity of the particles, according to the electrochemical measurements (Figure 12). Persistent cathodic activity on the particles therefore causes a significant rise in pH and extensive oxide film deposition, particularly under stagnant conditions.

Deposition of the Ti-Zr based conversion layer as a result of local alkalisation at cathodic sites is similar to the mechanism described for the rare earth conversion coatings [17]. This mechanism is fundamentally different from chromating, which involves a *redox reaction* between hexavalent chromate ions in the solution and aluminium resulting in the formation of a hydrated chromium oxide conversion coating on the aluminium matrix, and significantly thinner film on the intermetallic particles. Contrary to chromating, the nature of the Ti-Zr oxide layer forming process implies considerable variations in the extent of deposition on different alloy substrates. This variability is due to changes in the area fraction, size and distribution of intermetallic phases in the surface. Moreover, the cathodic activity of different types of intermetallic particles may vary significantly. For aluminium alloys in the 1000, 3000, 5000 and 6000 series the cathodic particles present are predominantly Fe containing compounds. The Fe impurity level in these alloys is therefore expected to influence the coating weight obtained for a given process. In general, a better understanding of how substrate microstructure, bulk pH and convection of the conversion solution affect the extent and distribution of Ti-Zr oxide deposition is required. In order to achieve this, use of rotating disc electrodes would seem appropriate to control the flow conditions at the surface.

For a reliable characterisation of the non-uniform conversion layers and heterogeneous composition of the surface oxide resulting from Ti-Zr based pre-treatment, surface analytical methods with high lateral resolution are required. In particular, field emission SEM can be very useful in documenting the morphology of the deposited oxide films, as demonstrated by the observation of a particulate type of structure in apparently un-coated areas on the surface. The formation and significance of this particulate structure with respect to performance of coated or adhesive bonded joints should be addressed in future work, as it constitutes a major fraction of the pre-treated surface.

CONCLUSIONS

Ti-Zr conversion layers normally form by deposition at and in the vicinity of cathodic -Al(Fe,Mn)Si particles on AA6060 aluminium. The deposition is a result of local alkalisiation at these sites due to oxygen reduction and hydrogen evolution. The conversion layers formed consequently exhibit considerable lateral variations in thickness.

Reducing the bulk pH or increasing the convection in the conversion bath inhibits growth of this layer. These parameters, in addition to surface microstructure, are therefore important in controlling the extent of layer deposition and its distribution over the surface.

The cathodic activity of the particles is only slightly reduced by formation of the conversion coating. In general, the electrochemical behaviour of AA6060 in 0.1 M NaCl solution is not significantly influenced by the Ti-Zr based pre-treatment. Hence, these conversion coatings are not expected to improve the corrosion resistance of aluminium significantly.

On areas away from the cathodic -Al(Fe,Mn)Si particles, as well as on the iron-free AlMg0.5Si0.4 alloy, a high density of small (< 50 nm) oxide particles are deposited, presumably with a composition similar to the continuous conversion layer. Adhesive properties of such coating morphology require further study.

ACKNOWLEDGEMENTS

The EPMA analyses were performed by M. Raanes at the Norwegian University of Science and Technology. The GDOES analysis was performed at the Swedish Institute for Metals Research in Stockholm, and XPS results obtained by S. Jørgensen, University of Oslo. The AES analysis was performed by P. Mack, Thermo VG Scientific, England. This work was funded by the Norwegian Research Council.

REFERENCES

1. J. H. Nordlien, J. Walmsley, H. Østerberg and K. Nisancioglu, *Surface and Coatings Technology*, **153**, 72 (2002).
2. L. F. Mondolfo, *Aluminium Alloys: Structure and Properties*, Butterworths, London (1976).
3. K. Nisancioglu, *J. Electrochem. Soc.*, **137**, 69 (1990).
4. H. Leth-Olsen, Dissertation, Norwegian University of Science and Technology, Trondheim (1996).
5. A. E. Hughes, R. J. Taylor, K. J. H. Nelson, B. R. W. Hinton and L. Wilson, *Materials Science and Technology*, **12**, 928 (1996).
6. G. M. Brown, K. Shimizu, K. Kobayashi, G. E. Thompson and G. C. Wood, *Corrosion Science*, **33**, 1371 (1992).
7. P. D. Deck, M. Moon and R. J. Sujdak, *Progress in Organic Coatings*, **34**, 39 (1998).
8. T. Schram, G. Goeminne, H. Terryn, W. Vanhoolst and P. Van Espen, *Trans I.M.F.*, **73**, 91 (1995).
9. A. Nylund, *Aluminium Transactions*, **2**, 121 (2000).
10. M. A. Smit, J. M. Sykes, J. A. Hunter, J. D. B. Sharman and G. M. Scamans, *Surface Engineering*, **15**, 407 (1999).
11. P. D. Deck and D. W. Reichgott, *Metal Finishing*, **90**, 29 (1992).
12. L. Fedrizzi, F. Deflorian and P. L. Bonora, *Electrochimica Acta*, **42**, 969 (1997).
13. K. Nisancioglu, O. Lunder and H. Holtan, *Corrosion*, **41**, 247 (1985).
14. E. H. Hollingsworth and H. Y. Hunsicker, in ASM Handbook, Vol 13: Corrosion, ASM International (1987).
15. O. Lunder and K. Nisancioglu, *10th European Corrosion Congress*, Barcelona, 1993. Progress in the Understanding and Prevention of Corrosion, J. M. Costa, A. D. Mercer (eds.), **1**, 1249, The Institute of Materials, London (1993).
16. M. Pourbaix, *Atlas of Electrochemical Equilibria in Aqueous Solutions*, CEBELCOR, Brussels (1974).
17. A. E. Hughes and K. J. H. Nelson, *Interfinish 96 World Congress*, Birmingham (1996).

Chapter 5 is not included due to copyright

6. Pre-treatment of AA6060 aluminium alloy for adhesive bonding*

O. Lunder^{1,2}, B. Olsen² and K. Nisancioglu²

¹SINTEF Materials Technology, N-7465, Trondheim, Norway

²Norwegian University of Science and Technology, Department of Materials Technology and Electrochemistry, N-7491, Trondheim, Norway

ABSTRACT

AA6060-T6 aluminium extrusions have been subjected to various surface treatments before bonding with an epoxy based adhesive and subsequent exposure to chloride and humid atmosphere (82 % RH, 40°C) for 50 days. Single lap joints given an alkaline etch pre-treatment before bonding suffered a 7 % reduction in strength as a result of environmental exposure. Desmutting in nitric acid after a similar alkaline etch pre-treatment to remove the Mg rich hydroxide film resulted in still higher loss in strength. Application of an experimental phosphate-permanganate conversion coating to the alkaline etched substrate also had no beneficial effect. Examination of the bonded surfaces after lap shear testing revealed the presence of filiform corrosion (FFC) filaments, providing paths for rapid ingress of moisture to the substrate/adhesive interface. The best results were obtained by AC anodising in hot sulphuric acid to a film thickness of about 0.2 µm.

INTRODUCTION

The use of adhesive bonded aluminium joints for automotive applications has several advantages in comparison with other joining techniques. Dissimilar materials can be bonded with a reduced risk of galvanic corrosion, and better control of tolerances is obtained since distortion resulting from the heat of welding is avoided. Other benefits include improved stiffness, rigidity, impact behaviour and energy absorption, less vibration and sound deadening [1]. However, a major concern is deterioration of the mechanical performance of the joints as a result of exposure to a wet and corrosive environment. The pre-treatment of the aluminium substrate is essential in this respect [2,3].

* Published in *Int. Journal of Adhesion and Adhesives*, **22**, 143 (2002).

In order to obtain a strong and stable bond between the metal and the adhesive, the naturally formed surface oxide on aluminium has to be removed and replaced with a new, continuous, solid and corrosion resistant oxide layer. The most successful and widely used treatments in the aerospace industry all use hexavalent chromium in their processing, and phosphoric acid anodising (PAA) or chromic acid anodising (CAE) are essential steps in the pre-treatments. For automotive applications, simpler, cheaper and more environmentally friendly processes are required.

In the present work, AA6060-T6 extrusions have been subjected to various chrome-free pre-treatments, including thin film AC anodising in hot sulphuric acid, alkaline etching and a phosphate-permanganate conversion coating. A chromic-sulphuric acid pre-treatment (FPL etch), commonly used for bonding of aluminium, was included as a reference. Hot AC anodising is a process developed to prepare aluminium strip or sheet for painting on a continuous basis. However, the method should be of interest also as a batch pre-treatment process. In addition to being chrome-free, no degreasing or etching stage is necessary due to the cleaning action of hydrogen evolved from the surface during the cathodic cycle of the AC current. Thus, processing time is very short.

Degradation of adhesive joints is associated with diffusion of water to the adhesive/substrate interface causing hydration of the oxide conversion coating and loss of adhesive strength. A moderate temperature increase, which in the absence of water does not have an adverse effect on a structural joint, leads to a much more pronounced loss in strength. Presence of chloride ions is further expected to accelerate the loss of adhesion, e.g., by propagation of localised corrosion of the metal beneath the adhesive. Earlier unpublished work at our laboratories has indicated that filiform corrosion (FFC) could be an important factor in the degradation of adhesive joints in corrosive environments. Hence, we have presently chosen to expose the adhesive joints in a climate chamber under conditions known to promote FFC on aluminium.

EXPERIMENTAL

The adherends used were aluminium AA6060-T6 (composition by weight 0.40%Si, 0.46% Mg, 0.18%Fe, 0.021%Mn, 0.002%Cu, 0.015%Zn, 0.01%Ti, Al balance) which were cut from extrusions (width 80 mm, thickness 2 mm and with 0.2 mm ridges on one side) into coupons 125 mm in length. After surface treatment the coupons were assembled into single lap shear joints with

20 mm overlap in which a ridged surface was pressed against a flat surface. The adhesive used was a commercial epoxy based structural adhesive, Betamate XD4600 from Gurit-Essex. Curing was performed for 30 min at 180°C in an air circulation furnace. Metallic clips were used to keep the two coupons together during curing, the extrusion ridges providing a uniform glue line with thickness 0.2 mm. Three replicates of all joints were prepared. The following surface pre-treatments were employed prior to bonding:

1. AC anodising of the as-received extrusions in hot (80°C) 15% sulphuric acid at a current density of 10 A/dm² (rms) for 4 s, rinsing under tap then distilled water, and drying in hot air.
2. As pre-treatment 1, but with anodising time of 12 s.
3. Degreasing in acetone, then etching in 10wt% NaOH solution for 50 s at 60°C, rinsing under tap then distilled water, and air drying.
4. As pre-treatment 3, but with a 15 s de-smutting in concentrated nitric acid following the alkaline etch.
5. As pre-treatment 3, but with a 15 s de-smutting in 15wt% sulphuric acid + 2vol% nitric acid following the alkaline etch.
6. Pre-treatment 3 followed by conversion coating in phosphate permanganate solution (100 g/l NaH₂PO₄, 30 g/l KMnO₄ and 0.5 g/l NaF adjusted to pH2 with sulphuric acid) for 3 min at 60°C, rinsing under tap and distilled water, and air drying.
7. FPL etch pre-treatment: Degreasing in acetone, hot water rinse, immersion in FPL etch solution (16.3vol% H₂SO₄, 6wt% Na₂Cr₂O₇) for 20 min at 60°C, 20 min rinse under tap water, drying with hot air stream.

Adhesive bonding was carried out within 3 h of the FPL pre-treatment, and within 48 h of pre-treatments 3-6. The AC anodised samples were stored for two weeks in ambient laboratory air before bonding.

Ageing of the lap joints was performed by exposure for 50 days in climate chamber at 82%RH and 40°C, corresponding to standard conditions employed in filiform corrosion testing (DIN EN 3665). Initiation of pitting corrosion, eventually leading to FFC at the substrate/adhesive interface, was accomplished by placing a few drops of 16% HCl solution along one of the lap joint edges for about 10 min before excessive liquid was removed and the joints transferred to the climate chamber. Tensile testing was performed within 2 h after completion of the FFC test on an automated 500 kN capacity Instron machine. The initial jaw separation was set at 100 mm, and a cross-head speed of 10 mm/min was used.

Electrochemical behaviour of pre-treated surfaces was evaluated by use of potentiodynamic polarisation experiments in aerated 0.1 M NaCl solution at room temperature. Shortly after immersion in the electrolyte, the specimens were polarised to $-1.0 V_{SCE}$ and the potential swept in anodic direction to $-0.5 V_{SCE}$ at a rate of 10 mV/min. Five replicates of each pre-treatment were examined, each with an exposed area of 1.33 cm^2 .

Topography and composition of pre-treated surfaces was analysed using SEM, AFM (contact mode) and GDOES, glow discharge optical emission spectroscopy [4]. GDOES combines sputtering and atomic emission to provide an extremely rapid technique for element depth profiling. During operation, a plasma is generated in the analysis chamber by the applied voltage between the anode and the cathode (the sample) in presence of argon under low pressure. Ionised Ar atoms cause sputtering of the sample area. Sputtered atoms excited in the plasma rapidly de-excite by emitting photons with characteristic wavelengths. The sensitivity of the method is at the ppm level due to the relatively large area analysed, in this case 4 mm in diameter. Measurements were conducted at the Swedish Institute for Metals Research, where a method for quantitative depth profile analysis has been developed based on the concept of emission yield and compensation for variations in excitation parameters [5].

RESULTS AND DISCUSSION

Surface characterisation of pre-treated surfaces

Typical surface morphologies of pre-treated surfaces are shown by SEM micrographs in Figure 1 and by AFM surface plots in Figure 2. The as-extruded surface exhibits a directional topography in the extrusion direction. This topography is essentially retained after AC anodising (pre-treatments 1-2) since the oxide film thickness is considerably smaller than the transverse roughness of the profile. Alkaline etching under the present conditions removes about $5 \mu\text{m}$ of metal and much of the directionality. In addition, a scalloped surface is formed (pre-treatments 3-6). After FPL etching (pre-treatment 7) scallops are also observed, but of a considerably smaller size than those formed during alkaline etching, in agreement with earlier work [6]. FPL etching removes about $1 \mu\text{m}$ of the surface, and directionality of the topography is largely retained also in this case. On a micrometre scale, the

FPL etched surface is considerably rougher than that obtained after AC anodising in hot sulphuric acid.

Quantitative GDOES depth profiles of the pre-treated surfaces are shown in Figure 3. Profiles for the AC anodised specimens agree fairly well with oxide film thickness results obtained from gravimetric measurements, shown in Table 1, and TEM examination (Figure 4). Increasing the anodising time from 4 to 12 seconds does not result in a threefold increase in film thickness due to simultaneous film formation and dissolution during anodising at elevated temperatures. Oxide film thickness of the etched surfaces estimated from the GDOES profiles are also shown in Table 1. As expected, these films are considerably thinner than the AC anodised films, particularly the ones given a final acid etch (desmuted and FPL etched specimens).

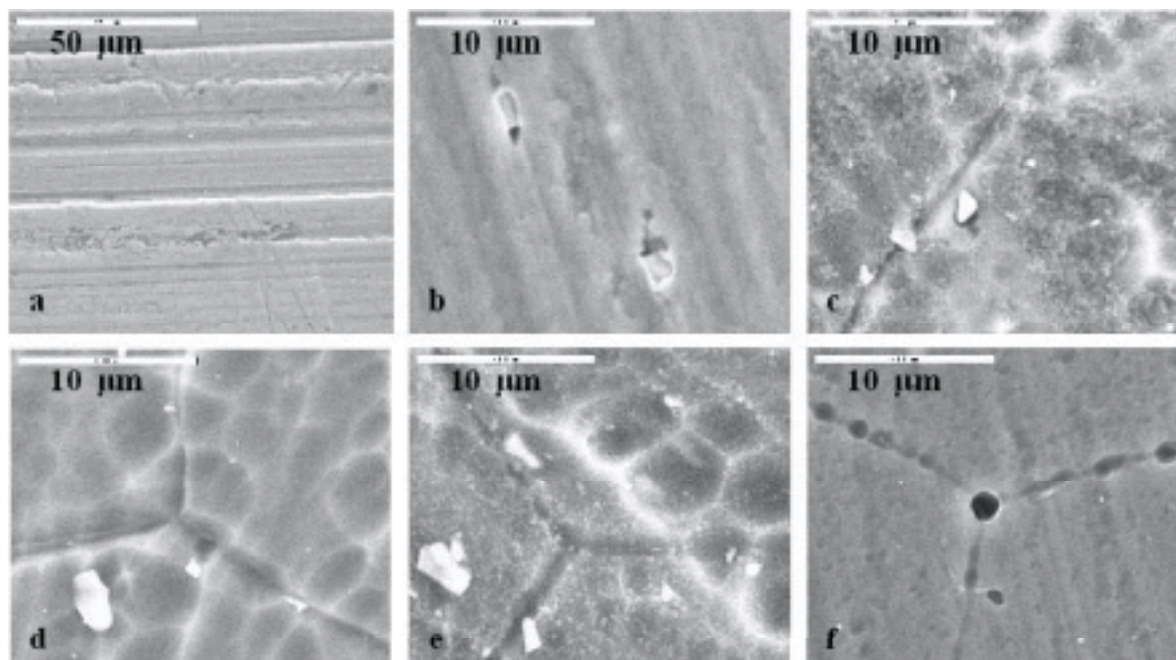


Figure 1. SEM micrographs of extruded aluminium AA6060-T6. a) Degreased, b) Hot AC anodised for 12s, c) NaOH etched, d) NaOH etched and desmuted in nitric acid, e) Phosphate-permanganate treated, f) FPL etched. Particles protruding from the surface in b, c, d and e are Fe rich intermetallic phases.

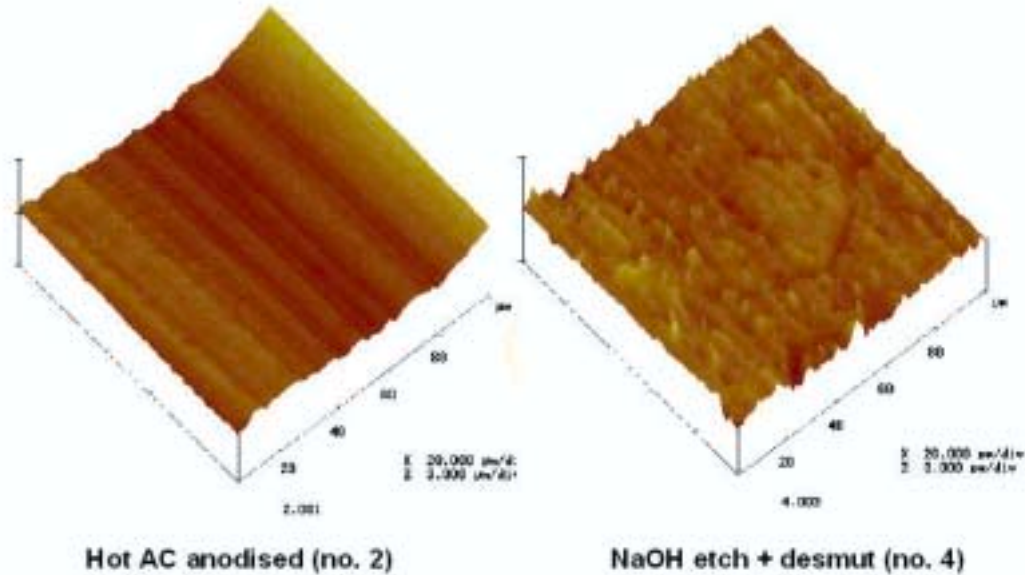


Figure 2. AFM images of AA6060-T6 surfaces after pre-treatments 2 and 4.

Table 1. Aluminium metal removed by the different pre-treatments and approximate thickness of conversion oxide films based on gravimetric measurements. Numbers in italics are estimated from GDOES profiles.

	Pre-treatment	Metal removed (μm)	Oxide thickness (μm)
1	Hot AC anodising (4s)	0.08	0.10
2	Hot AC anodising (12s)	0.24	0.22
3	NaOH etch	5	<i>0.01</i>
4	NaOH + desmut in nitric acid	5	<i>0.002</i>
5	NaOH + desmut in sulphuric acid	5	<i>0.002</i>
6	Phosphate permanganate	5	<i>0.02</i>
7	FPL etch	1	<i>0.004</i>

According to the GDOES results the AC anodised films contain about 15% S, and a significant amount of carbon (Figure 3a and 3b). Presence of sulphur is expected in sulphuric acid anodised films [7]. Some carbon contamination (e.g. adsorbed CO₂ from the atmosphere) is always detected, and carbon is in this case present throughout the oxide film because of its porous nature. It should also be noted that a significant Si enrichment is detected in the outer part of the oxide film.

Alkaline etching causes formation of a “smut” layer rich in Mg hydroxide. The Mg concentration is of the order 10%, i.e. a factor 20 higher than in the bulk metal (Figure 3c). A similar enrichment of Si is observed, and a more moderate enrichment of Fe and Mn (not shown in Figure 3) due to selective dissolution of Al from the Fe containing intermetallic particles [8]. By desmutting practically all Mg is removed regardless of whether nitric or sulphuric acid is used, whereas a Si concentration of nearly 10% remains in the oxide (Figure 3d and 3e).

The phosphate-permanganate treated surface exhibited a golden-brown colour, indicative of the transformation of initially applied Mn (VII) to manganese dioxide, Mn (IV). The GDOES profiles indicate a conversion layer of about 20 nm in thickness and with a non-uniform composition judging from the shapes of the P and Mn profiles (Figure 3f). The Mg concentration is very low, while significant Si enrichment is found in the outer part of the conversion film.

The FPL etched surface exhibits a very thin oxide, with significant amounts of S and C present (Figure 3g). No Mg enrichment is observed due to the low pH of the etching solution. The Cr concentration in the oxide is only about 1%.

Quantitative GDOES depth profiles were obtained to a depth of 2-3 µm into the metal. Bulk concentrations in the ranges 0.40-0.43%Mg, 0.31-0.36%Si, 0.15-0.17%Fe and 0.026-0.029%Mn were obtained. This is in good agreement with the alloy composition as determined from spectrographic analysis.

6. Pre-treatment of AA6060 aluminium alloy for adhesive bonding

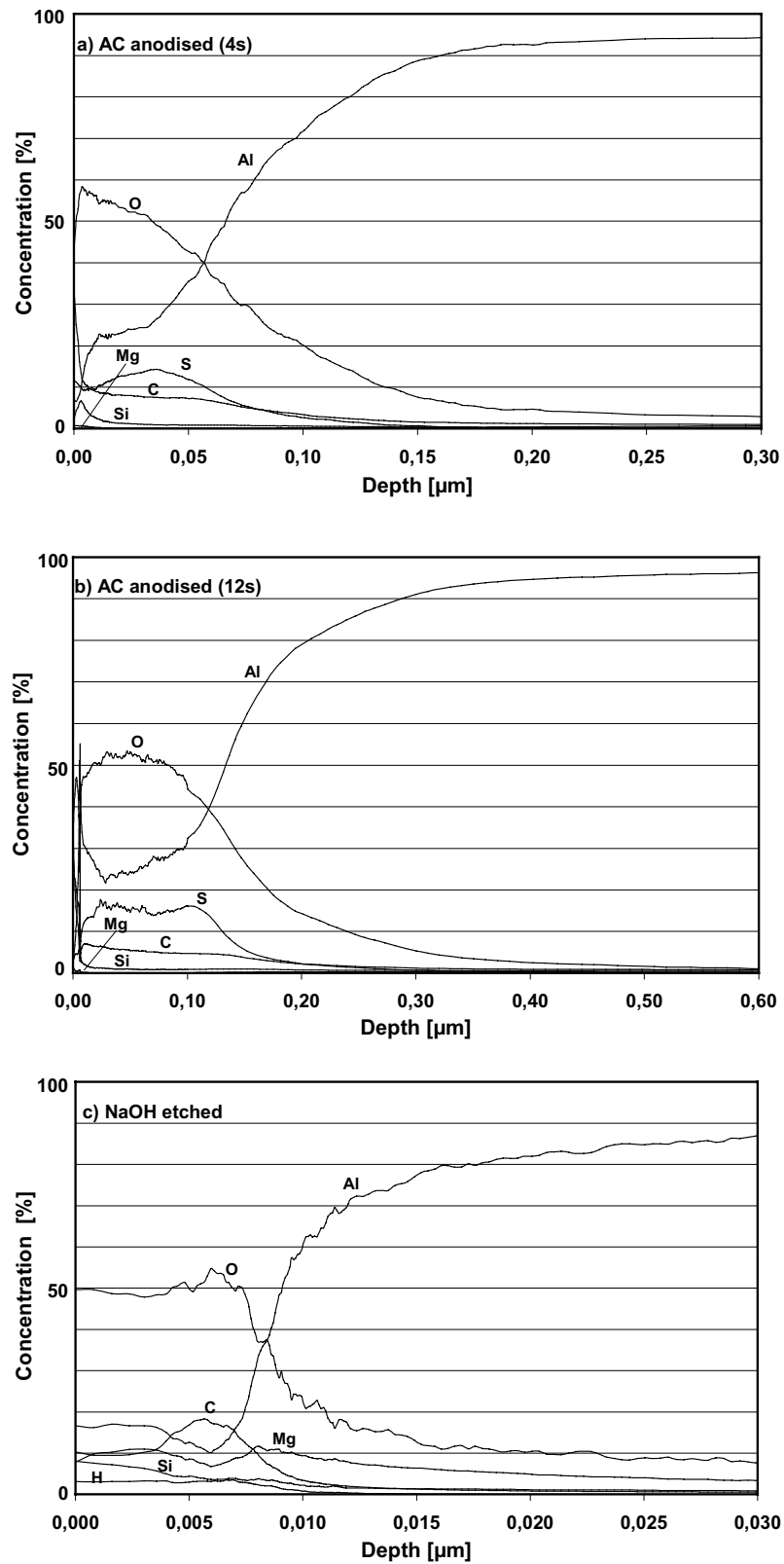


Figure 3. GDOES depth profiles of pre-treated surfaces. a) Hot AC anodised for 4s, b) Hot AC anodised for 12s, c) NaOH etched.

6. Pre-treatment of AA6060 aluminium alloy for adhesive bonding

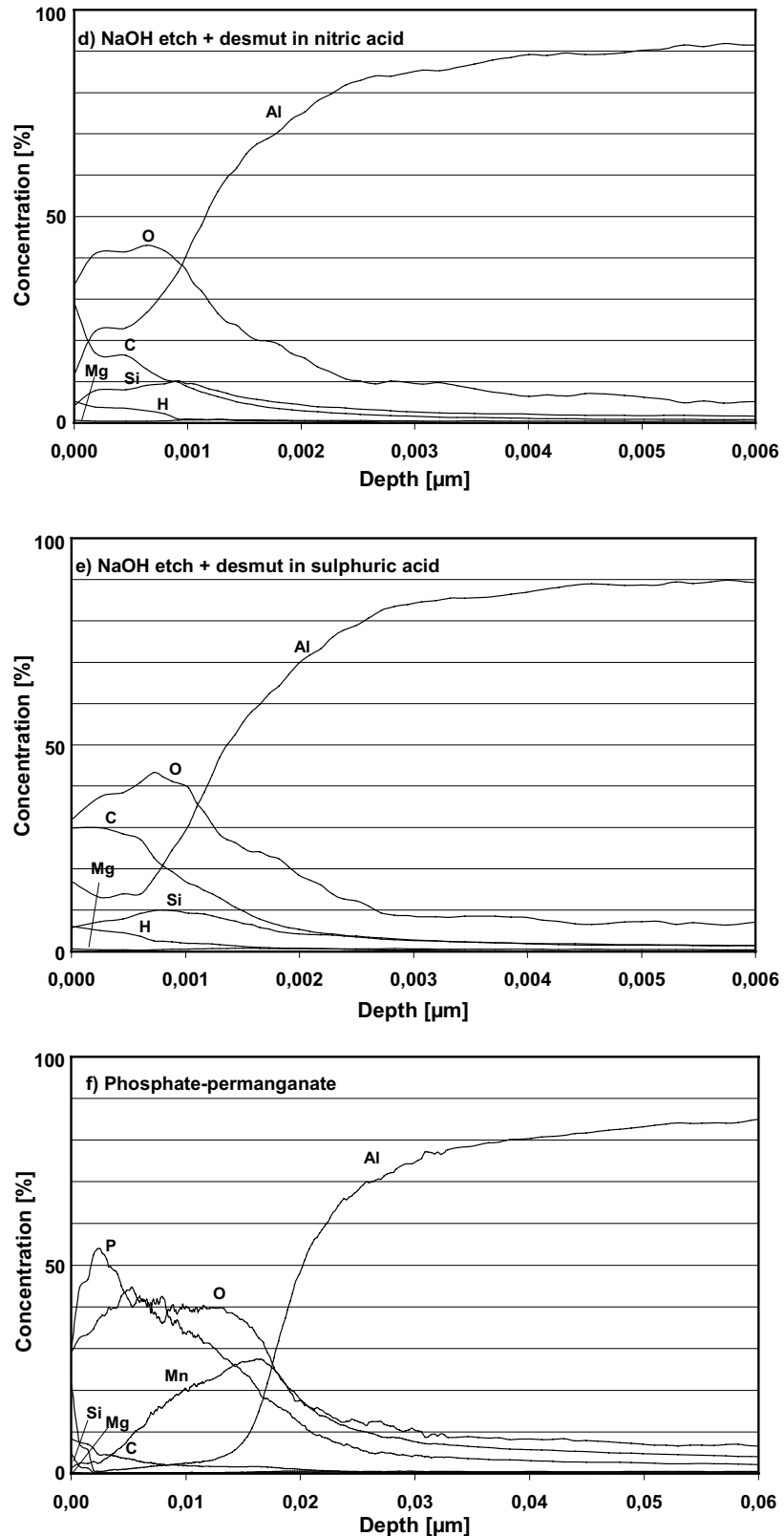


Figure 3. (cont.) GDOES depth profiles of pre-treated surfaces. d) NaOH etched and desmuted in nitric acid, e) NaOH etched and desmuted in sulphuric acid, f) Phosphate-permanganate treated.

6. Pre-treatment of AA6060 aluminium alloy for adhesive bonding

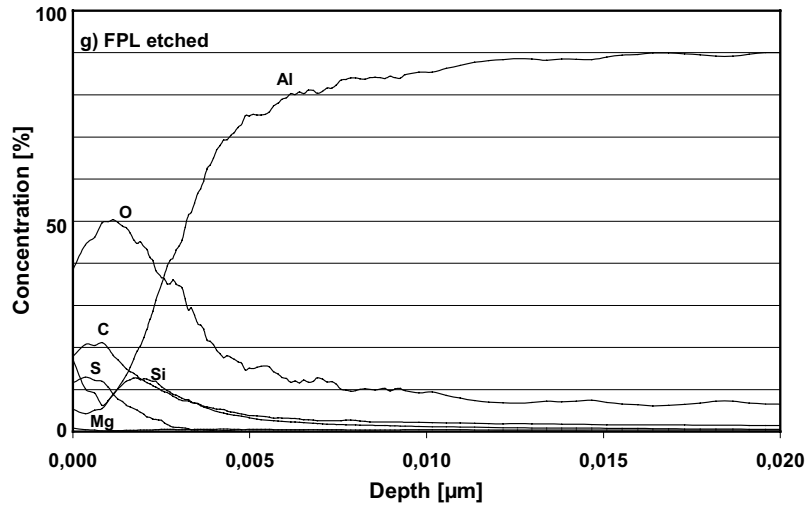


Figure 3. (cont.) GDOES depth profiles of FPL etched surface.

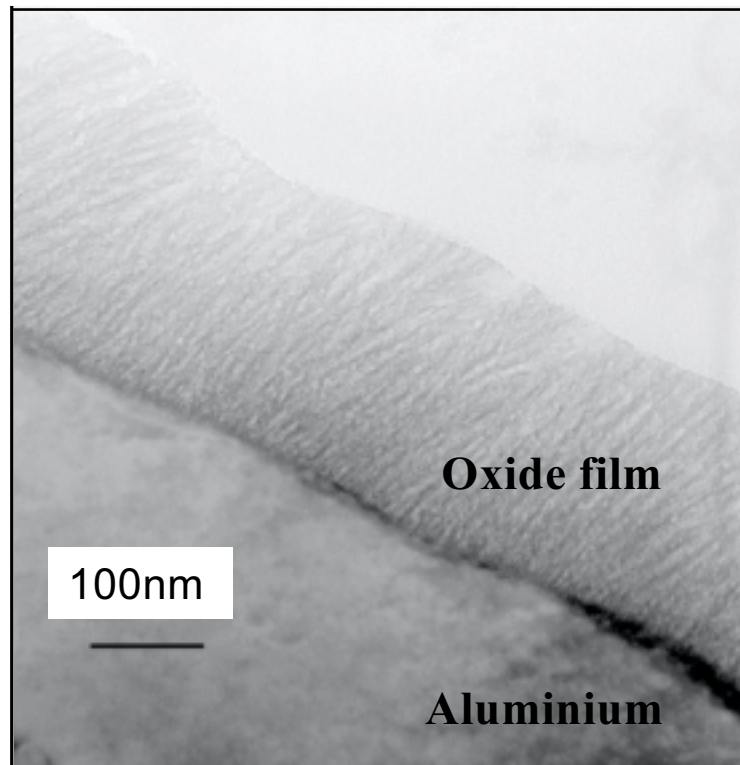


Figure 4. TEM image of hot AC anodised film, pre-treatment 2.

Electrochemical behaviour of pre-treated surfaces

Polarisation curves of pre-treated AA6060-T6 specimens are shown in Figure 5. The phosphate-permanganate treated surface exhibits a reduced cathodic reaction rate compared with the other pre-treatments, presumably due to partial coverage of the Fe containing phases by the conversion coating. By alkaline etching (pre-treatments 3-5) the cathodic current densities are increased relative to the degreased surface. This is most likely a result of surface modification as well as an increase in the effective area of these intermetallics [8]. The fact that AC anodised and etched surfaces exhibit similar cathodic polarisation behaviour indicate that an insulating oxide film is not formed on the Fe rich particles during the short anodisation period employed, as might be inferred also from the SEM observations, Figure 1b.

As expected, the thin oxide film formed on the matrix of AC anodised surfaces clearly leads to a reduced current density during anodic polarisation. Thus, while pre-treatment 6 appears to provide some corrosion protection by inhibiting the cathode reaction, AC anodising improves the corrosion resistance by reducing the anodic reaction rate. Another evidence for the improved corrosion resistance obtained by the AC anodising pre-treatment is a significant reduction in the hydrogen evolution rate observed visually during inoculation of lap joints with HCl solution.

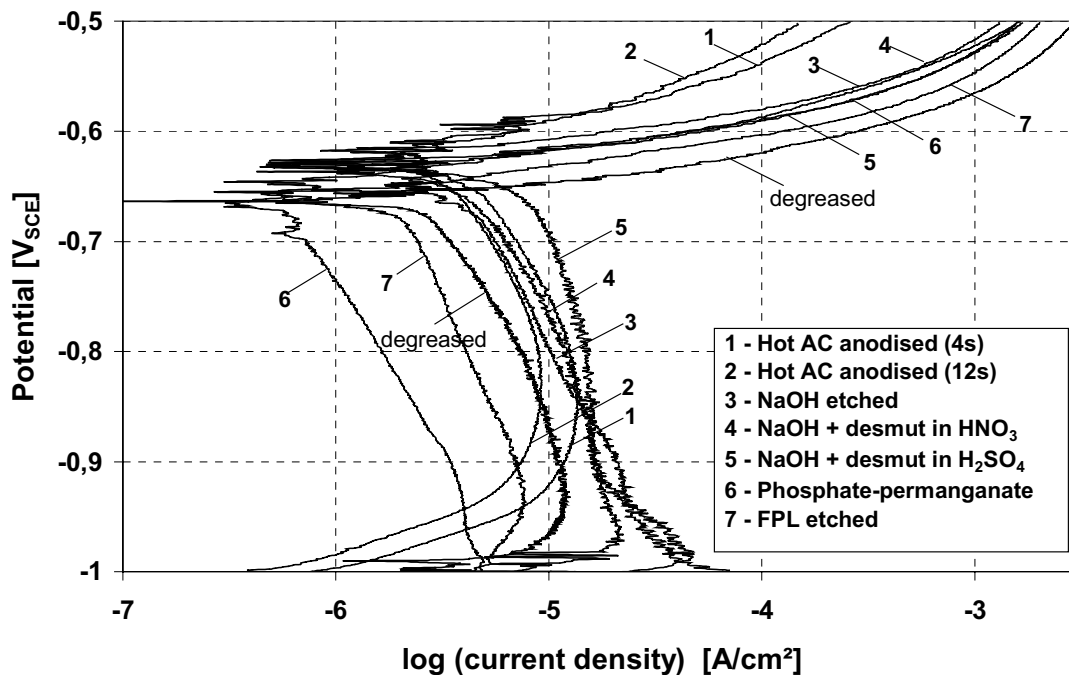


Figure 5. Polarisation curves for pre-treated AA6060-T6 in aerated 0.1 M NaCl solution. Each curve is the average of five replicate specimens.

Tensile strength of lap joints

The use of single lap joints is a convenient test geometry that is simple and representative of commonly used joint designs in industry. However, the stresses generated in the adhesive layer are not uniform. Eccentricity of the tensile axis of a single lap joint gives rise to transverse or peel stresses. The peel stresses are most significant at the ends of the overlap joint and constitute a major factor in the fracture of lap joints, i.e., by enabling cracks to initiate and propagate from the ends of the overlap [3].

As the true shear strength is not readily obtained from such experiments, the tensile test results of the lap joints are given in terms of maximum load in Figure 6. The results show hardly any degradation of hot AC anodised (pre-treatments 1 and 2) and FPL etched (pre-treatment 7) specimens as a result of the climate chamber exposure. A significant reduction in joint strength is observed for the alkaline etched specimens (pre-treatment 3), and the relative strength loss is further increased when specimens are desmuted after alkaline etching (pre-treatments 4 and 5). Application of the phosphate-permanganate conversion coating (pre-treatment 6) after alkaline etching results in still poorer results, both in terms of initial strength and degree of degradation.

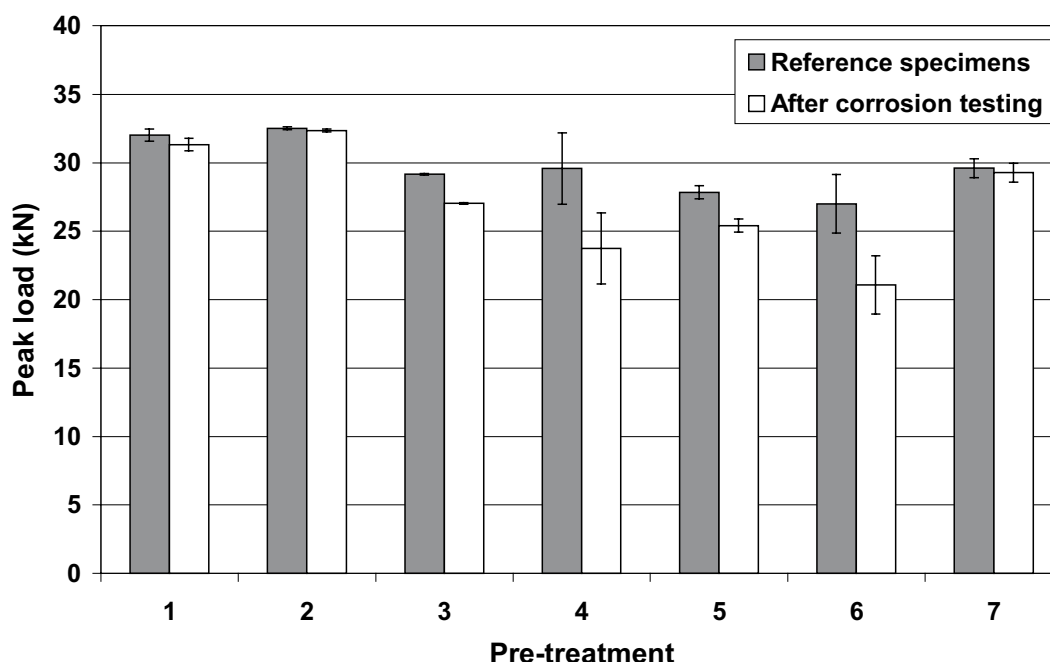


Figure 6. Tensile test results obtained for adhesive bonded AA6060-T6 single lap joints before and after exposure in climate chamber (82%RH, 40°C, 50 days). Error bars indicate standard deviation for three replicate specimens.

In a previous investigation at our laboratory [9] it was shown that degreasing with acetone as a pre-treatment resulted in a 85% loss in strength when using a similar substrate alloy, adhesive, joint design and test conditions. Hence, alkaline etching is superior to degreasing in terms of bond durability. It was further observed that desmutting after alkaline etching had a significant detrimental effect on the joint durability, in agreement with the present results. The GDOES profiles of the elements Al, Mg, O and H in Figure 3 indicate that the alkaline etched surface exhibits a mixture of Al and Mg hydroxides, which are removed by desmutting. It has been suggested that a high MgO concentration in the oxide layer is unfavourable for the bond durability [3,10-12]. A general correlation between Mg surface concentration and poor joint durability is obviously not supported by the present results. Whether Mg is present as an oxide or a hydroxide is probably of significance. The Mg enriched oxide formed as a result of heat treatment may be more susceptible to hydration and subsequent delamination than the Mg rich hydroxide formed as a result of alkaline etching. The issue is worth further investigation.

The adhesive type is probably also important in determining the effect of Mg surface concentration on bond durability. The adhesive used in the present work contains dicyandiamide as a curing agent. It has been reported that epoxies which are hardened with dicyandiamide may react with water to form products that are strongly alkaline in nature [13] and consequently tend to destabilise the aluminium oxide. However, presence of Mg oxide in the aluminium oxide film is expected to improve the stability in alkaline environment due to the fact that Mg oxides are thermodynamically passive at high pH. Thus, the reduced durability observed presently as a result of Mg removal by desmutting may be rationalised.

The so-called STAB (3) treatment [14], involving a dip in highly concentrated NaOH solution followed by a hard spray rinse in de-ionised water, also leaves a surface film with high Mg concentration on AA2024-T3 aluminium. Bonding with dicyandiamide containing epoxies still gives durability results comparable to standard FPL etching [14]. On the other hand, the results obtained by Kinloch and Smart [10,11] suggesting an adverse effect of Mg on joint durability were obtained using a phenolic-based adhesive. The pH of residues from phenolic-based adhesives is generally acid [3]. As Mg oxides dissolve readily in acid solutions the presence of Mg in the aluminium oxide film in this case should have an unfavourable effect, if any. Whether there is a general correlation between Mg surface concentration, pH of the adhesive and joint durability has yet to be established, though.

Examination of fracture surfaces

Examples of the macroscopic appearance of fracture surfaces after tensile testing of corroded lap joints are shown in Figure 7. On hot AC anodised specimens (pre-treatment 1, Figure 7a) discoloration of the substrate shows that a fairly uniform corrosion front has propagated about 5 mm under the joint area, starting from the edge of the lap joint where HCl was inoculated. There appears to be a region of adhesive failure ahead of the corrosion front, a region of cohesive failure in the middle of the joint, and then an adhesive failure region again as the fracture crosses over to the other interface towards the opposite overlap edge. All specimens exhibit a similar failure mode pattern as a result of the peel forces acting predominantly at the ends of the overlap joints, but there are characteristic differences in corrosion behaviour and degree of adhesive failure depending on the pre-treatment. For example, by increasing the AC anodising time to 12 s the corrosion resistance is improved significantly and virtually no corrosion occurred on these specimens during the test period. On all the other variants, corrosion of the substrate propagated some 4-7 mm under the overlap joint. While alkaline etched and desmutted specimens exhibit a more or less uniform corrosion front, FFC primarily occurred on the NaOH etched, phosphate-permanganate coated (pre-treatment 6, Figure 7b) and FPL etched specimens.

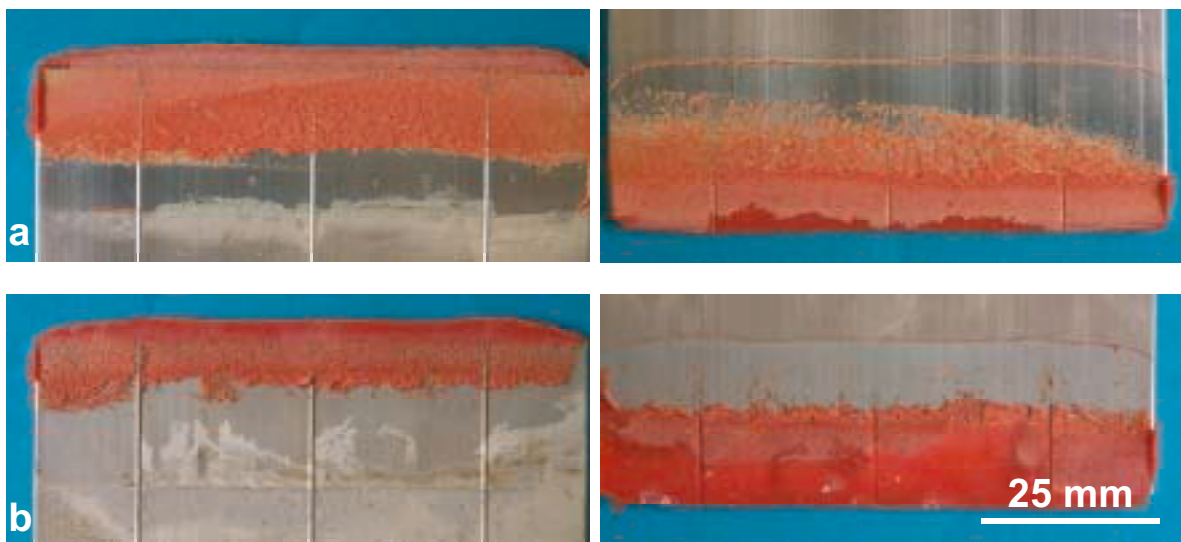


Figure 7. Appearance of fractured surfaces after tensile testing of corroded lap joints. a) Hot AC anodised surface displaying a relatively uniform corrosion front (bright region, left image). b) Phosphate-permanganate coated surface showing significant FFC in adhesive failure region.

Recent studies have shown [15,16] that FFC is predominantly controlled by the microstructural characteristics of very thin ($< 1 \mu\text{m}$) and heavily deformed metal surface layers on rolled sheet. The FFC susceptibility of extruded materials also appears to be significantly enhanced by presence of surface layers with different composition and microstructure than the bulk material [17]. The present results demonstrate, however, that FFC is not fully prevented by removal of about $5 \mu\text{m}$ of the substrate metal by alkaline etching. In corrosive, chloride-containing environments FFC may therefore play an important role in the degradation mechanism of adhesive bonded joints by providing paths for rapid ingress of moisture to the substrate/adhesive interface. Moreover, the formation of corrosion products at the joint interface is expected to result in transverse stresses that would further accelerate the loss of adhesion.

Figure 8 shows a correlation between the joint strength after corrosion testing and the extent of cohesive failure as assessed by visual examination of the fractured joints. As might be expected, the results indicate a higher degree of adhesive failure for the inferior pre-treatments, although surface analysis (*e.g.* AES or XPS) is required to identify precisely the locus of failure. Furthermore, the degree of adhesive failure is generally increased on all variants as a result of environmental exposure, also on the AC anodised joints (pre-treatment 2) where a negligible strength loss is observed.

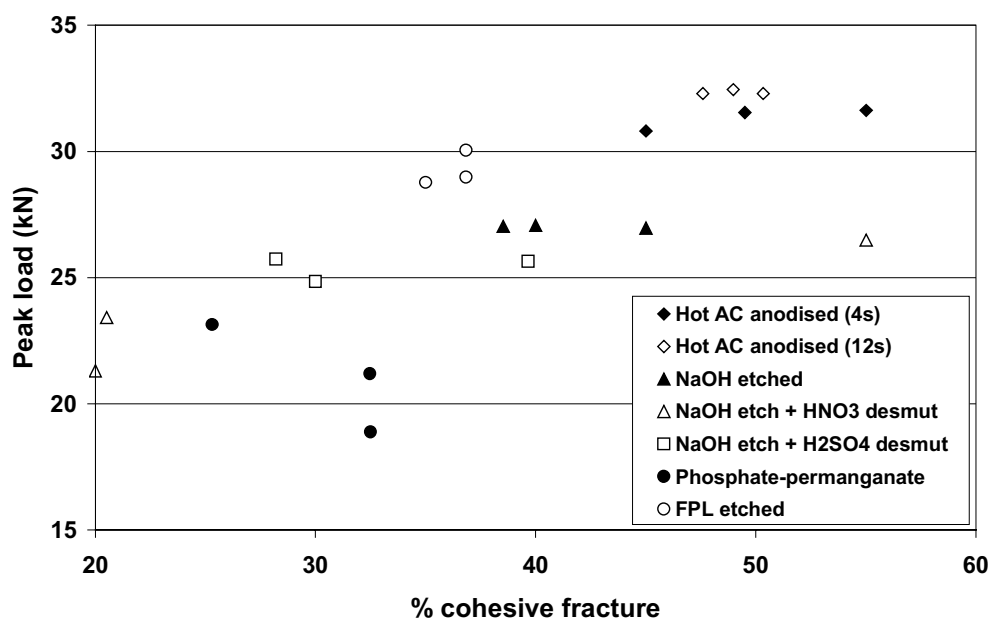


Figure 8. Correlation between (apparent) mode of fracture and peak load during tensile testing of corroded lap joints.

The phosphate-permanganate treated joints showed a high degree of adhesive fracture (about 70%) both before and after FFC testing. Hence, whether the significant loss in joint strength observed for these specimens can be attributed to a high FFC susceptibility cannot be ascertained, particularly since FFC propagates from the overlap edge where peel stresses are high during single lap shear testing. For more conclusive evidence on the role of FFC on joint durability, a different joint design or longer exposure times are required. Climate chamber tests performed in the absence of chlorides to avoid FFC may provide further insight into the role of corrosion on the degradation mechanism.

SUMMARY AND CONCLUSIONS

Surface characteristics and durability of adhesive bonded AA6060 aluminium alloy joints with different pre-treatments have been studied. The results indicate that thin film AC anodising in hot sulphuric acid is promising as a simple, very rapid and environmentally friendly pre-treatment for adhesive bonding. Hot AC anodised single lap joints subjected to standard filiform corrosion (FFC) test conditions exhibited no significant loss in strength after 50 days of exposure at 82% RH and 40°C. Reference FPL etched joints also showed no significant strength loss after similar exposure, but had a slightly lower tensile strength than AC anodised joints.

Pre-treatment of the AA6060 material by alkaline etching in hot NaOH solution resulted in the formation of a scalloped surface with a Mg enriched hydroxide film. A significant reduction in joint strength of about 7% was observed for these specimens as a result of corrosion testing. Desmutting in nitric or sulphuric acid to remove the Mg enriched hydroxide film resulted in still higher losses in strength. Application of a phosphate-permanganate conversion coating to the alkaline etched substrate also had no beneficial effect. However, all pre-treatments employed are superior to acetone degreasing alone.

Examination of fractured surfaces after tensile testing revealed evidence of FFC on the alkaline etched, phosphate-permanganate coated and FPL etched specimens. Corrosion filaments provide paths for ingress of moisture to the substrate/adhesive interface and corrosion products may also have contributed to loss of adhesion by creating transverse stresses. To what extent the rate of degradation of adhesive bonded joints is affected by FFC requires further investigation.

ACKNOWLEDGEMENTS

J. Walmsley, G. Pettersen and I. Lindseth at SINTEF Materials Technology are acknowledged for their assistance in undertaking the TEM, AFM and GDOES work, respectively. The GDOES analyses were conducted at the Swedish Institute for Metals Research, Stockholm, Sweden.

REFERENCES

- [1] Barnes TA and Pashby IR, *J. Materials Processing Technology*, **99**, 72 (2000).
- [2] Kozma L, Olefjord I, *Materials Science and Technology*, **3**, 860 (1987).
- [3] Kinloch AJ, *Adhesion and Adhesives*, Chapman and Hall, London (1987).
- [4] Payling R, *Materials Forum*, **18**, 195 (1994).
- [5] Bengtson A, *Spectrochimica Acta*, **49B**(4), 411 (1994).
- [6] Arrowsmith DJ, Moth DA, Vickery CM, *Trans. IMF*, **66**, 112 (1988).
- [7] Wernick S, Pinner R, Sheasby PG, *The Surface Treatment and Finishing of Aluminium and Its Alloys*, ASM International, Ohio (1987).
- [8] Lunder O, Nisancioglu K, *Corrosion*, **44**, 414 (1988).
- [9] Nordlien JH, *Unpublished results* (1999).
- [10] Kinloch AJ, Smart NR, *J. Adhesion*, **12**, 23 (1981).
- [11] Kinloch AJ, Bishop HE, Smart, NR, *J. Adhesion*, **14**, 105 (1982).
- [12] Rijkhoff MJ, Bleeker R, Bottema J, Proceedings of the *International Symposium on Aluminium Surface Science and Technology*, 125, Antwerpen (1997).
- [13] Brockmann W, Hennemann OD, Kollek H, Matz C, *Int. Journal of Adhesion and Adhesives*, **6**, 115 (1986).
- [14] Smith T, Proceedings of the *26th National SAMPE Symposium*, Los Angeles (1981).
- [15] Leth-Olsen H, Nordlien JH, Nisancioglu K, *J. Electrochem Soc*, **144**, L196 (1997).
- [16] Afseth A, PhD Thesis, Norwegian University of Science and Technology (1999).
- [17] Nordlien JH, Defrancq J, Züst W, Benmalek M, Stuckart R, *Materials and Corrosion*, **51**, 473 (2000).

6. Pre-treatment of AA6060 aluminium alloy for adhesive bonding

7. Effect of pre-treatment on the durability of epoxy-bonded AA6060 aluminium joints

O. Lunder^{1,2}, F. Lapique¹, B. Johnsen² and K. Nisancioglu²

¹ SINTEF Materials Technology, N-7465, Trondheim, Norway

² Norwegian University of Science and Technology,
N-7491, Trondheim, Norway

ABSTRACT

Extruded AA6060 aluminium has been subjected to various surface pre-treatments before application of a one component structural epoxy adhesive, XD4600. The durability of joints has been assessed by wedge adhesion and filiform corrosion (FFC) testing of panels coated with adhesive. A chromate-free Ti-Zr based pre-treatment provided improved durability relative to an alkaline etch and deoxidation pre-treatment, but was clearly inferior to chromating in terms of adhesion and FFC resistance. Excessive Ti-Zr oxide deposition occurred in the vicinity of intermetallic -Al(Fe,Mn)Si particles during pre-treatment, which significantly reduced the performance of bonded joints during wedge test. The intermetallics furthermore played a crucial role in promoting FFC, as demonstrated by complete FFC immunity of an AA6060 model analogue alloy (AlMg0.5Si0.4) free from -Al(Fe,Mn)Si particles. The Ti-Zr based pre-treatments provided limited protection against FFC on AA6060, apparently due to a limited effect of the Ti-Zr oxide conversion coating in reducing the cathodic activity of the intermetallic particles. In search for chromate-free pre-treatments for painted or adhesive bonded aluminium, inhibition of the cathodic activity on the Fe containing particles is suggested as an important factor to prevent FFC.

INTRODUCTION

Surface pre-treatment is an extremely important factor affecting the durability of adhesive bonded aluminium [1]. Although high initial strength may be obtained by removal of gross contamination [2], the pre-treatment of aluminium is crucial to reduce the rate of joint degradation in humid and hot environment, especially under stressed conditions. Water diffusion through the adhesive, and along the interface between the substrate and the adhesive [3], may cause hydration of the aluminium oxide on the adherend surface [4]

and promote adhesive failure. Presence of chloride ions may further accelerate loss of adhesion due to corrosion of the substrate. It has been pointed out that degradation of epoxy-bonded aluminium joints can occur by an alkaline as well as an acid failure mechanism [5]. The former is related to the influence of amines leaching from the epoxy and reacting with water to produce an alkaline medium, which destabilises the aluminium oxide at the adhesive-substrate interface. The latter is related to the “bondline corrosion” observed on high strength aluminium alloy joints [5]. However, corrosion of the substrate may occur also on more corrosion resistant aluminium alloy joints, *e.g.* under conditions promoting filiform corrosion (FFC) [6].

In order to obtain optimum durability of adhesive bonded aluminium joints, anodising processes are extensively used in the aerospace industry [7-10]. The oxides formed by chromic acid anodising (CAA) or phosphoric acid anodising (PAA) exhibit a higher resistance against hydration than the significantly thinner oxides formed by etch pre-treatment [8], and also provide some corrosion protection of the metal substrate. The porous structure of the anodised oxide films is favourable as low viscosity primers may fill the pores to form a “micro-composite” layer with an increased area for interfacial bonding compared to a planar surface [11,12]. Furthermore, the micro-composite layer has an intermediate stiffness compared with the low-modulus adhesive and the high-modulus aluminium alloy, which reduces local stress concentrations and contributes to the superior durability observed in environmental cyclic-fatigue tests [12].

Under less demanding conditions, simpler pre-treatments may be good enough. Chromate conversion coatings (CCC) have been successfully used for decades to improve corrosion resistance and provide adhesion to paints and adhesives. CCCs inhibit corrosion by reducing the activity of both cathodic and anodic sites on the aluminium surface, and exhibit self-healing behaviour due to storage and release of hexavalent Cr that interacts with bare metal and prevents pit initiation [13]. Moreover, the CCCs are inert, hydrophobic and stable over a broad pH range [14]. These factors are probably important in order to maintain excellent adhesion to paints and adhesives [9] in wet environments.

A number of different Ti-Zr based conversion coatings, often including a polymeric constituent, are commercially available as a more environmentally friendly alternative to the chromate based treatments. The Ti-Zr conversion coatings may be applied by dipping, spraying or no-rinse processes. The films formed are of the order 10-50 nm in thickness [15-17] and generally exhibit inferior corrosion resistance in comparison with the CCCs [18].

However, the performance of painted AA6063 aluminium subjected to Ti-Zr based pre-treatments appeared to be significantly affected by the choice of polymer in the conversion bath [19]. Stressed durability testing of epoxy bonded aluminium showed that Zr based treatments performed similarly to a chromate-phosphate treatment [20]. Ti-Zr based processes have also performed relatively well in cyclic stress durability tests [10], although the aerospace PAA treatment is yet unrivalled under such conditions.

Recent work [21,22] has shown that the presence of cathodic intermetallic particles on the aluminium surface promoted deposition of Ti-Zr based conversion coatings. Preferential deposition occurred at the particles since precipitation of Ti and Zr oxide was favoured by the increased pH developing at these sites as a result of cathodic activity. Hence, under similar coating conditions, significant differences in coating weight may be obtained on different aluminium alloys [22]. Limited information is available in the accessible literature on the relationship between Ti-Zr conversion coating weight and durability of adhesive bonded joints. However, for painted AA3105 aluminium subjected to Ti-Zr based no-rinse pre-treatments it has been generally observed that “adhesion is enhanced at lower coating weights, while corrosion resistance is improved with higher coating weights, provided adhesion is sufficient” [15].

The purpose of this work is to examine the influence of a Ti-Zr based pre-treatment on durability of epoxy-bonded AA6060 aluminium extrusions. Specifically, the influence of coating weight on durability is addressed. Uncoated and chromated specimens were included as reference pre-treatments. Adhesion degradation was assessed by use of wedge test specimens [23]. The corrosion resistance was evaluated using panels coated with the epoxy adhesive, which were subjected to FFC test conditions for 1000 h. Recent work has shown that FFC will take place only if there is microgalvanic coupling between the aluminium matrix and electrochemically nobler second phase particles [24]. Iron impurities in AA6060 cause precipitation of -Al(Fe,Mn)Si particles [25]. An AlMg0.5Si0.4 model analogue alloy free from -Al(Fe,Mn)Si particles was included in the FFC test to evaluate the importance of these particles in promoting FFC on AA6060.

EXPERIMENTAL

Materials

The composition of the test materials, determined by spectrographic analysis, is given in Table 1. Commercially produced AA6060-T6 extrusions from two different batches were used. All profiles were air cooled from 520°C to below 200°C in less than 4 min after exit from the die. Ageing to T6 temper was done at 195°C for 3.25 h. The material used in the wedge test (batch 1) was 2 x 110 mm² in cross-section, while the material employed in the FFC and lap-shear tests (batch 2) was 2 x 80 mm² in cross-section and with 0.2 mm ridges on one side. In addition, an AlMg0.5Si0.4 alloy with Mg and Si concentrations similar to AA6060 was prepared in the laboratory from its pure components. This alloy was cast into extrusion billets, homogenised at 575°C for 4 h and water quenched. The billets were then machined to a diameter of 95 mm, preheated to 470°C and extruded to profiles with a cross-sectional area of 3.2 x 60 mm². The profiles were water quenched immediately after the exit from the die.

Table 1. Composition of test materials (wt%, bal. Al).

Alloy	Si	Fe	Mg	Mn	Cu	Zn	Ti	Cr	Zr
AA6060 (1)	0.42	0.21	0.46	0.022	0.006	0.0069	0.0013	0.0003	0.0020
AA6060 (2)	0.40	0.18	0.46	0.021	0.002	0.015	0.01	-	-
AlMg0.5Si0.4	0.38	<0.001	0.47	0.001	0.001	0.0015	0.0005	0.0009	0.0002

Surface treatment

The following surface pre-treatments were employed prior to adhesive bonding of the wedge and lap shear test samples:

1. *NaOH etched and deoxidised:* Degreased in a commercial degreasing agent (A. D. Chemicals Z19, 50 g/l, pH 1.6, 50°C, 20 s), rinsed in tap water, etched in 100 g/l NaOH solution (60°C, 50 s), rinsed in tap water, deoxidised in fluoride/sulphuric/phosphoric acid based solution (4% Alfideox 73, 25°C, 1 min), rinsed in tap then distilled water, and dried in hot air stream.
2. *Ti-Zr based treatment, pH 2.9:* Pre-treated as in 1 followed by immersion in hexafluorotitanate/zirconate based solution (4% Gardobond X4707, 90 s, 20°C, adjusted to pH 2.9 by Gardolene 6800), rinsed in tap then distilled water, dry in hot air stream.

7. Effect of pre-treatment on the durability of epoxy-bonded AA6060 aluminium joints

3. *Ti-Zr based treatment, pH 4.0:* As pre-treatment 2, except that conversion coating was performed in a solution of pH 4.0.
4. *Chromated:* Pre-treated as in 1 followed by immersion in chromate solution (15 g/l Alodine C6100, 3 min, pH 2, 20°C), rinsed in tap then distilled water, and dried in hot air stream.

Ti-Zr based pre-treatments 2 and 3, differing from each other only by the pH of the conversion bath, were employed to produce specimens with “low” and “high” coating weights in a controlled manner. Care was taken to maintain similar convection conditions in the baths during coating formation.

Two additional pre-treatments were included in the FFC test:

5. *NaOH etched:* As pre-treatment no. 1, but without the deoxidation step.
6. *Degreased:* Degreased in acetone.

Lap-shear testing

AA6060 extrusions from batch 2 were cut into coupons, 110 mm in length and 80 mm in width. Within 24 h of surface treatment, the coupons were glued with an epoxy based structural adhesive, Betamate XD4600, to form single lap joints in which a ridged surface was pressed against a flat surface, giving a glue-line thickness of 0.2 mm. The overlap was 20 mm. Metallic clips were used to keep the two coupons together during curing for 30 min at 180°C. Three replicates of each variant were prepared. Specimens were then stored for about two weeks in laboratory air before tensile testing was performed on an automated Instron machine. The initial jaw separation was set at 125 mm, and a cross-head speed of 10 mm/min was used.

Wedge testing

Wedge testing was performed according to the procedure described in ASTM D3762-79 [23]. Within 24 h of surface treatment, the AA6060 adherends were bonded by use of the XD4600 epoxy adhesive. In order to increase the stiffness of the wedge samples, a 6 mm thick AA7021-T1 backing material (Yield strength > 360 MPa) was glued on each side to form a sandwich assembly, 16 mm in thickness. Spacers were inserted at the edges to obtain a glue-line thickness of 0.1 mm between the AA6060 surfaces. Metallic clips were used to keep the sandwich assemblies together during curing, which was performed for 30 min at 180°C in an air circulation furnace. After curing, the

sandwich assemblies were machined into reinforced double cantilever beam (RDCB) specimens, 25.4 mm in width, 154 mm in length and 16 mm in height, as shown in Figure 1. Six replicate RDCB specimens were manufactured for each surface treatment.

The cut edges were polished to facilitate measurement of the crack lengths under a stereo microscope. Wedges were introduced at a controlled rate of 1 mm/s. The RDCB specimens were stored at room temperature for 24 h before the initial crack lengths were measured. The specimens were then exposed at 96% RH and 40°C in a climate chamber. The crack length (denoted “a” in Figure 1) was determined as the average of visible crack lengths measured on the two sides of a sample. Measurements were carried out frequently during the first two days of exposure, then after 1, 2, 4 and 8 weeks, when the test was terminated and the specimens opened for examination of the fracture surfaces.

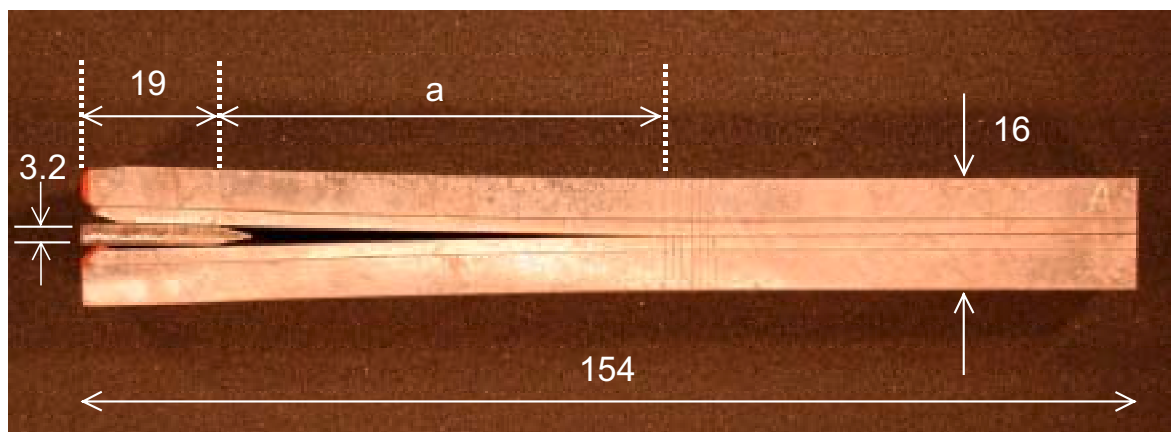


Figure 1. Dimensions (in mm) of RDCB specimen used in the wedge test.

Filiform corrosion testing

AA6060 and AlMg0.5Si0.4 alloy profiles were cut into test coupons, 120 x 80 mm and 80 x 60 mm in size, respectively. Within one hour of surface treatment, specimens were coated with XD4600 adhesive by use of a spatula. The coating thickness was 0.2 mm, obtained by utilising the ridges on the AA6060 profile and spacers along the edges of the AlMg0.5Si0.4 alloy during application of the adhesive. Two specimens were prepared for each

material/surface treatment combination. After curing, a diagonal scribe line was made on each specimen to expose the metal underneath. Initiation of pitting corrosion, eventually leading to FFC, was accomplished by placing 16% HCl solution along the scribe. After 5 min of exposure, excessive liquid was removed, and the specimens were transferred to a climate chamber. The specimens were exposed to 82% RH and 40°C for 1000 h, corresponding to standard FFC test conditions according to DIN EN 3665.

Surface characterisation

The surface morphology of pre-treated AA6060 specimens were studied in a field emission SEM (Hitachi S4300 SE) with X-ray EDS capability. Fracture surfaces of selected wedge test RDCB specimens were studied in the SEM to obtain clues about the locus of environmental crack growth. A few Ti-Zr treated specimens (pre-treatment 2) were also analysed by glow discharge optical emission spectroscopy (GDOES), using a LECO GDS 750A instrument.

RESULTS

Characterisation of pre-treated AA6060 surfaces

Typical surface morphologies of pre-treated AA6060 surfaces are shown in Figure 2. Alkaline etching without subsequent deoxidation (pre-treatment 5) resulted in significant amounts of smut on the surface (Figure 2a). X-ray EDS analysis indicated that the smut mainly consisted of Mg hydroxide, as expected, since Mg oxides are stable in high pH solutions [26]. By subsequent deoxidation (pre-treatment 1) the smut was effectively removed and a scalloped topography, which was developed during alkaline etching, became visible. GDOES analyses indicated that the Al/Mg ratio in the oxide increased from about 2 to about 20 as a result of deoxidation. Deoxidation also caused formation of small crystallographic etch pits, particularly along the grain boundaries (Figure 2b).

The surfaces produced by the Ti-Zr based pre-treatments are shown in Figure 2c (pre-treatment 2) and Figure 2d (pre-treatment 3), respectively. Earlier studies [21,22] have shown that Ti-Zr oxide deposition occurs predominantly on and in the vicinity of cathodic $-Al(Fe,Mn)Si$ particles on the surface of AA6060 aluminium. X-ray EDS analyses of surfaces treated at pH 2.9

(Figure 2c) showed Ti and Zr only on the particles themselves. Treatment at pH 4.0 resulted in more extensive coating deposition, and significant Ti and Zr signals were detected on and around the particles, corresponding to the dark areas in Figure 2d. Typical EDS spectra acquired from these areas are shown in Figure 3. Hence, the conversion coating formed in pH 4.0 solution was relatively thick over a considerable area fraction of the AA6060 surface. Under similar coating conditions, the thickness of deposited Ti-Zr oxide layer surrounding the particles was observed to be of the order 50-100 nm [22].

In the areas well away from the intermetallic particles, and on the surfaces treated in a solution of pH 2.9, closer examination in field emission SEM revealed a particulate type of oxide deposit, shown in Figure 2e. The oxide particles were far too small (< 50 nm) to be detected by X-ray EDS analysis, but their composition was probably similar to that of the thicker deposits at the intermetallic particles. Quantitative GDOES depth profiles acquired from such surfaces indicated that the overall oxide film thickness was a few nm (Figure 4), which is typical of air formed films on aluminium. However, the low Ti concentration observed ($< 1\%$) suggests that the deposited Ti (and Zr) oxide only covered a small fraction of the total surface area, mainly located at the cathodic $-Al(Fe,Mn)Si$ particles [21,22]. GDOES analyses further indicated that the Al/Mg ratio in the oxide (20 ± 5) was similar to the values obtained for the deoxidised surface.

The CCC formed on the AA6060 aluminium matrix (pre-treatment 4) was characterised by a porous morphology and poor coverage at the grain boundaries (Figure 2f). The intermetallic $-Al(Fe,Mn)Si$ particles appeared to be unaffected by the chromate treatment. However, Auger analysis of AA6060 subjected to similar pre-treatment indicated that a thin Cr oxide film was formed on these particles. Moreover, the chromate treatment was significantly more effective than the Ti-Zr based pre-treatments in reducing the cathodic activity of the particles during subsequent exposure in chloride solution [27].

7. Effect of pre-treatment on the durability of epoxy-bonded AA6060 aluminium joints

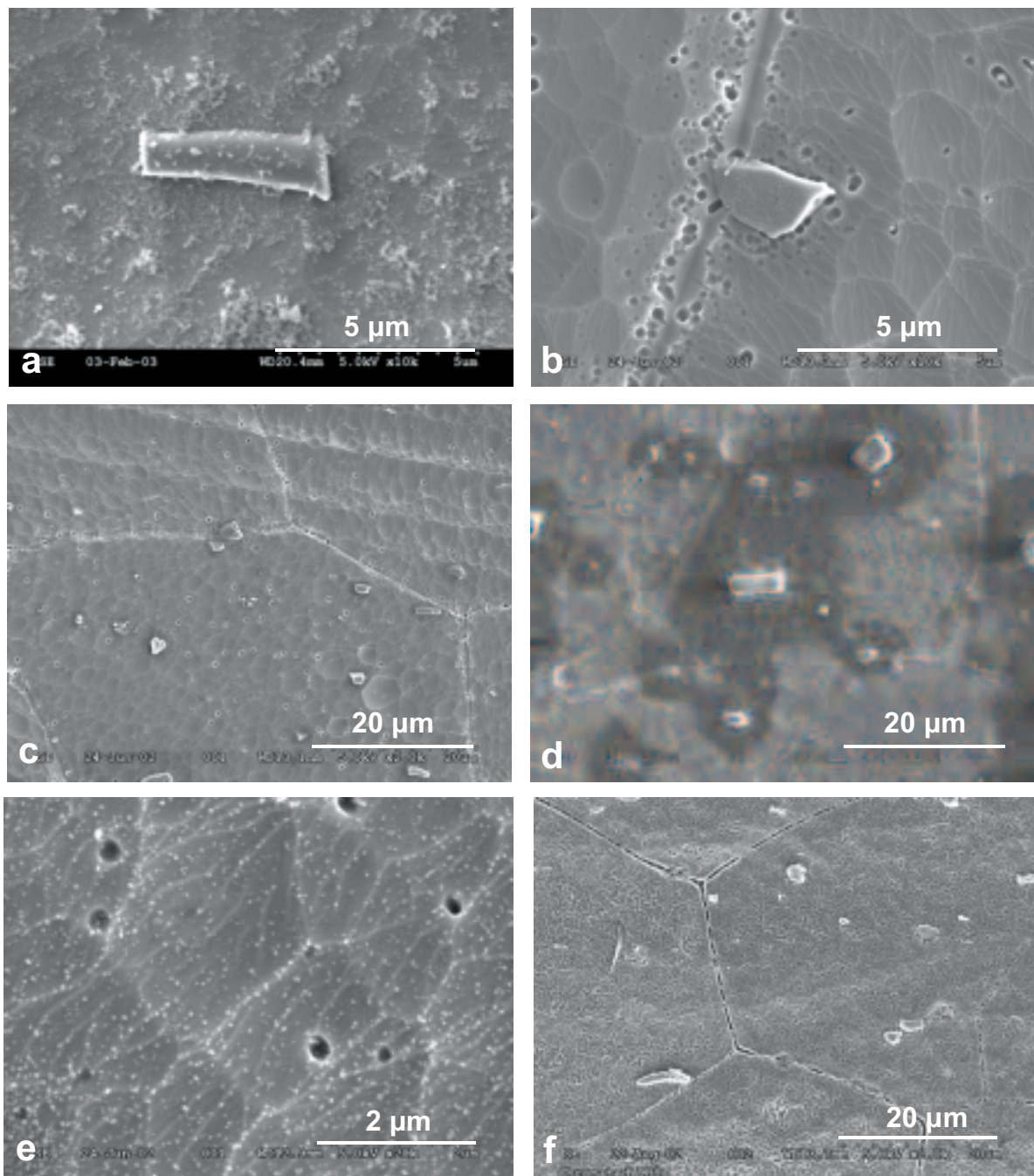


Figure 2. SEM images of AA6060 subjected to pre-treatment 5 (a), 1 (b), 2 (c), 3 (d,e) and 4 (f). The appearance of a dark zone surrounding the intermetallic particles in d) was caused by presence of a relatively thick Ti-Zr oxide conversion layer. In the remaining areas on the aluminium matrix a particulate oxide structure was formed, as shown in e). A similar particulate structure was observed as a result of Ti-Zr treatment at pH 2.9 (not shown here).

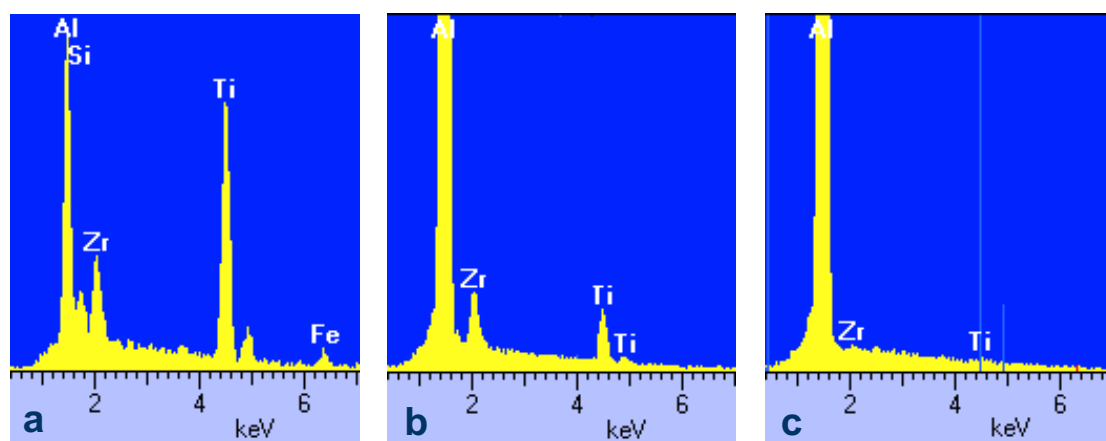


Figure 3. X-ray EDS spectra acquired at 10 kV from different locations on AA6060 aluminium subjected to pre-treatment 3 (Figure 2d). The spectra were acquired from a) intermetallic $-Al(Fe,Mn)Si$ particle, b) the dark region surrounding the intermetallic particles and c) bright area of the aluminium matrix well away from the particles.

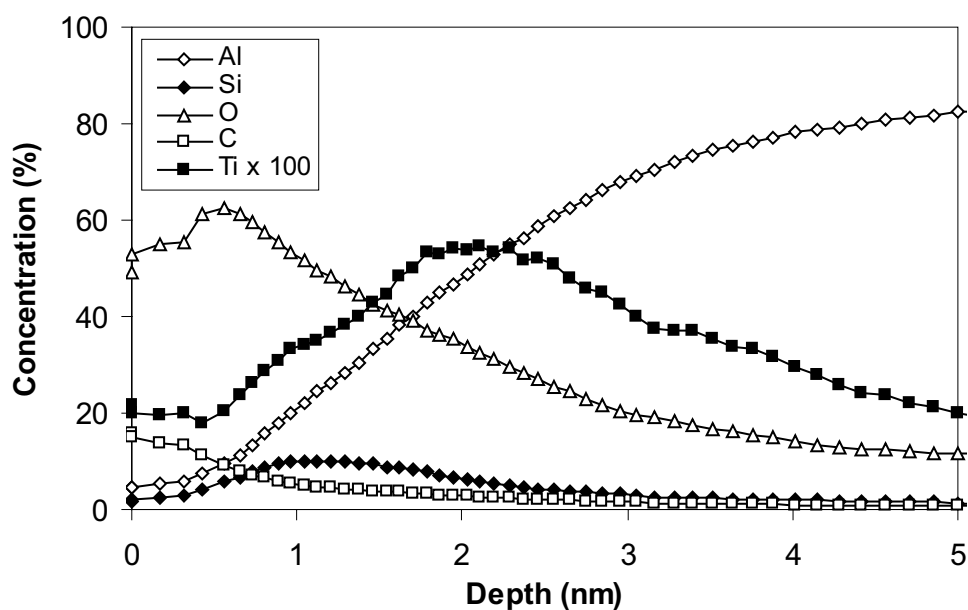


Figure 4. GDOES depth profiles obtained for AA6060 aluminium subjected to Ti-Zr based pre-treatment at pH 2.9, resulting in a particulate type of deposit similar to that shown in Figure 2e. The analysis area was circular, with a diameter of 4 mm. Note that the Ti profile is plotted on an expanded scale. Zr and F are omitted due to lack of reference specimens for quantification.

Single lap shear testing

During tensile testing of single lap joints, significant transverse stresses are generated in addition to shear stresses in the adhesive layer [1]. As true shear strength is not readily obtained, the tensile test data of as-cured (not exposed to wet conditions) lap joints in Table 2 are therefore presented in terms of maximum load before fracture occurred. While the etched and Ti-Zr treated specimens, respectively, showed maximum loads of about 30 kN, the chromated specimens consistently failed at only about 20 kN.

Table 2. Max. load (kN) during tensile testing of as-cured single lap joints.

No.	Surface Treatment	Max. load (kN) \pm std. dev.
1	NaOH etched and deoxidised	30.3 \pm 0.2
2	Ti-Zr, pH 2.9	(not tested)
3	Ti-Zr, pH 4.0	31.0 \pm 0.2
4	Chromated	20.6 \pm 0.1

Visual examination of the fracture surfaces showed that the etched and Ti-Zr treated specimens exhibited a relatively large area of cohesive fracture in the adhesive layer as well as areas of adhesive fracture towards the edges of the overlap region, where peel forces become high during tensile testing [1]. For chromated specimens, the fractures occurred by 100% interfacial failure. The fracture surface on the metal side was bright and shiny, and distinctly different from the golden brown colour of the chromate conversion coating (CCC) on the remaining part of the specimen. Hence, the locus of failure appeared to be predominantly at the interface between the CCC and the aluminium substrate.

Wedge testing

Figure 5 and Table 3 summarise the wedge test results obtained for the different pre-treatments. Initial crack lengths appeared to be influenced to some extent by the pre-treatment, despite the fact that formation of initial cracks occurred by cohesive failure of the adhesive. Compared with the chromated specimens, longer initial cracks were observed for NaOH etched and deoxidised specimens, while the specimens subjected to Ti-Zr based pre-treatment exhibited somewhat shorter initial cracks.

Figure 5a shows mean crack lengths as a function of time during the initial stage of environmental exposure. Significant crack propagation was observed already after one hour on the NaOH etched and deoxidised as well as the Ti-Zr treated specimens, but not on the chromated ones. Results obtained for the entire test period (Figure 5b) show that the crack growth rate generally decreased with time, which is mainly related to a reduction of the stress intensity at the crack tip with increasing crack length. However, the long-term crack growth was obviously also affected by the pre-treatment of the adherend surfaces. In this respect, chromating was clearly superior to the other treatments. The two Ti-Zr based variants exhibited a similar behaviour during the first couple of weeks. During the remaining time the crack growth rate was significantly higher on the specimens subjected to Ti-Zr treatment at pH 4.0, which had a “high” conversion coating weight. The total crack length measured after eight weeks of testing was similar to the results obtained for the uncoated specimens.

The crack growth data presented in Table 3 further show that the NaOH etched and deoxidised specimens exhibited the highest crack growth rate during the first week of exposure, in spite of relatively long initial cracks and hence lower stress levels at the crack tip. The total crack growth measured after completed exposure (26.1 mm) was similar to that observed for specimens subjected to Ti-Zr treatment at pH 2.9 (25.5 mm). However, comparisons based on crack growth alone may be misleading since differences in the stress level also need to be considered. Ranking of the pre-treatments should rather be based on the total crack length after completed testing. Hence, the following ranking can be made based on the present results: Chromated (best) >> Ti-Zr, pH 2.9 > Ti-Zr, pH 4.0 \approx NaOH etched and deoxidised.

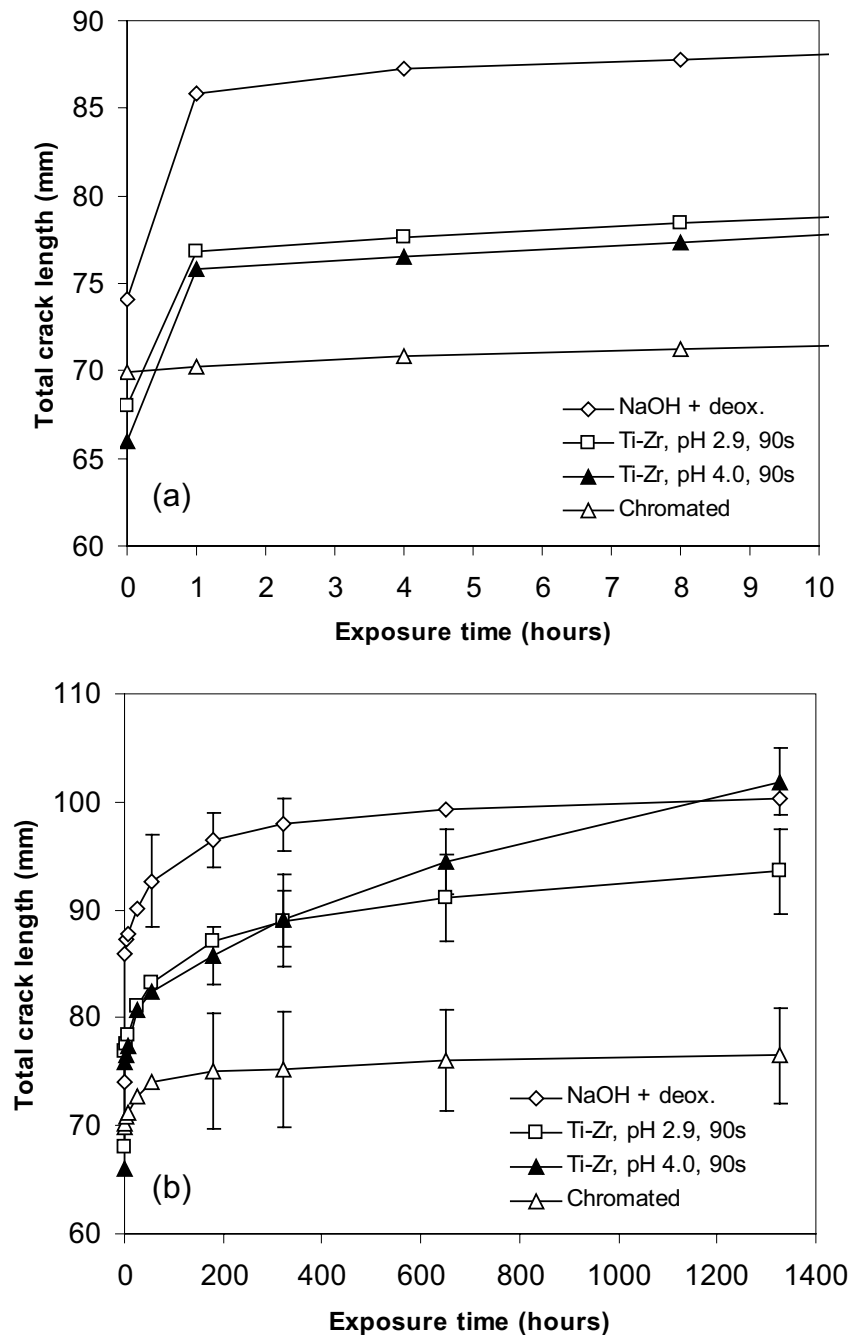


Figure 5. Crack length vs. time for AA6060 wedge test specimens during exposure to 96% RH and 40°C. a) Initial stage of environmental crack growth, indicating immediate start of crack propagation for specimens subjected to pre-treatments 1, 2 and 3, but not for the chromated specimens. b) Crack growth during 8 weeks of exposure. Error bars, indicating standard deviation among the replicates, are not shown for all points to enhance the clarity of the diagram.

Table 3. Initial crack lengths and crack growth on the RDCB specimens during environmental exposure for a week (178 h), two weeks (321 h) and eight weeks (1328 h). Average \pm standard deviation for six replicate specimens are shown.

Pre-treatment	Initial crack length (mm)	Crack growth (mm)		
		178 h	321 h	1328 h
1. NaOH + Deox.	74.1 \pm 5.5	22.4 \pm 6.9	23.8 \pm 6.2	26.1 \pm 6.1
2. Ti-Zr, pH 2.9	68.0 \pm 1.8	19.1 \pm 4.4	21.0 \pm 3.9	25.5 \pm 3.5
3. Ti-Zr, pH 4.0	66.0 \pm 2.3	19.8 \pm 2.1	23.1 \pm 1.7	35.9 \pm 1.2
4. Chromated	69.9 \pm 4.6	5.1 \pm 1.0	5.4 \pm 1.2	6.6 \pm 1.3

Examination of fracture surfaces

Macroscopic examination of the fracture surfaces showed that the initial crack, formed during insertion of the wedge, propagated cohesively in the adhesive layer on all RDCB specimens. For pre-treatments 1, 2 and 3 the cracks immediately moved to and propagated along the adhesive-substrate interface during exposure in the climate chamber. In contrast, the chromated specimens (pre-treatment 4) exhibited nearly 100% cohesive fracture of the adhesive under similar conditions. Typical appearance of the two types of fracture surfaces is shown in Figure 6.

The interfacial fracture surfaces of specimens subjected to pre-treatment 3 were studied in SEM in an attempt to determine the locus of failure more precisely. SEM images of the two fracture surfaces are shown in Figure 7. On the “aluminium side” of the joint (Figure 7a), intermetallic -Al(Fe,Mn)Si particles and surrounding darker areas indicative of a relatively thick Ti-Zr oxide deposit were seen, similar to the appearance of the pre-treated surface before adhesive bonding (Figure 2d). Strong Ti and Zr signals were detected by X-ray EDS point analysis of the particles. Ti and Zr were also detected in the dark zone surrounding the particles, although the intensity of the characteristic Ti K and Zr L_{2,3} peaks was significantly weaker in these areas. On the opposite “adhesive side” of the joint, the fracture surface exhibited depressions (Figure 7b) caused by protruding -Al(Fe,Mn)Si particles on the AA6060 aluminium surface. Ti and Zr were detected occasionally at the bottom of or along the periphery of these depressions in the adhesive, indicating localised cohesive fracture of the Ti-Zr oxide conversion coating. Otherwise, no Ti or Zr could be detected by X-ray EDS analyses on the adhesive side of the fracture.

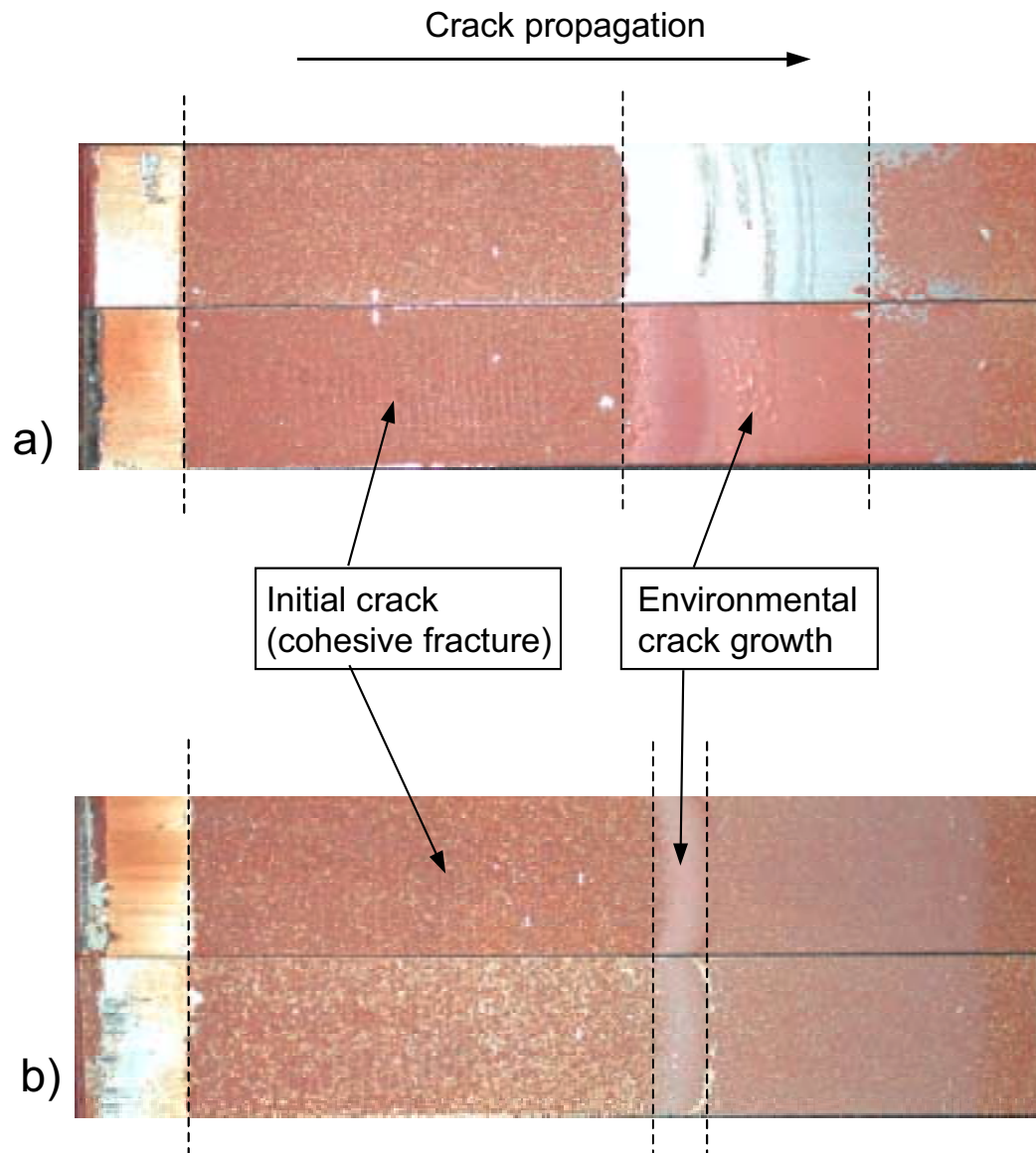


Figure 6. Fracture surfaces of AA6060 wedge test specimens. a) Ti-Zr treated at pH 4.0, showing interfacial failure during environmental exposure. b) Chromated specimen exhibiting slow, cohesive crack growth under similar conditions.

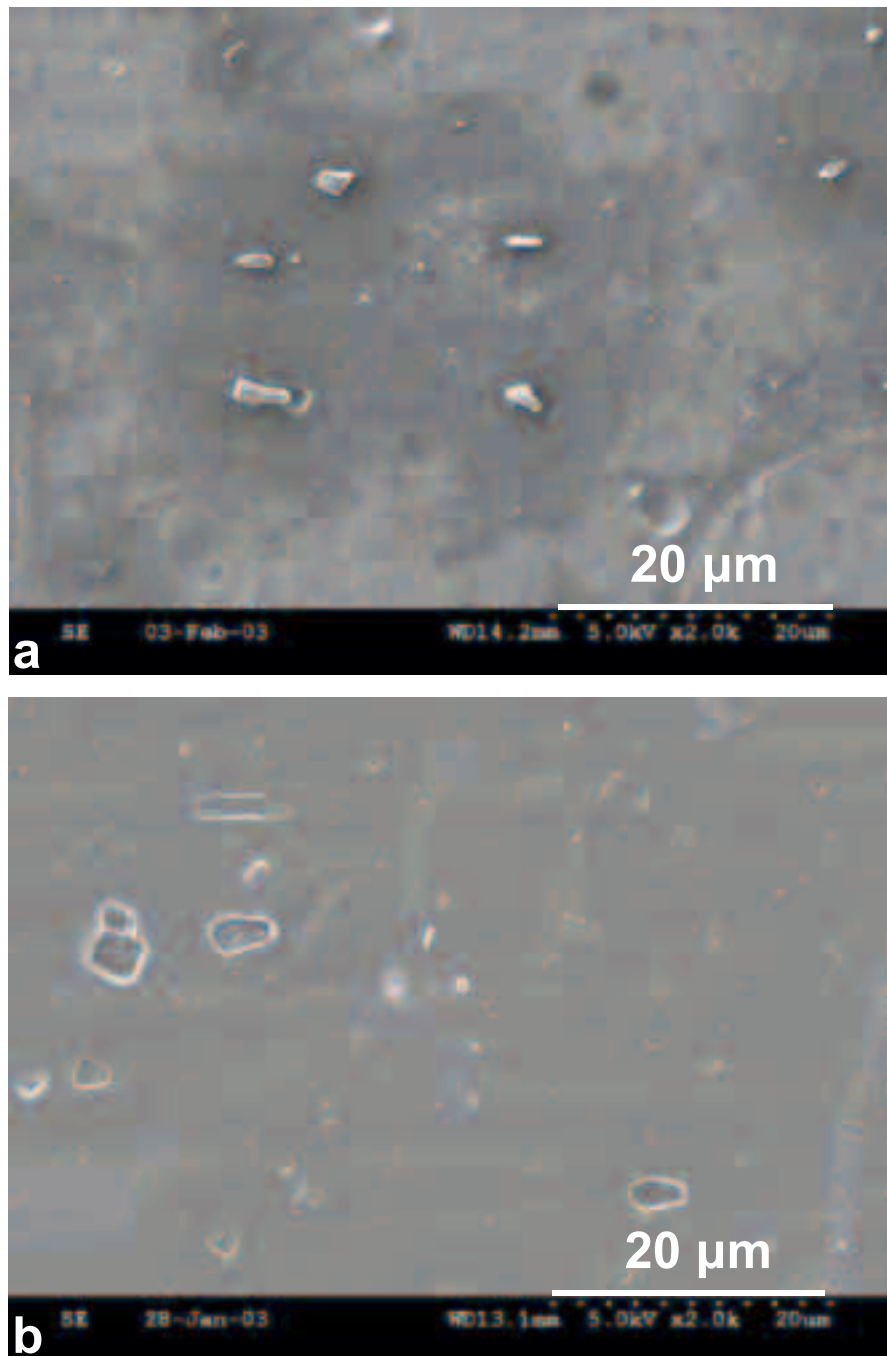


Figure 7. SEM images of fracture surfaces of AA6060 prepared using Ti-Zr based pre-treatment at pH 4.0 (pre-treatment 3). Specimens were cut from adhesive fracture region formed during environmental exposure. a) Aluminium fracture side, b) adhesive side of fracture exhibiting depressions where intermetallic particles were located before failure.

Filiform corrosion testing

The corrosion test results, assessed by the average maximum length of attack measured perpendicular to the scribe, are summarised in Figure 8. The corrosion susceptibility of the AA6060 specimens was significantly affected by the pre-treatment prior to coating with the epoxy adhesive. NaOH etched and de-oxidised specimens (pre-treatment 1) exhibited extensive disbonding of the epoxy coating on a continuous front along the scribe, such that the coating could be removed without difficulty after the test (Figure 9a). The Ti-Zr based pre-treatments caused a significant improvement relative to the etched and deoxidised specimens. However, FFC and some continuous disbonding still occurred close to the scribe (Figure 9b), probably due to lifting of the coating by corrosion products formed in the filament tails.

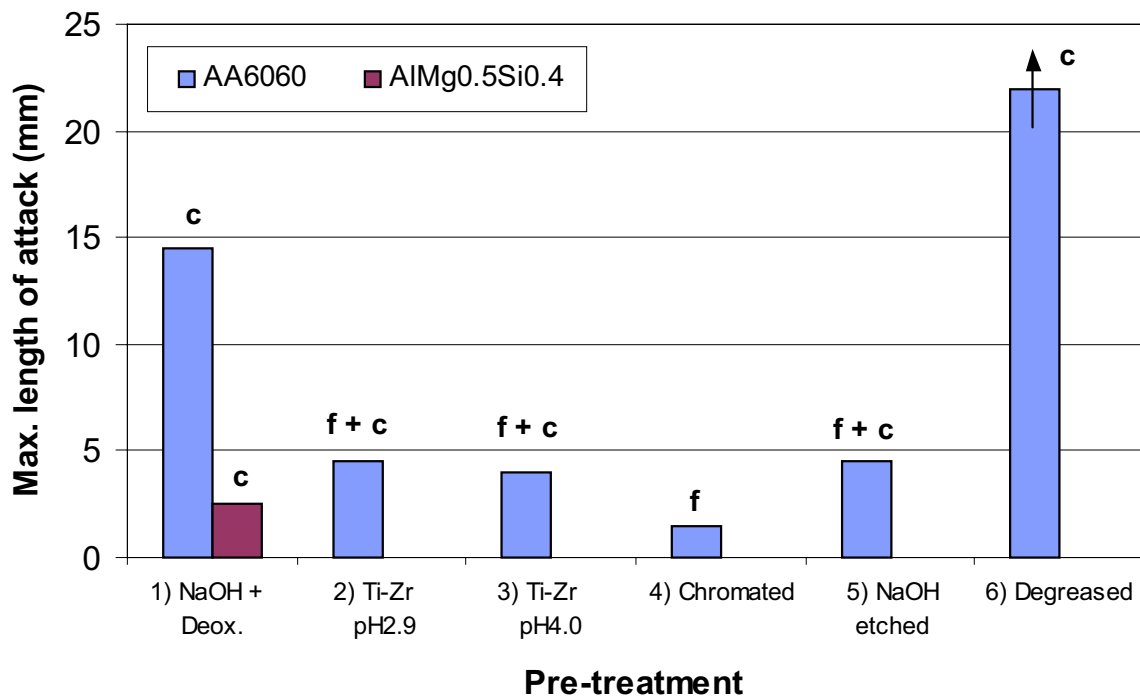


Figure 8. Maximum length of attack from scribe on epoxy coated AA6060 and AlMg0.5Si0.4 specimens after 1000 h of FFC testing. The maximum lengths of attack reported include filiform corrosion and continuously disbonded areas along the scribe, referred to as “f” and “c” in the diagram.

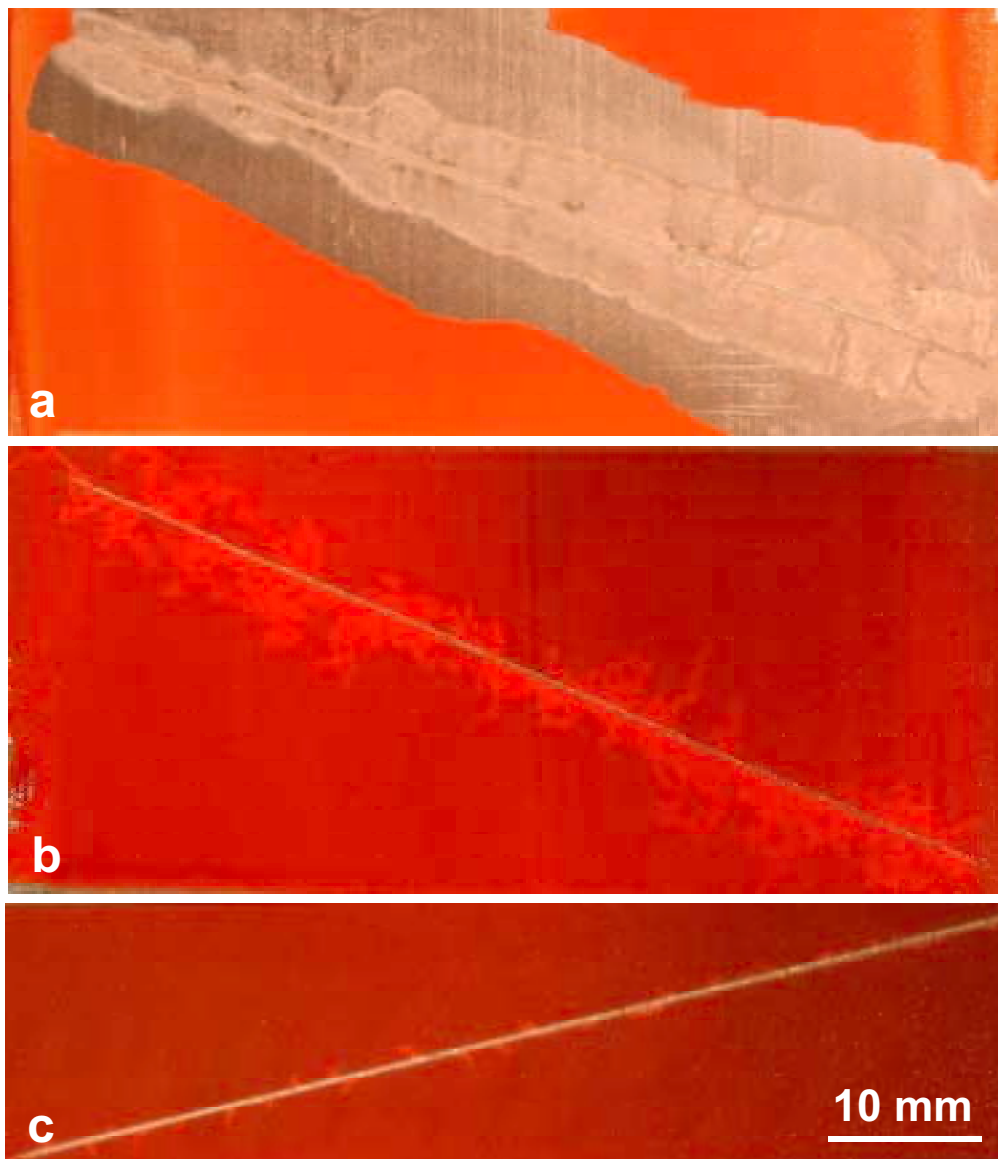


Figure 9. Macrographs of epoxy coated AA6060 specimens after 1000 h of FFC testing. a) NaOH etched and deoxidised. The disbonded epoxy coating was removed to show an etched zone next to the scribe, and apparently unaffected metal surface farther away from the scribe, b) Ti-Zr treated at pH 4.0, c) chromated in Alodine C6100.

The chromated specimens exhibited the best performance (Figure 9c), both in terms of filament length and disbonded area. Disbonding appeared to be limited to the trail of the corrosion filaments, indicative of good adhesion between the CCC and the epoxy coating. AA6060 specimens subjected to NaOH etching alone (pre-treatment 5) performed similarly to the Ti-Zr treated specimens. Hence, the adhesion of the epoxy coating to the AA6060 substrate was significantly reduced by the deoxidation treatment. A similar effect was observed previously on epoxy bonded AA6060 lap shear joints [6]. Acetone degreasing was inferior to all the other pre-treatments and extensive disbonding of the coating occurred in the course of only a few days of environmental exposure.

In contrast to AA6060, the AlMg0.5Si0.4 alloy specimens were virtually immune against FFC, independent of pre-treatment. Apart from a tendency to continuous disbonding of the coating in local areas on NaOH etched and deoxidised specimens (pre-treatment 1), no signs of FFC or disbonding were observed after 1000 h of exposure on any of the other variants, including the acetone degreased surfaces.

DISCUSSION

Wedge test

Several mechanisms have been proposed to account for environmental failure of adhesive bonded aluminium [28,29]. Diffusion of water to the adhesive-substrate interface may plasticise the adhesive and cause cohesive fracture of the adhesive close to the interface. True interfacial failure may occur if water displaces atomic bonds between the adhesive and the oxide-covered aluminium. A third possibility is that the oxide layer itself becomes hydrated and fractures cohesively. In an earlier study [30] of chromic acid etched and epoxy bonded AA3103 aluminium joints it was concluded, based on AES analyses, that locus of failure was mainly interfacial with small amounts of cohesive failure within the adhesive. A similar interfacial failure mode was observed [31] as a result of fatigue testing of XD4600 epoxy bonded AA5083 aluminium joints in wet environment. However, in this case the surfaces were grit-blasted and degreased before bonding. For chromic acid etched adherends, exhibiting a thin (< 40 nm) aluminium oxide film on the surface [8,30], cracks propagated mainly through the aluminium oxide.

The Ti-Zr based pre-treatments used in this study produced highly heterogeneous surfaces in terms of distribution of the deposited conversion coating. The failure mechanism may therefore be complex. Examination of the fracture surfaces by SEM/X-ray analyses indicated that crack growth occurred in or very close to the Ti-Zr oxide-adhesive interface. However, if the mechanism of environmental attack is to be established reliably, the locus of environmental crack growth must be identified more precisely, *e.g.* by use of XPS or AES.

Qualitatively, the wedge test results are in line with general observations made in earlier work [15], where the wet adhesion of a polyester paint to AA3105 aluminium was reduced by increasing the coating weight of a no-rinse Ti-Zr based conversion coating. As shown in Figure 5, the crack growth behaviour of the two Ti-Zr treated variants was nearly identical during the first two weeks of exposure. However, during prolonged testing the specimens with a high coating weight (pre-treatment 3) exhibited a significantly higher crack growth rate than the other specimens, eventually resulting in longer cracks than on the uncoated specimens.

Water diffusion is clearly an important factor in the failure mechanism. Water may enter the interface region by diffusion through the bulk adhesive, by wicking or “capillary diffusion” along the adhesive-oxide interface [3], or by diffusion through the oxide layer [32]. Bulk diffusion coefficients of water in epoxy adhesive can be estimated from gravimetric measurements, while interfacial diffusion is difficult to measure directly. However, water uptake also causes a reduction in the elastic modulus of the adhesive. By mechanical testing of epoxy-bonded torsional joints it was observed [3] that the elastic modulus decreased considerably faster than expected based on bulk diffusion of water alone. Thus, interfacial diffusion contributed significantly to the ingress of water in the system studied.

Surface treatment must be an important factor controlling interfacial diffusion of water, which again affects the rate of adhesion degradation. The poor performance of specimens subjected to pre-treatment 3 may therefore be related to a high interfacial diffusion rate of water, *e.g.* due to presence of cracks or defects in the thicker parts of the conversion coating. During the initial stages, crack propagation was fast (due to high stress intensity) and influenced mainly by the water present at the crack tip. After longer exposure times, the intact joint ahead of the crack tip became increasingly affected by water diffusing in from the edges of the wedge specimen, promoting loss of strength. Hence, the effect of enhanced water ingress during wedge testing is expected to become pronounced with time, which could explain the

increasingly divergent crack growth curves of the Ti-Zr treated specimens in Figure 5b.

The wedge test provides a qualitative, but fairly reliable, ranking of the environmental durability of adherend surface pre-treatments [23]. Thus, the results in Figure 5 indicate that, to achieve improved durability by Ti-Zr based treatment, the conversion coating weight must not become too high. This conclusion is supported by tensile test results [33] of AA6060 lap joints formed by the same XD4600 adhesive as in this work. Figure 5 further shows that chromate treatment provided superior durability, in spite of the relatively low strength obtained by tensile testing of unexposed lap-shear joints (Table 2). Apparently, the chromate pre-treatment employed in this work is not intended for structural adhesive bonding. However, similar treatment has been shown to provide very good adhesion and FFC resistance of polyurethane painted aluminium sheet materials [34].

Filiform corrosion

Recent research on FFC of painted aluminium [24,34,35] has emphasised the significance of the near surface substrate microstructure. Highly deformed surface layers (of the order 1 μm in thickness) on rolled aluminium sheet may become electrochemically active as a result of subsequent heat treatment. The high susceptibility to FFC was primarily attributed to a fine distribution of cathodic intermetallic particles in the surface layer [24,35]. Electrochemically active surface layers have not been shown to exist on extruded material, and in this work the outer 5 μm on all AA6060 surfaces (except pre-treatment 6) was removed by alkaline etching. Nevertheless, the importance of the $-\text{Al}(\text{Fe},\text{Mn})\text{Si}$ particles in promoting FFC on AA6060 is clearly demonstrated by the fact that FFC did not occur at all on the particle-free AlMg0.5Si0.4 alloy. Hence, efficient inhibition of the reduction reactions occurring at the cathodic particles should be an important characteristic of conversion coatings to prevent FFC.

The superior performance of the chromate treated specimens in the FFC test is due to a combination of excellent adhesion (Figure 5) as well as efficient passivation of the cathodic particles [27]. Present results obtained for the Ti-Zr based pre-treatments indicate that formation of a relatively thick Ti-Zr oxide on the intermetallic particles does not pay off in terms of improved FFC resistance. However, in comparison with the NaOH etched and deoxidised specimens, Ti-Zr treatment significantly reduced the extent of continuous disbonding along the scribe. This is in partial agreement with the wedge test

results, which showed a significant improvement in adhesion by pre-treatment 2, but not by pre-treatment 3.

As can be inferred from Figure 8, deoxidation of the NaOH etched surface increased the susceptibility to continuous disbonding along the scribe considerably. In general, acid solutions will effectively remove the Mg rich oxide formed on the surface of Mg containing alloys as a result of alkaline etching [8], as observed also in this work. A recent investigation [36] of several aluminium alloy/epoxy systems demonstrated superior hydrolytic stability of bonded joints made from simply degreased AlMg3 alloy. The good performance was attributed to a high surface concentration of magnesium oxides and their high stability in alkaline media. The alkaline environment originates from amines set free during curing of epoxy adhesives, and reacting with water according to the reaction



Similar results were obtained by tensile testing of epoxy-bonded AA5251 aluminium lap joints [37]. Degreased specimens, with a surface Al/Mg ratio of about 2 as determined by AES, had a higher durability in hot water than grit blasted specimens with an Al/Mg ratio $\gg 10$. These results bear resemblance with present observations in that the NaOH etched specimens with a surface Al/Mg ratio of about 2 exhibited better adhesion, *i.e.* considerably lower susceptibility to continuous disbonding (Figure 8), than the NaOH etched and deoxidised specimens with a surface Al/Mg ratio of about 20.

Since the Ti-Zr based pre-treatment 2 performed significantly better than pre-treatment 1 (both with a surface Al/Mg ratio of about 20) in the wedge test as well as the FFC test, the particulate type of Ti-Zr oxide formed (Figure 2e) does promote adhesion in wet environment. However, the mechanism by which this particulate type of oxide improves the adhesion remains unclear and requires further investigation.

CONCLUSIONS

- Ti-Zr based pre-treatment provided improved durability of epoxy bonded AA6060 aluminium joints relative to an alkaline etch and deoxidation pre-treatment, but was inferior to a chromate treatment in terms of adhesion and resistance against filiform corrosion (FFC).

- The presence of cathodic intermetallic -Al(Fe,Mn)Si particles in AA6060 is detrimental in two ways:
 1. The particles cause excessive Ti-Zr oxide deposition in their vicinity during pre-treatment, resulting in poor durability of epoxy-bonded joints in humid environments.
 2. The particles promote FFC in presence of chlorides. A particle-free AlMg0.5Si0.4 model alloy similar to AA6060 was virtually immune against FFC, independent of pre-treatment.
- As the amount of Ti-Zr oxide deposited during Ti-Zr based pre-treatment is affected by the type, fractional area and distribution of cathodic particles present on the aluminium surface, the pre-treatment conditions should be adapted to the specific alloy in order to achieve optimum performance.
- While the Ti-Zr based pre-treatment promoted adhesion, such treatment did not provide significant protection against FFC because the Ti-Zr oxide deposit did not inhibit the cathodic activity on the particles as effectively as a chromate pre-treatment. Effective passivation of the cathodic particles, which are always present in commercial aluminium alloys, should be an important issue in the search for chromate-free pre-treatments exhibiting high FFC resistance.

ACKNOWLEDGEMENTS

The GDOES analysis was performed by S. Hånström at the Swedish Institute for Metals Research, Stockholm. This work was funded by the Norwegian Research Council.

REFERENCES

1. A. J. Kinloch, *Adhesion and Adhesives*, Chapman and Hall, London (1990).
2. A. J. Kinloch and N. R. Smart, *J. Adhesiom*, **12**, 23 (1981).
3. M. P. Zanni-Deffarges and M. E. R. Shanahan, *Int. Journal of Adhesion and Adhesives*, **15**, 137 (1995).
4. G. D. Davis, P. L. Whisnant and J. D. Venables, *J. Adhesion Sci. Technol.*, **9**, 433 (1995).

5. W. Brockmann, O. D. Hennemann, H. Kollek and C. Matz, *Int. Journal of Adhesion and Adhesives*, **6**, 115 (1986).
6. O. Lunder, B. Olsen and K. Nisancioglu, *Int. Journal of Adhesion and Adhesives*, **22**, 143 (2002).
7. K. B. Armstrong, *Int. Journal of Adhesion and Adhesives*, **17**, 89 (1997).
8. L. Kozma and I. Olefjord, *Materials Science and Technology*, **3**, 869 (1987).
9. G. W. Critchlow and D. M. Brewis, *Int. Journal of Adhesion and Adhesives*, **16**, 255 (1996).
10. P. Briskham and G. Smith, *Int. Journal of Adhesion and Adhesives*, **20**, 33 (2000).
11. D. J. Arrowsmith, D. A. Moth and S. P. Rose, *Int. Journal of Adhesion and Adhesives*, **12**, 67 (1992).
12. A. J. Kinloch, M. S. G. Little and J. F. Watts, *Acta. Mater.*, **48**, 4543 (2000).
13. G. S. Frankel and R. L. McCreery, *Interface*, **10** (4), 34 (2001).
14. M. Kendig, S. Jeanjaquet, R. Addison and J. Waldrop, *Surface and Coatings Technology*, **140**, 58 (2001).
15. P. D. Deck and D. W. Reichgott, *Metal Finishing*, **90**, 29 (1992).
16. T. Schram, G. Goeminne, H. Terryn, W. Vanhoolst and P. Van Espen, *Trans I.M.F.*, **73**, 91 (1995).
17. M. A. Smit, J. M. Sykes, J. A. Hunter, J. D. B. Sharman and G. M. Scamans, *Surface Engineering*, **15**, 407 (1999).
18. L. Federizzi, F. Deflorian and P. L. Bonora, *Electrochimica Acta*, **42**, 969 (1997).
19. P. D. Deck, M. Moon and R. J. Sujdak, *Progress in Organic Coatings*, **34**, 39 (1998).
20. G. W. Critchlow and D. M. Brewis, *J. Adhesion*, **61**, 213 (1997).
21. J. H. Nordlien, J. C. Walmsley, H. Østerberg and K. Nisancioglu, *Surface and Coatings Technology*, **153**, 72 (2002).
22. O. Lunder, J. Walmsley, Y. Yu, A. Aytac and K. Nisancioglu, *15th International Corrosion Congress*, Granada, 22-27 Sept 2002.
23. ASTM D3762-79: Standard Test Method for Adhesive-Bonded Surface Durability of Aluminum (Wedge Test).
24. A. Afseth, J. H. Nordlien, G. M. Scamans and K. Nisancioglu, *Corros. Sci.*, **44**, 2491 (2002).
25. L. F. Mondolfo, *Aluminium Alloys: Structure and Properties*, Butterworths, London (1976).
26. M. Pourbaix, *Atlas of Electrochemical Equilibria in Aqueous Solutions*, CEBELCOR, Brussels (1974).
27. O. Lunder, J. Walmsley, P. Mack and K. Nisancioglu, *To be published*.

28. A. J. Kinloch, L. S. Welch and H. E. Bishop, *J. Adhesion*, **16**, 165 (1984).
29. M. R. Bowditch, *Int. Journal of Adhesion and Adhesives*, **16**, 73 (1996).
30. D. M. Brewis and G. W. Critchlow, *Int. Journal of Adhesion and Adhesives*, **17**, 33 (1997).
31. R. A. Dickie, L. P. Haack, J. K. Jethwa, A. J. Kinloch and J. F. Watts, *J. Adhesion*, **66**, 1 (1998).
32. D. M. Brewis, J. Comyn, B. C. Cope and A. C. Moloney, *Polymer Engineering and Science*, **21**, 797 (1981).
33. H. Leth-Olsen, Hydro Aluminium, *unpublished results* (2001).
34. H. Leth-Olsen and K. Nisancioglu, *Corrosion Science*, **40**, 1179 (1998).
35. K. Nisancioglu, J. H. Nordlien, A. Afseth and S. Scamans, *Materials Science Forum Vols. 331-337*, 111, Trans Tech Publications Ltd, Switzerland (2000).
36. M. Bremont and W. Brockmann, *J. Adhesion*, **58**, 69 (1996).
37. G. W. Critchlow and D. M. Brewis, *Int. Journal of Adhesion and Adhesives*, **15**, 173 (1995).

7. Effect of pre-treatment on the durability of epoxy-bonded AA6060 aluminium joints

8. Discussion

Since this thesis is structured as a compilation of separate papers intended for individual publication the discussion of results in these papers is confined to those presented within each chapter. The purpose of this chapter is therefore to provide an overall discussion of the main experimental results presented in the chapters 3 through 7, and to suggest possibilities for further developments on the subject of pre-treatment for adhesive bonding of aluminium.

Formation and properties of the chemical conversion coatings

The results presented in chapters 3 and 4 show that chromate conversion coatings (CCC) and Ti-Zr based conversion layers were formed by different mechanisms. The CCC was formed by an oxidation-reduction reaction, building a relatively thick, hydrated chromium oxide film over the aluminium matrix and a significantly thinner oxide film on the intermetallic particles. Conversely, the Ti-Zr oxide conversion layer was deposited on the surface as a result of local alkalisiation at cathodic sites, *i.e.* at the -Al(Fe,Mn)Si particles on the AA6060 surface. This mechanism caused significant lateral variations in the thickness of the conversion layers, which was essentially controlled by the distribution of cathodic sites as well as pH and agitation of the conversion bath. However, a particulate type of Ti-Zr oxide was deposited all over the aluminium surface, also on an iron-free AA6060 model analogue alloy without any cathodic -Al(Fe,Mn)Si particles.

Despite the relatively thick Ti-Zr oxide depositing on the cathodic particles (Figures 4d and 7a in chapter 4), electrochemical measurements of treated AA6060 surfaces in chloride solution showed only a small reduction in the cathodic activity on the surface due to the Ti-Zr based treatment. This observation again contrasted the behaviour of AA6060 surfaces subjected to chromate treatment. Although the CCC formed on the -Al(Fe,Mn)Si particles was very thin (Figures 3f and 4b in chapter 3), chromate treatment caused a considerable reduction in the cathodic activity of AA6060 during polarisation in chloride solution, even when the chromating time was only a few seconds. Figure 1 illustrates the effect of chromate and Ti-Zr based treatment, respectively, on the polarisation behaviour of AA6060 and the -Al(Fe,Mn)Si phase in 0.1 M NaCl solution. Oxygen reduction was the main cathodic reaction under the experimental conditions employed. The results presently obtained are in line with recent research [1,2] on AA2024 alu

minium, indicating that inhibition of the oxygen reduction reaction at cathodic Cu-rich particles is an important part of the overall corrosion inhibition mechanism of CCCs. However, the detailed mechanism of chromate inhibition of the oxygen reduction reaction is still a subject of continuing investigation [2].

To summarise, the results obtained in the present study demonstrate that Ti-Zr based pre-treatment affects the electrochemical behaviour of AA6060 in chloride solution only to a small extent. This treatment is therefore not expected to improve the corrosion resistance of the alloy significantly. The effective cathodic inhibition of the γ -Al(Fe,Mn)Si particles in AA6060 by chromate treatment is expected to have a favourable effect on the corrosion resistance.

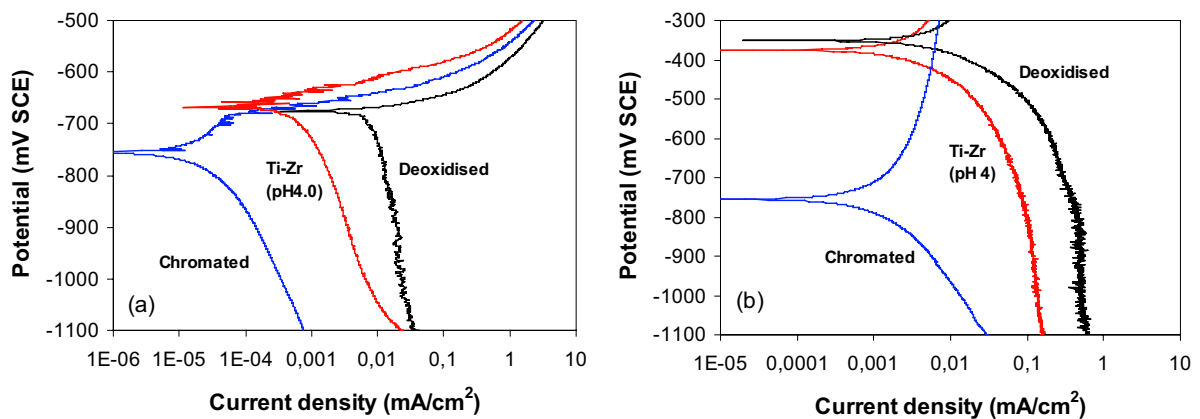


Figure 1. Polarisation curves of a) AA6060 and b) γ -Al(Fe,Mn)Si phase particles in 0.1 M NaCl solution, indicating a more efficient cathodic inhibition by chromate treatment than by Ti-Zr based pre-treatment. Experiments were conducted by potential sweeps at a rate of 30 mV/min in the positive direction, and under similar stirring conditions.

Durability of adhesive joints subjected to chemical pre-treatment

Corrosion of the substrate material

The presence of cathodic particles has previously been shown to have a crucial effect on the susceptibility of aluminium alloys to filiform corrosion (FFC) [3,4] and other types of localised corrosion [5,6]. In fact, corrosion tests have demonstrated that the presence of electrochemically noble second phase particles is a necessity for FFC to occur [4]. The immunity against FFC observed for the iron-free AA6060 model analogue alloy (chapter 7) is there

fore in accordance with earlier conclusions obtained for various single phase binary alloys [4]. Furthermore, the results of the present study indicate that the superior FFC resistance of chromated AA6060 relative to the Ti-Zr treated specimens can probably be largely attributed to a more effective inhibition of the oxygen reduction reaction occurring on the -Al(Fe,Mn)Si particles, as shown in Figure 1. Thus, inhibition of the cathodic activity on the iron containing phases is clearly a desirable feature, which should be considered in search for CCC replacements.

On this background, removal of the detrimental particles from the surface of the aluminium substrate would seem feasible as an alternative pre-treatment method to improve the FFC resistance. Indeed, the results presented in chapter 5 showed that the -Al(Fe,Mn)Si particles could be effectively removed from the AA6060 alloy surface. However, such pre-treatment did not prevent FFC corrosion of the epoxy-coated surface. Apparently, filament growth was supported by cathodic activity on the particles that became exposed as a result of aluminium corrosion, initiated by placing hydrochloric acid in the scribe. The use of 16 wt.% HCl solution was convenient to promote onset of FFC in the accelerated test. It should be noted, though, that this solution is very aggressive compared to the environments that adhesive aluminium joints would be expected to withstand in practice. Before superficial particle removal treatment is rejected as a method to enhance the FFC resistance of coated aluminium it would be desirable to extend the present work, which was limited to one substrate material and one type of adhesive only.

Another factor contributing to the superior performance of chromated AA6060 with respect to FFC is probably the strong adhesion between the CCC and the epoxy adhesive in wet environment, as demonstrated by the wedge test results in chapter 7. It has been suggested [7] that chromating may reduce filament growth on painted aluminium by inhibiting disbonding at the filament head caused by mechanical forces originating from expanding corrosion products in the filament area. Good adhesion is particularly believed to be important when filaments propagate by formation of successive pits beneath the paint [7]. The area of freshly exposed substrate caused by lifting of the paint would then be limited, restricting the available area for initiation of new pits.

In the case of an adhesive bonded aluminium-to-aluminium joint localised lifting of the adhesive due to corrosion products formed at one interface is constrained by the opposite aluminium substrate. Clearly, the formation of voluminous corrosion products must therefore exert a tensile stress on the

joint, promoting loss of adhesion in a larger region surrounding the corroded area. Attempts have been made [8] to observe the disbonding process *in-situ* under FFC test conditions by employing a transparent epoxy adhesive (Araldite 2020) and a glass plate as one of the adherends, allowing visual observation of the corrosion propagation at the aluminium-adhesive interface. It was observed that the disbonded area associated with corrosion propagation depended strongly on the pre-treatment of the AA6060 adherend, as expected. On degreased samples, extensive superficial corrosion of the substrate occurred, causing disbonding over large areas ahead of the corrosion front. Alkaline etching of the substrate prior to bonding significantly reduced the lateral corrosion propagation extending from the edges. However, disbonded regions surrounding the localised corrosion attacks were still observed, apparently due to mechanical lifting of the adhesive from the substrate.

In addition to the mechanical factor, any localised corrosion attack extending from the joint edge obviously represents a path for rapid ingress of water to the interface. The interface area affected by a propagating corrosion filament is therefore generally expected to be significantly larger than the filament area itself.

Loss of adhesion due to moisture

As pointed out above, the presence of cathodic intermetallic particles and a chloride environment may accelerate adhesive joint degradation due to FFC of the substrate alloy. In the absence of chlorides the Fe-rich particles commonly found in commercial alloys are not expected to affect adhesive joint degradation directly, as these particles typically constitute a very small area fraction of the aluminium surface. However, such particles may indirectly have a strong influence by controlling the characteristics of the conversion coating formed during pre-treatment. This was specifically demonstrated by the wedge test results in chapter 7, where excessive Ti-Zr oxide formation on and around the cathodic $-\text{Al}(\text{Fe},\text{Mn})\text{Si}$ particles significantly reduced the performance of bonded joints in humid atmosphere. The practical implication of these observations is that the amount of Ti-Zr oxide deposited, *i.e.* the coating weight, may be strongly affected by the type, fractional area and distribution of cathodic sites on the aluminium surface. Thus, the pre-treatment conditions should be adapted to the specific alloy in order to achieve optimum durability of adhesive joints. In any case it would be important to have good control of the pH and agitation of the conversion bath, which are important factors with respect to the kinetics of the Ti-Zr oxide deposition.

Although there may be controversy regarding the reasons for the reduction in joint strength under adverse environmental conditions, there seems to be general agreement on the need for a stable and cohesively strong surface oxide layer [9-11]. Anodising produces aluminium joints exhibiting superior durability. Phosphoric acid anodising (PAA) is particularly effective due to the hydrolytic stability of the oxide [9,10]. CCCs provide excellent adhesion to paints and adhesives, apparently because hydrated chromium oxide films are particularly inert, hydrophobic and stable over a broad pH range [12]. The oxides formed by these pre-treatments cover nearly 100% of the surface area, although the films may contain a high density of pores and cracks, as shown for the CCC studied in chapter 3.

It has been suggested [13-15] that the deposition of Ti oxide or Zr oxide films on the aluminium surface is beneficial because both these oxides are thermodynamically stable over a wider pH range than aluminium oxide, particularly on the alkaline side. However, for a conversion coating to perform satisfactorily, good coverage of the metal substrate should be an important requirement. Although previous work based mainly on AES and XPS [13,16] seems to indicate the presence of relatively uniform Ti-Zr based conversion coatings, electron microscopy has shown [17,18] that the coatings may be highly heterogeneous. The non-uniform distribution and poor coverage of the Ti-Zr oxide was presently confirmed by field emission SEM observations (chapter 4) and GDOES analyses (chapter 7). In fact, it appeared that the particulate oxide covered only a small fraction of the surface as a result of treatment at the recommended pH of about 3, which could explain the inferior durability of Ti-Zr treated specimens relative to the chromated ones during wedge testing.

Addition of various polymers to the conversion bath is claimed to enhance the uniformity of the coatings [17]. It is also possible that more uniform conversion coatings are formed by no-rinse application. Ti based, polymer free conversion coatings deposited on AA3003 aluminium by spin coating appeared to have a relatively uniform film thickness of about 30 nm according to cross-sectional TEM observations [19]. Interestingly, this coating provided no cathodic inhibition in chloride solution, in accordance with the present results (chapter 4), while significant anodic inhibition occurred. However, the performance of the Ti based conversion coating for adhesive bonding was not investigated.

Present results, obtained from lap shear testing (chapter 6) and FFC testing (chapter 7), indicated that alkaline etching of the AA6060 surface prior to bonding significantly improved the interface stability compared to the

degreased surface. By subsequent desmutting of the etched surface, performance was considerably reduced. Removal of the Mg-rich oxide formed as a result of alkaline etching was suggested as a possible cause for the detrimental effect of desmutting. The role of Mg surface concentration on joint durability has been subject of discussion in the literature, and it has been reported that the presence of Mg may have a detrimental [10,20], beneficial [21,22] or apparently indifferent [23] influence on the durability of aluminium joints. Obviously, the Mg surface concentration is far from being the only factor determining the joint durability. However, the cumulative evidence provided by the literature data and present findings strongly indicates that the significance of Mg is related to the type of adhesive used. It has been observed that an alkaline environment may develop due to a chemical reaction of components in the epoxy with water [24]. The high surface concentration of Mg oxides is believed to increase the hydrolytic stability of the interface due to the high stability of these oxides in alkaline media. In addition to effectively removing the Mg oxides, desmutting of the alkaline etched AA6060 surface also resulted in a reduction of the overall oxide film thickness from about 10 nm to 2 nm, according to the GDOES depth profiles in chapter 6. With such thin oxides, the deterioration of adhesive bonds in humid environment could be due to direct corrosion of the aluminium substrate as well as hydration of the oxide [10].

To conclude, it is not possible to fully explain the performance provided by various pre-treatments independent of the substrate material, adhesive and environmental conditions. Because of the many variables involved, it is often difficult to compare different studies on durability. Some of the published work performed to characterise the changes occurring during hydration has been conducted on oxide surfaces exposed to moist environment. The specific environment created under an adhesive may be much more complex. It remains to be seen whether the mechanisms of oxide weakening are exactly the same when the oxide is covered by an adhesive layer [11].

Pre-treatment by hot AC anodising

The experimental results obtained from the lap shear testing of AA6060 specimens subjected to AC anodising in hot sulphuric acid (chapter 6) were very encouraging. No significant loss of strength was observed for these specimens after 50 days (1200 h) of exposure under FFC test conditions, while significant strength reductions occurred for the various etch pre-treatments tested. The chromate based FPL etch treatment also performed well, although the joint strength was somewhat lower than measured for the

AC anodised specimens. Furthermore, examination of the fracture surfaces after tensile testing indicated a high FFC resistance for the anodised specimens. While hot AC anodising for 4 s, producing an oxide film thickness of about 0.1 μm , resulted in interfacial corrosion extending a few mm from the overlap edge, no signs of interfacial corrosion were observed when the oxide thickness was increased to about 0.2 μm . Specimens subjected to etch pre-treatment, exhibiting an oxide film thickness in the range 0.002-0.02 μm , were all attacked by interfacial corrosion, including the FPL etched surface.

According to the results obtained from polarisation experiments in chloride solution (Figure 5 in chapter 6), no significant reduction in the cathodic activity on AA6060 was observed as a result of hot AC anodising. In view of previous research [25], some oxide film formation probably occurred on the -Al(Fe,Mn)Si particles during anodising. However, the anodising time was apparently too short to cause any insulating film to be formed on the particles. The high resistance against FFC observed for these surfaces must therefore be attributed to the continuous oxide film covering the entire aluminium matrix.

Corrosion tests of painted aluminium sheet alloys [26] indicated that hot AC anodising, performed under similar conditions as in this work, provided high resistance to FFC as long as no active layer formed by thermo-mechanical processing [5] was present beneath the oxide film. It has been argued that reactive surface layers may form on extruded aluminium as well [27]. This conclusion was based on results obtained from FFC testing of chromated and powder coated AA6060 and AA6063 profiles. For some of the materials tested it was necessary to etch away up to about 1 g/m^2 (corresponding to about 0.4 μm) of metal prior to chromate treatment in order to obtain the required performance (<2 mm from scribe after 1000 h). It was not evaluated, though, whether pre-etching influenced the CCC and its adhesion to the powder coating, which could also affect the extent of corrosion attack. It seems that further work is required to understand the detailed structure, composition and corrosion behaviour of the near surface region of extruded aluminium alloys. Anyhow, hot AC anodising should still effectively transform any reactive surface layer into a porous oxide film, thereby reducing the risk of FFC and providing a favourable substrate for adhesive bonding.

A direct comparison of the durability of hot AC anodised and chromated epoxy-bonded joints, respectively, is not possible based on the results presented in this thesis, since different test methods were used. However, due to the promising results presently obtained by lap shear testing, and in view of the rapid and chromate-free processing involved, hot AC anodising is being exploited as a pre-treatment of aluminium for adhesive bonding of automotive





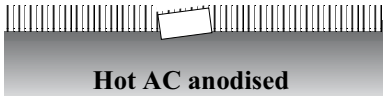
structures [28-30]. Crack growth measurements obtained from wedge tests, performed under exactly the same experimental conditions as those described in chapter 7, have confirmed that the hot AC anodised adherends provide excellent durability. The growth rate was similar to that of the chromated specimens, and visual examination of the fracture surfaces indicated that the locus of failure was partly cohesive and partly interfacial. In general, hot AC sulphuric acid anodised (SAA) joints performed considerably better than both FPL etched and conventional DC SAA joints. However, still better performance was obtained by anodising in phosphoric acid, including DC PAA according to the Boeing procedure as well as hot AC PAA. The excellent performance of the PAA treatments was attributed to a more open pore structure and a higher hydration resistance of these oxides.

Comparison of pre-treatments employed in present work

On the basis of the results presented in this thesis, a qualitative comparison of the pre-treatments examined is given in Table 1, including schematic illustrations of the coating distribution in the vicinity of an -Al(Fe,Mn)Si particle exposed at the AA6060 surface. In general, the selection of pre-treatment for a specific application should be based on a balance between the necessary service life required and the economics of the adhesive bond operation. This balance is difficult to address with confidence due to the lack of engineering data in the area of adhesive bonding [11] and the many variables affecting the performance of adhesive joints. Nevertheless, the performance versus cost issue probably requires particular consideration in the automotive industry, where both safety and cost efficiency are matters of prime concern.

In terms of durability it appears that, among the chromate-free pre-treatments studied in this work, hot AC anodising was the only one matching the performance of the chromate based processes. In addition to being rapid, recent work [28-30] has confirmed that good and reproducible durability is obtained by such pre-treatment. Robustness of the process, and the possibility to increase the coating thickness for increased corrosion protection, should also be attractive features of a chromate-free surface treatment for structural adhesive bonding in automotive applications. While CCCs effectively inhibit the cathodic reactions on the intermetallic particles, hot AC anodising primarily inhibit the anodic reaction (corrosion) by forming a protective oxide over the aluminium matrix. In both cases, the microgalvanic process between the aluminium matrix and the cathodic particles is inhibited, causing a considerable reduction in the rate of localised corrosion propagation.

Table 1. General assessment of pre-treatments investigated in this work.

	Coating thickness (nm)	Coverage	Durability	
			Corrosion resistance	Adhesion
 Etched	2 - 10	-	Low	Low / Medium
 Chromated	150 - 200	High	Medium / High	High
 Ti-Zr treated	0 - 200	Low	Low	Low / Medium
 Particle removal	2	-	Low	Low
 Hot AC anodised	100 - 500	High	Medium / High	Medium / High

Suggestions for further work

It is believed that the observations made in this work clarify several issues concerning the influence of the aluminium substrate on the formation and properties of conversion coatings for adhesive bonding, and the degradation of joints in corrosive environment as listed in the next, concluding chapter. However, further work is required to meet the increasing demand for adhesive systems that are cheaper and more environmentally acceptable, while still exhibiting long-term durability under wet and corrosive conditions. On the basis of the present work, the following topics are specifically suggested for further study:

- Ti-Zr based processes have already gained commercial acceptance as a pre-treatment for painted aluminium. However, much further work is required to obtain the high and consistent performance required for adhesive bonding of automotive aluminium structures. As the Fe-rich

particles of the aluminium substrate are shown to have a significant effect on the coating deposition, experiments should be performed using alloys with different distribution, area fraction and type of cathodic particles. Surface characterisation of the pre-treated surfaces must be combined with environmental testing of bonded joints in an attempt to correlate coating characteristics (*e.g.* coating weight) and durability.

- Further work is called for to precisely determine the locus of failure on adherends subjected to Ti-Zr pre-treatment, such that the degradation mechanisms can be determined. To achieve this, surface analyses of both the metal and the adhesive side of the fractured surface, using techniques such as XPS, AES and SIMS, are required.
- The significance of the low coverage, particulate type of Ti-Zr oxide formed on the aluminium surface, apparently independent of the presence of intermetallic particles, should be investigated further. It has been observed [17] that polymer additions seem to modify the particulate oxide formed in fluorotitanate solutions, and can improve paint adhesion and corrosion resistance. Further studies of Ti-Zr based pre-treatments for adhesive bonding should include the role of polymers.
- Formation of the Ti-Zr oxide deposit in a dipping process may be significantly different from spray or no-rinse application. No-rinse processing implies that a liquid film on the surface is “dried-in-place”. The composition, coverage and morphology of these coatings may therefore be significantly different from those formed as a result of a dipping and rinsing process. A better understanding of the properties and performance of coatings applied by the different methods is desirable.
- The promising results obtained by hot AC anodising in sulphuric acid need to be validated. Such work is already in progress at SINTEF, including TEM characterisation of oxide films, wedge testing and cyclic fatigue testing in humid atmosphere [28-30].
- The performance of an adhesive system is the result of complex interaction between the substrate, the oxide formed by pre-treatment, and the adhesive. It would be interesting to see how the pre-treatments used in this work perform using a different type of adhesive, *e.g.* a phenolic based adhesive giving a slightly acidic pH as a result of reaction with water. The role of Mg in the surface oxide should be addressed in this connection.

References

1. G. S. Frankel and R. L. McCreery, *Interface*, **10**, (4), 34 (2001).
2. G. O. Ilevbare and J. R. Scully, *J. Electrochem. Soc.*, **148**, B196-B207 (2001).
3. A. Afseth, J. H. Nordlien, G. M. Scamans and K. Nisancioglu, *Corrosion Science*, **44**, 2491 (2002).
4. A. Afseth, J. H. Nordlien, G. M. Scamans and K. Nisancioglu, *Corrosion Science*, **44**, 2529 (2002).
5. K. Nisancioglu, J. H. Nordlien, A. Afseth and S. Scamans, *Materials Science Forum Vols. 331-337*, 111, Trans Tech Publications Ltd, Switzerland (2000).
6. K. Nisancioglu, Proceedings of *The 3rd International Conference on Aluminium Alloys: Their Physical and Mechanical Properties*, Trondheim, Norway, **3**, 239 (1992).
7. H. Leth-Olsen, *Dissertation*, Norwegian University of Science and Technology, Trondheim (1996).
8. J. H. Nordlien, *unpublished results* (1999).
9. D. M. Brewis, *Materials Science and Technology*, **2**, 761 (1986).
10. L. Kozma and I. Olefjord, *Materials Science and Technology*, **3**, 869 (1987).
11. A. J. Kinloch, *Adhesion and Adhesives*, Chapman and Hall, London (1990).
12. M. Kendig, S. Jeanjaquet, R. Addison and J. Waldrop, *Surface and Coatings Technology*, **140**, 58 (2001).
13. P. D. Deck and D. W. Reichgott, *Metal Finishing*, **90**, 29 (1992).
14. R. A. Haaksma and J. R. Weir, *Proc. of the 27th International SAMPE Technical Conference*, 1074, Albuquerque, New Mexico, 2-12 Oct 1995.
15. A. Nylund, *Aluminium Transactions*, **2**, 121 (2000).
16. T. Schram, G. Goeminne, H. Terryn, W. Vanhoolst and P. Van Espen, *Trans I.M.F.*, **73**, 91 (1995).
17. P. D. Deck, M. Moon and R. J. Sujdak, *Progress in Organic Coatings*, **34**, 39 (1998).
18. J. H. Nordlien, J. Walmsley, H. Østerberg and K. Nisancioglu, *Surface and Coatings Technology*, **153**, 72 (2002).
19. M. A. Smit, J. M. Sykes, J. A. Hunter, J. D. B. Sharman and G. M. Scamans, *Surface Engineering*, **15**, 407 (1999).
20. A. J. Kinloch, H. E. Bishop and N. R. Smart, *J. Adhesion*, **14**, 105 (1982).
21. M. Bremont and W. Brockmann, *J. Adhesion*, **58**, 69 (1996).
22. T. Smith, *J. Adhesion*, **14**, 145 (1982).

23. P. Poole and J. F. Watts, *Int. Journal of Adhesion and Adhesives*, **5**, 33 (1985).
24. W. Brockmann, O. D. Hennemann, H. Kollek and C. Matz, *Int. Journal of Adhesion and Adhesives*, **6**, 115 (1986).
25. K. Shimizu, G. M. Brown, K. Kobayashi, P. Skeldon, G. E. Thompson and G. C. Wood, *Proc. of Int. Symposium on Aluminium Surface Science and Technology*, 188, Antwerp, Belgium, 12-15 May 1997.
26. H. Leth-Olsen and K. Nisancioglu, *Corrosion Science*, **40**, 1179 (1998).
27. J. H. Nordlien, J. Defrancq, W. Züst, M. Benmalek and R. Stuckart, *Materials and Corrosion*, **51**, 473 (2000).
28. A. Bjørgum, F. Lapique, J. Walmsley and K. Redford, submitted to *Int. Journal of Adhesion and Adhesives*.
29. B. Johnsen, F. Lapique and A. Bjørgum, submitted to *Int. Journal of Adhesion and Adhesives*.
30. B. Johnsen, F. Lapique, A. Bjørgum, J. Walmsley, B. S. Tanem and T. Luksepp, submitted to *Int. Journal of Adhesion and Adhesives*.

9. Conclusions

Formation and properties of the chemical conversion coatings

- Intermetallic particles present in aluminium alloys have a significant effect on the formation and properties of chromate-free conversion coatings and on the degradation of adhesive-bonded joints in corrosive environment. During Ti-Zr based pre-treatment, hydrated Ti and Zr oxides deposit at and in the vicinity of cathodic -Al(Fe,Mn)Si particles on AA6060 aluminium. The deposition is a result of local alkalisation at these sites due to oxygen reduction and hydrogen evolution.
- Substrate microstructure, bulk pH and agitation of the conversion bath are important factors controlling the extent of Ti-Zr oxide deposition and its distribution on the surface. On areas well away from the cathodic particles, a high density of small (<50 nm) oxide particles is deposited, presumably with a composition similar to the continuous conversion layer.
- The cathodic activity of the particles is only slightly reduced by formation of the Ti-Zr oxide conversion coating. In general, the electrochemical behaviour of AA6060 in chloride solution is not significantly influenced by such Ti-Zr based pre-treatment. In combination with poor coverage of the aluminium matrix, these conversion coatings are therefore not expected to improve the corrosion resistance of aluminium significantly.
- Contrary to Ti-Zr oxide deposition, chromate conversion coatings (CCC) form by a reduction-oxidation reaction between hexavalent chromate ions in the solution and aluminium. As a result, a hydrated chromium oxide layer (about 200 nm in thickness) is formed over the aluminium matrix of AA6060, while a significantly thinner film is formed on the -Al(Fe,Mn)Si particles. The CCC presently studied is characterised by a porous morphology, with cracks extending down to the base metal and incomplete coverage at the grain boundaries. The morphology of the CCC is influenced by the presence of precipitation hardening Mg_2Si phase, which promotes nucleation of the CCC to give a more homogeneous coating on a macroscopic scale.
- Chromate treatment results in a significant reduction in the cathodic activity on AA6060 in chloride solution. This is attributed to rapid

formation of a thin (<50 nm) chromium oxide film on the γ -Al(Fe,Mn)Si particles. Effective suppression of the cathodic reactivity of intermetallic particles is an important part of the overall corrosion inhibition mechanism of chromate pre-treatments.

Durability of epoxy-bonded aluminium joints

- The degradation of epoxy-bonded aluminium joints in humid environment is strongly affected by the pre-treatment of aluminium adherends. Ti-Zr based pre-treatment can provide improved durability of epoxy-bonded AA6060 aluminium joints relative to alkaline etching and deoxidation treatment. However, Ti-Zr based pre-treatment is inferior to CCC in maintaining adhesion to epoxy adhesive in humid atmosphere.
- Excessive Ti-Zr oxide deposition in the vicinity of cathodic γ -Al(Fe,Mn)Si particles on AA6060 during pre-treatment results in poor durability of bonded joints. As the amount of Ti-Zr oxide deposited during Ti-Zr based pre-treatment is affected by the type, fractional area and distribution of cathodic particles present on the aluminium surface, the pre-treatment conditions should be adapted to the specific alloy in order to achieve optimum performance.
- In the presence of chlorides, degradation of adhesive-bonded joints may be accelerated by a filiform corrosion (FFC) type of mechanism, which causes tensile stresses by expanding corrosion products and provides paths for rapid ingress of water to the interface. Cathodic particles in the alloy are required for FFC to occur on an epoxy-coated surface. Ti-Zr based pre-treatment provides less protection against FFC than chromate pre-treatment, because the Ti-Zr oxide deposit does not inhibit the cathodic activity on the particles as effectively as a CCC.
- The cathodic γ -Al(Fe,Mn)Si particles present on the surface of AA6060 aluminium can be effectively removed by different etch treatments. However, selective removal of surface intermetallics does not prevent FFC because filament growth is supported by cathodic activity on particles that become exposed in the filament tail as a result of the corrosion process.
- Thin film AC anodising in hot sulphuric acid is promising as a very rapid and chromate-free pre-treatment for adhesive bonding. Based on lap shear testing of joints exposed to FFC test conditions, hot AC anodising to a film

9. Conclusions

thickness of about 0.2 μm gave better performance than the chromate based FPL etch. While hot AC anodising does not significantly inhibit the cathodic activity on the $-\text{Al}(\text{Fe},\text{Mn})\text{Si}$ particles on AA6060, good resistance against FFC is still obtained due to the oxide film covering the whole aluminium matrix. In view of separate, recent results about good and reproducible durability of joints pre-treated by hot AC anodising, this method should prove to be an attractive chromate-free and robust pre-treatment for adhesive bonding of aluminium in certain industrial applications.